

Copyright
by
Breanna R Tercero
2020

**The Dissertation Committee for Breanna R. Tercero certifies that this is the
approved version of the following dissertation:**

**INVESTIGATING THE MECHANISM OF RNA PACKAGING IN
RIFT VALLEY FEVER PHLEBOVIRUS**

Committee:

Shinji Makino, D.V.M., Ph.D.

Dennis Bente, D.V.M., Ph.D.

Alexander Freiberg, Ph.D.

Andrew Routh, Ph.D.

Kylene Kehn-Hall, Ph.D.

**INVESTIGATING THE MECHANISM OF RNA PACKAGING IN
RIFT VALLEY FEVER PHLEBOVIRUS**

by

Breanna R. Tercero, B.S.

Dissertation

Presented to the Faculty of the Graduate School of

The University of Texas Medical Branch

in Partial Fulfillment

of the Requirements

for the Degree of

Doctor of Philosophy

The University of Texas Medical Branch

November 2020

Dedication

I wish to thank my family and friends for their constant love and support throughout my journey. For my father, Rene Rios, who has always provided encouragement since the very beginning of my Ph.D. For my siblings, Carlos Duran, Jose Valadez, Jessica Rios, and Anee Vigueras Duarte and my siblings-in-law, Elizabeth Duran, Luis Vigueras Duarte, and Loreanna Alvarez, who have always been there for me. For my dear friends, Heidy Penate, Krishna Narayanan, and Lola Alcorn, who all helped maintain my sanity throughout my Ph.D and have been there in my times of need. I especially would like to dedicate my dissertation to two of the strongest women in my life; my two grandmothers Romelia Valadez and Irma Bedaro.

Acknowledgements

I wish to acknowledge those who were vital for this scientific achievement. Dr. Anthony Griffiths and Dr. Melanie Amen, who both served as my mentors during my internship at Texas Biomed which ignited my career path. Dr. David Niesel and Dr. Clifford Houston, who accepted me into the PREP program. Mrs. Aneth Zertuche and Dr. Lynn Soong, who have both been there to help me throughout my graduate career.

I would like to acknowledge the Makino laboratory, past and present, who have all helped shape me into the scientist I am today. Dr. Shinji Makino, who not only accepted me into his lab during PREP but also gave me the opportunity to be directly admitted into his lab for my graduate school. Dr. Kaori Terasaki, who was my mentor throughout my graduate career. I would like to thank Dr. Krishna Narayanan for his thoughtful scientific discussions about my project and for challenging me throughout my Ph.D. I would like to thank him for constantly keeping my morale up throughout the many failed experiments and troubleshooting required for my dissertation project.

INVESTIGATING THE MECHANISM OF RNA PACKAGING IN RIFT VALLEY FEVER PHLEBOVIRUS

Publication No. _____

Breanna R. Tercero, B.S.

The University of Texas Medical Branch, 2020

Supervisor: Shinji Makino

Rift Valley fever phlebovirus (RVFV) is a trisegmented, single-stranded, negative-sense RNA genome, consisting of L, M and S segments. The virion carries two envelope glycoproteins, Gn and Gc, along with ribonucleoprotein complexes (RNPs), composed of encapsidated genomes carrying the nucleocapsid protein, N, and the RNA-dependent RNA polymerase, L protein. Understanding the mechanisms that govern the recognition and recruitment of viral RNPs for packaging into RVFV particles is valuable for understanding the regulation of virus replication, virus evolution, and genetic reassortment. However, the mechanisms of viral RNA packaging in RVFV and other bunyaviruses are largely unknown. To study the accumulation kinetics and packaging profile of RVFV RNAs into virions, we established a novel strand-specific RT-qPCR assay that selectively quantifies the genomic and antigenomic RNAs of each of the three RVFV RNA segments. Using this assay, we were able to determine the accumulation kinetics of genomic and antigenomic viral RNAs in RVFV-infected cells and conduct a quantitative analysis of RNA packaged inside purified RVFV particles. Our analysis revealed similar packaging abilities among genome segments but among antigenomic segments, antigenomic S displayed a significantly higher packaging ability. Our data suggests the preferential incorporation of

antigenomic S RNA compared to antigenomic L and M RNA. To delineate the factor(s) governing the differential packaging abilities of RVFV RNA segments, we characterized the molecular interactions between Gn and viral RNPs in RVFV-infected cells. Co-immunoprecipitation analysis demonstrated an interaction of Gn with viral RNPs in infected cells. Furthermore, UV-crosslinking and immunoprecipitation analysis showed that Gn also directly binds to genomic and antigenomic viral RNAs, revealing the presence of a direct interaction between Gn and viral RNAs in infected cells for the first time in bunyaviruses. Strikingly, among the antigenomic RNAs, Gn exhibited a significantly higher binding ability to antigenomic S RNA, which correlated with its higher packaging ability, suggesting the presence of a mechanism for the preferential packaging of antigenomic S RNA. Collectively, our study strongly suggests that a direct interaction between Gn and specific RNA elements in viral RNAs could be the primary factor that governs the packaging efficiency of RVFV RNA segments into virus particles.

TABLE OF CONTENTS

List of Tables	x
List of Figures	xi
List of Illustrations	xiii
List of Abbreviations	xiv
CHAPTER 1: INTRODUCTION	16
Overview of the <i>Bunyavirales</i> order	16
Virion structure and organization	17
Replication and genome coding strategy	19
RNA packaging.....	23
Assembly of viral RNPs into virus particles.....	25
Rift Valley Fever phlebovirus.....	28
RNA Replication.....	28
NSs and the innate immune response	30
RNA packaging.....	32
Assembly	34
Questions addressed in this dissertation	36
CHAPTER 2: A STRAND-SPECIFIC REAL-TIME QUANTITATIVE RT-PCR ASSAY FOR DISTINGUISHING THE GENOMIC AND ANTIGENOMIC RNAs OF RIFT VALLEY FEVER PHLEBOVIRUS	38
Introduction.....	38
Materials and methods	41
Cell culture and virus infection.....	41
Intracellular RNA extraction from virus-infected cells	42
Plasmid construction.....	42
<i>In-vitro</i> RNA synthesis	43
Reverse transcription	43
Standard PCR.....	44

Quantitative PCR	45
Results	45
Strand-specific RT-PCR assay design using unmodified primers fails to selectively amplify target viral RNA segments	45
Primer-independent cDNA synthesis prevents selective amplification of target viral RNAs	53
Strand-specific RT-PCR using ‘tagged’ RT primers selectively amplifies the target viral RNA segment	56
Establishment of strand-specific RT-qPCR assays for genomic and antigenomic RVFV RNAs	64
Kinetics of viral RNA accumulation in RVFV-infected cells	68
Discussion	71
CHAPTER 3: CHARACTERIZATION OF THE MOLECULAR INTERACTIONS THAT GOVERN THE PACKAGING OF RIFT VALLEY FEVER PHLEBOVIRUS RNA SEGMENTS INTO VIRUS PARTICLES	76
Introduction	76
Materials and methods	78
Cell culture	78
Virus infection	78
Virus and VLP purification	79
Co-immunoprecipitation assay	79
Western blot	80
Northern blot	81
Reverse transcription	81
Standard PCR	81
Quantitative PCR	82
VLP RNA packaging assay	82
UV light cross-linking immunoprecipitation (CLIP)	83
Protein dot blot	84
Results	84
Antigenomic S RNA is efficiently incorporated into purified RVFV-virions ..	84

Packaging profiles of S and M RNAs in VLPs	90
Demonstration of the interaction of Gn with viral RNPs in RVFV-infected cells	93
Gn directly interacts with viral RNAs in infected cells	96
Discussion	101
CHAPTER 4: SUMMARY AND FUTURE PERSPECTIVES	105
References	111
Vita	123

List of Tables

Table 2.1: Unmodified RT primers	47
Table 2.2: Unmodified PCR primers	48
Table 2.3: Tagged primers used for reverse transcription	57
Table 2.4: Primers used for strand-specific PCR	60
Table 2.5: Validation parameters for qPCR	66
Table 2.6: Demonstration of strand-specific RT-qPCR in the presence of opposite-sense RNA transcripts.....	67

List of Figures

Figure 1.1: Schematic diagram of bunyavirus genome organization and coding strategies	21
Figure 2.1: RVFV RNA species and coding strategies	40
Figure 2.2: Standard RT-PCR using modified primers does not display strand-specificity	50
Figure 2.3: Absence of residual plasmid DNA after DNase treatment in RNA preparations	52
Figure 2.4: Primer-independent cDNA synthesis of viral RNA impairs standard RT-PCR strand-specificity	54
Figure 2.5: Schematic diagram of modified RT-qPCR with tagged RT primers and modified PCR primer sets	58
Figure 2.6: Modified tagged PCR primer sets do not amplify cDNAs generated by primer-independent reverse transcription	61
Figure 2.7: Validation of a strand-specific RT-qPCR using modified tagged RT primers and PCR primer sets	63
Figure 2.8: Standard curves for genomic and antigenomic segments.....	65
Figure 2.9: Accumulation kinetics of genomic and antigenomic viral RNA segments in RVFV-infected cells	69

Figure 2.10: Comparison of accumulation kinetics of L, M and S segments in RVFV-infected cells	70
Figure 2.11: Possible mechanisms for primer-independent cDNA synthesis	73
Figure 3.1: Quantitative analysis of RVFV RNA segments packaged inside purified virus.	86
Figure 3.2: Alternative representation of RVFV RNA packaged inside virions.	87
Figure 3.3: Packaging abilities of viral RNAs in MP-12-rLuc virus.	89
Figure 3.4: Single-segment RNA packaging assay	92
Figure 3.5: Gn-RNP interaction in RVFV-infected cells.	94
Figure 3.6: Direct interaction of Gn with viral RNAs in RVFV-infected cells. .	98
Figure 3.7: Quantitative analysis of RNA directly bound to Gn in RVFV-infected cells.	100

List of Illustrations

Illustration 1.1: Bunyavirus virion structure and organization	18
Illustration 1.2: Assembly of bunyavirus RNP complexes into mature virions .	27
Illustration 4.1: Future studies examining the biological significance of efficient antigenomic S RNA packaging	110

List of Abbreviations

UTMB	University of Texas Medical Branch
GSBS	Graduate School of Biomedical Science
RVFV	Rift Valley fever phlebovirus
CCHFV	Crimean-congo hemorrhagic fever virus
ANDV	Andes hantavirus
LACV	La Crosse virus
OROV	Oropouche virus
SBV	Schmallenberg virus
TSWV	Tomato spotted wilted virus
BUNV	Bunyamwera virus
NP	Nucleoprotein
RNP	Ribonucleoprotein
PS	Packaging signal
ER	Endoplasmic reticulum
GPC	Glycoprotein precursor complex
NCR	Noncoding regions
ORF	Open reading frame
RIG-I	Retinoic acid-inducible gene 1
IFN	Interferon
PKR	Protein Kinase R
VLP	Virus-like particle

RT	Reverse transcription
PCR	Polymerase chain reaction
qPCR	Quantitative polymerase chain reaction
UV-CLIP	Ultraviolet crosslinking immunoprecipitation
IGR	Intergenic region
TFIIH	Transcription factor II H
SAP30	Suppressor complex containing Sin3A associated protein
smFISH	Single molecule fluorescence <i>in situ</i> hybridization
HITS-CLIP	High throughput sequencing crosslinking immunoprecipitation

CHAPTER 1: INTRODUCTION

Overview of the *Bunyavirales* order

The *Bunyavirales* order is classified into 12 families and contain a large group of negative or ambisense, segmented RNA viruses (1). Bunyaviruses can infect a vast range of hosts including mammals, plants, invertebrates, and reptiles. Majority of these viruses are arboviruses that are maintained in specific arthropod-vertebrate-arthropod cycles, except for hantaviruses and arenaviruses that are maintained in vertebrate-vertebrate cycles without arthropod vectors. Bunyaviruses are distributed world-wide with many considered “emerging viruses”.

Within the order, five families, *Arenaviridae*, *Hantaviridae*, *Nairoviridae*, *Peribunyaviridae* and *Phenuiviridae*, contain many clinically relevant and economically important diseases in humans and animals. Transmission to humans can occur by being bitten by an infected arthropod vector, close contact with infected tissue or fluids, or in the case of hantaviruses and arenaviruses, exposure to the excretion of infected rodents (2-7). Infections with viruses that belong to the *Hantaviridae* family, such as Hantaan virus and Andes virus (ANDV), can cause hemorrhagic fever with renal syndrome and a severe respiratory disease called hantavirus pulmonary syndrome with mortality rates ranging from 10-50% in humans (5, 7). Crimean-Congo hemorrhagic fever virus (CCHFV) of *Nairoviridae*, which is widely distributed across Asia, Africa, Middle east, and Europe, can cause severe hemorrhagic fever with high fatality rates (3, 7). Members of the *Peribunyaviridae* family, including La Crosse virus (LACV) and Oropouche virus (OROV), have been linked to encephalitis leading to significant neurological sequelae (6, 7). Rift Valley Fever phlebovirus (RVFV), within the family *Phenuiviridae*, can cause

severe symptoms in humans including ocular damage, hemorrhagic fever, and late-onset encephalitis (4, 7).

Bunyaviruses are not only considered a threat to human public health but also pose a threat to agriculture due to severe disease in ruminants and crops that result in serious economic losses. For example, Schmallenberg virus (SBV) of the *Peribunyaviridae* family, causes a grave disease in ruminants leading to abortions and malformed newborns in cattle (8). Tomato spotted wilt virus (TSWV) of *Tospoviridae*, can infect a wide variety of plants leading to a decrease in yield and marketable value of crops. In Turkey, it was estimated that the yield loss due to TSWV in tomatoes was approximately \$0.9 million (9). RVFV infection in young livestock have a mortality rate ranging from 70-100% and causes “abortion storms” in pregnant animals. Outbreaks have a large negative impact on the economy due to large deaths within herds, reduction in the sales of animal products, and closures of live animal markets (4).

VIRION STRUCTURE AND ORGANIZATION

Bunyavirus virions are spherical, ranging from 80-120 nm in diameter and are composed of a lipid envelope with glycoprotein spikes (7, 10). The lipid envelope is comprised of two transmembrane glycoproteins, Gn and Gc, and contain lipids derived from host-cellular membranes. Additionally, arenaviruses incorporate host-cellular ribosomes into their virions, giving them a grainy appearance (11). Internally there are ribonucleoprotein (RNP) complexes consisting of individual genome RNA segments associated with the nucleocapsid protein, N, and the RNA-dependent RNA polymerase protein, or L protein (Illustration 1.1). The majority of bunyaviruses carry a tripartite genome consisting of the large (L) segment, medium (M) segment, and small (S) segment although most arenaviruses are comprised of only the L and S RNA segment. The 5' and 3' terminal ends of the viral RNAs contain palindromic sequences that form a panhandle structure (7). RNPs are densely packed inside virions and contain a thread-like helical

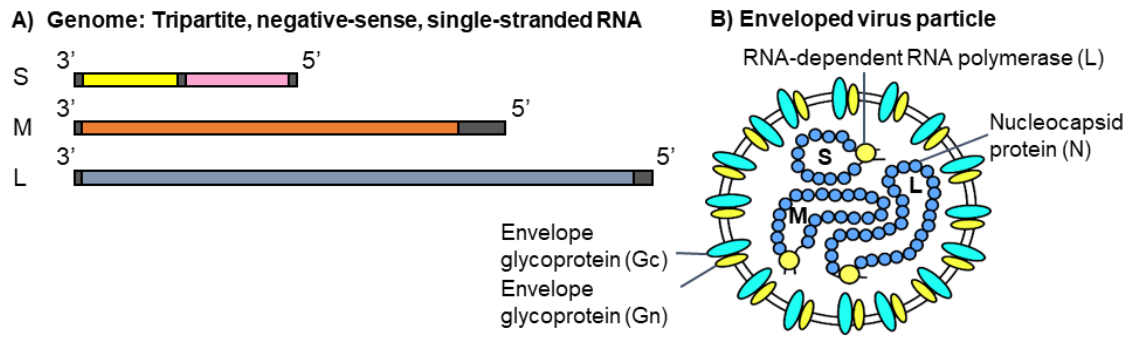


Illustration 1.1: Bunyavirus virion structure and organization

Schematic representation of the bunyavirus virion structure and organization. A) Most bunyavirus genomes have three negative-sense, single-stranded RNA segments that consist of the large (L), medium (M), and small (S) viral RNAs. B) The envelope is composed of a lipid bilayer and two envelope glycoproteins, Gn and Gc. The viral RNAs are encapsidated by the nucleocapsid protein and bound by the RNA-dependent RNA polymerase.

structure. Electron cryo-tomography revealed extensive contact between RNPs and the virion envelope, suggesting an interaction between RNPs and the cytoplasmic tails of the glycoproteins (12).

REPLICATION AND GENOME CODING STRATEGY

Most bunyaviruses have a trisegmented RNA genome comprised of L, M, and S segments. The length of each RNA segment differs in size among the families (7). Each RNA contains open reading frames (ORFs) that are flanked by non-coding regions (NCRs). These NCRs carry signals necessary for replication, transcription termination, and RNA packaging (13-17). The L segment is responsible for encoding L protein. The envelope glycoproteins, Gn and Gc, are produced by the cleavage of the glycoprotein precursor encoded by the M segment. For some bunyaviruses, cleavage of the glycoprotein precursor produces additional accessory proteins; the non-structural protein called NSm (7, 18) and the glycoprotein, 78kD (4). Further processing of the glycoprotein precursor for CCHFV leads to the production of secreted non-structural glycoproteins GP85, GP160, and GP38 (18). The S segment is responsible for encoding the N protein and for some bunyaviruses the non-structural protein, NSs. The coding strategy for S segment differs between the bunyavirus families. For *Peribunyaviridae*, the N and NSs proteins are encoded from two overlapping ORFs (7). Interestingly, some but not all members of the *Hantaviridae* family, such as ANDV, express the NSs protein in this manner (19). For *Phenuiviridae*, N and NSs proteins are produced using an ambisense coding strategy, wherein the N and NSs mRNAs are transcribed from the genomic and antigenomic S RNA, respectively (7). Notably, an additional ORF present in the antigenomic S RNA was found to be conserved in almost all strains of CCHFV (20) and the expression of NSs in CCHFV-infected cells has been demonstrated, although NSs undergoes active degradation during infection (21).

The *Arenaviridae* family have a negative sense, bisegmented genome consisting of L and S segments, with the exception of the genus *Antennavirus* that contain a trisegmented

genome (22, 23). Each segment consists of two ORFs flanked by NCRs and separated by an intergenic region (IGR), utilizing an ambisense coding strategy. The L segment encodes L protein and the matrix protein, Z. The S segment encodes the nucleoprotein, NP, and the glycoprotein precursor complex, GPC. The GPC is further cleaved to produce the glycoproteins GP1, and GP2 (23). The genome organization and coding strategies of representative virus members for the five families containing human and animal pathogens in the *Bunyavirales* order are illustrated in Figure 1.1.

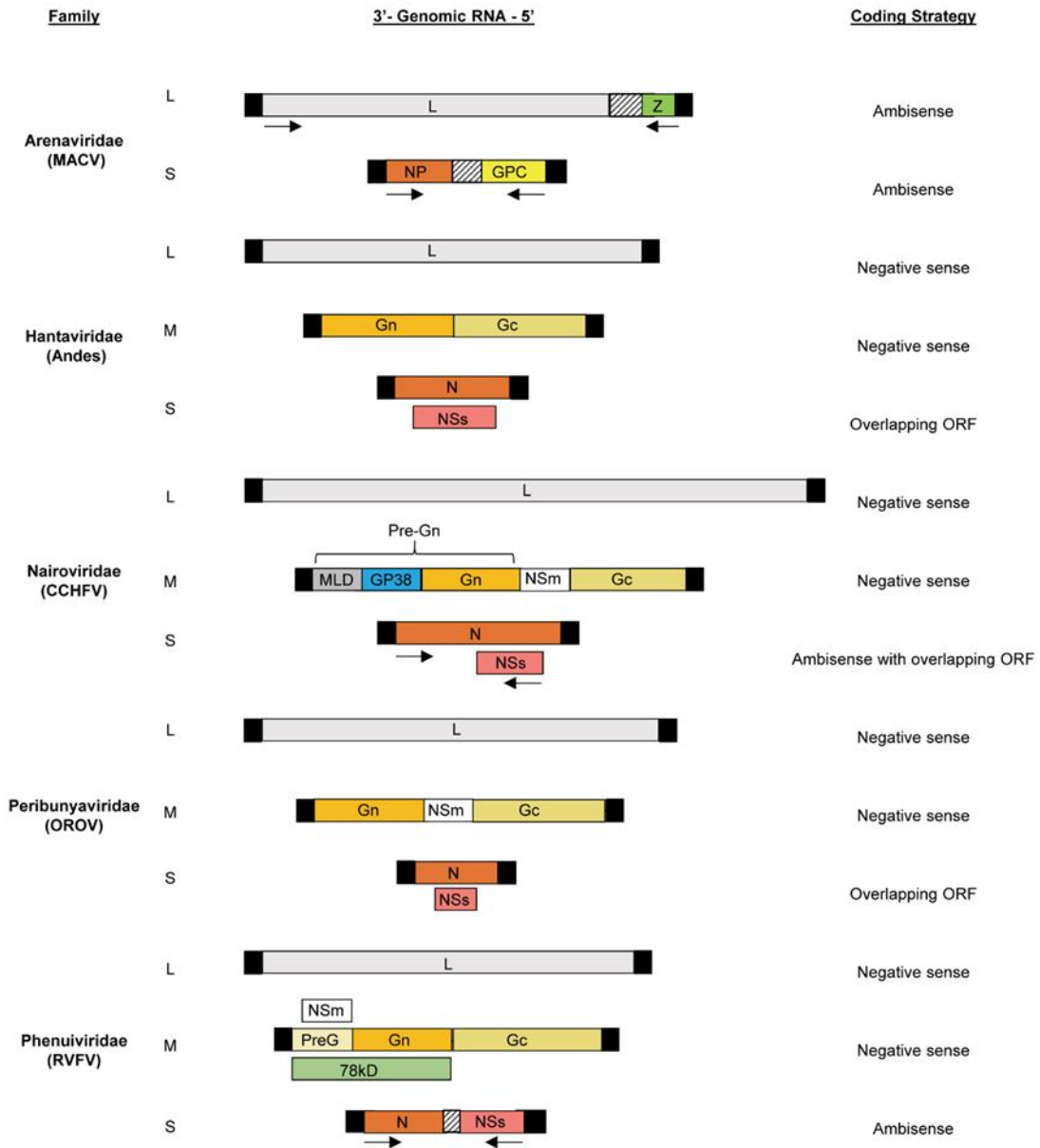


Figure 1.1: Schematic diagram of bunyavirus genome organization and coding strategies

Schematic diagram of the genome organization and coding strategies of representative virus members from selected families in the *Bunyavirales* order (24). The viral proteins encoded by each

viral RNA segments are indicated within boxes. The black boxes represent the terminal NCRs for each viral RNA segment. The intergenic regions are indicated by boxes with dashed lines. The figure is not drawn to scale. MLD; mucin-like domain

Bunyaviruses can replicate efficiently in a variety of cells and are generally cytolytic for mammalian cells but not in invertebrate cells (25). Bunyavirus infection begins when the envelope glycoproteins attach to cell receptors which triggers receptor-mediated endocytosis. Viruses are then internalized into endosomes by both clathrin-dependent and -independent endocytic pathways (7). Acidic conditions within the endosomes trigger a conformational change within the Gc fusion loop which allows endosome membrane fusion. After fusion, viral RNPs are released into the cytoplasm of infected cells, where replication and transcription occur with the involvement of N and L proteins (7, 23). As viral RNAs are negative sense, transcription requires the activation of the L protein that is complexed within the RNPs from the incoming virus. In virus-infected cells, three different viral RNA species are produced for each of the viral RNA segments, which include the genomic RNA, its complementary antigenomic RNA and cognate mRNAs. The L protein has endonuclease activity, cleaving 5'-methylated caps from host mRNAs and subsequently adding them to viral mRNAs to prime transcription in a process called cap-snatching (26, 27). Viral mRNAs lack the poly (A) sequence at the 3'-end, so transcription termination occurs at specific sequences located in the NCRs of viral RNAs. A unique characteristic of bunyaviruses are their ability to undergo transcription-coupled translation, wherein full-length mRNA transcriptions depend upon ongoing synthesis of viral proteins (7, 28, 29). It has been shown in Bunyamwera virus (BUNV) that “viral factories” are contained on tubular structures around the Golgi apparatus connecting viral replication and morphogenesis (30).

RNA PACKAGING

An important aspect of viral RNA packaging is the selection of viral genomic RNAs, from a large and diverse pool of cellular and viral-derived RNAs, that is required to produce infectious virus. Specific *cis*-acting RNA element(s) within the viral RNA genome, called the packaging signal (PS), allow the virus to preferentially incorporate the

viral RNAs into virus particles. PSs for many RNA viruses have been identified including Influenza A virus (IAV) (31), coronaviruses (32), alphaviruses (33), and retroviruses (34, 35). For bunyaviruses, these packaging signals are located within the NCRs of the viral genome segments but the exact nucleotide sequence has not been elucidated (36, 37). Packaging signals form specific secondary structures that are recognized by *trans*-acting element(s), like the viral nucleocapsid protein, which direct the packaging of RNA into virus particles. Interaction of the PS with the viral nucleocapsid protein is important for encapsidation of the viral RNA, which subsequently leads to the formation of the RNPs. Specificity and efficiency of RNA packaging can be coupled with nucleocapsid assembly but can also involve multiple factors such as additional PSs, RNA replication, viral factories, and RNA properties like length (38). Additional viral proteins may dictate efficiency of RNA packaging by interacting with viral RNPs. For example, the recognition of the packaging signal for coronaviruses is debated to be by the nucleocapsid protein and/or the membrane (M) protein (32, 39, 40). It should be noted that not all RNA packaging mechanisms depend on the presence of a PS such as polioviruses that have replication-mediated packaging (38).

An additional level of complexity for bunyavirus RNA packaging is the selective incorporation of segmented viral genomes as an infectious virus requires at least one copy of each viral RNA segment. IAV, an 8 segmented RNA virus, has been thoroughly studied and shown to have a selective co-packaging of its 8 RNA segments (31, 41-43). Selective packaging is defined as specific interactions that ensure all genomic RNA segments are packaged inside all virions. Electron micrographs and tomographs have shown that IAV viral RNPs are arranged in a specific “7 + 1” pattern, where a central RNP is surrounded by the remaining 7 RNPs (31, 42). Inter-viral RNA interactions via *cis*-acting stem-loop structures are essential for IAV genome packaging (31). Whether bunyaviruses employ a similar strategy for packaging their RNA segments is unknown.

ASSEMBLY OF VIRAL RNPs INTO VIRUS PARTICLES

For enveloped viruses, the specific recognition and recruitment of viral RNPs to the site of assembly is a crucial step for the egress of progeny virions. Many enveloped viruses use matrix proteins that serve as bridges between the virus envelope and the viral RNPs (44-46). Matrix proteins and RNP interactions have been reported for many enveloped viruses. The Ebola matrix protein, VP40, has been shown to associate with viral RNPs and is essential for virus assembly and budding (45). IAV matrix protein, M1, has been shown to interact with viral RNPs which is important for the translocation of viral RNPs from the nucleus to the cytoplasm (44). A key characteristic of matrix proteins is an intrinsic budding activity, mediated by a late-domain, that can induce the formation of virus-like particles (VLPs) in the absence of other viral proteins (47). RNA-binding motifs, such as zinc-finger domains, are also present within matrix proteins (44, 48).

A unique feature among most families within the *Bunyavirales* order is that they do not encode a matrix protein to facilitate the incorporation of viral RNPs into mature virions. Notably, arenaviruses are the only family in which they encode the matrix Z protein which interacts with the NP and L proteins to translocate the replication complex to the cell membrane for virus assembly and budding (23, 48). Multiple studies have suggested that the envelope glycoprotein, Gn, can serve as a surrogate matrix protein in which the cytoplasmic tail of Gn interacts with the viral RNPs subsequently leading to their packaging inside virions (Illustration 1.2) (36, 47, 49-53). The bunyavirus glycoproteins are synthesized as a precursor protein that undergoes N-linked glycosylation and cleavage in the endoplasmic reticulum (ER) (10, 23, 54). The Gn cytoplasmic tail contains a Golgi targeting signal that is important for the transit of the Gn/Gc heterodimer to the Golgi apparatus where virus assembly occurs. The Gn protein has been shown for RVFV to independently recruit L protein and N protein to the Golgi for assembly (53). Some bunyavirus glycoproteins can assemble into VLPs in the absence of viral RNPs, although

the efficiency of particle production is increased in the presence of viral RNPs (23, 36, 53, 55, 56). Late-domains have been found within the cytoplasmic tail of Gn for many bunyaviruses (47). Most bunyaviruses bud from the Golgi apparatus except for arenaviruses which bud from the plasma membrane (23). *In-vitro* experiments revealed that the Gn cytoplasmic tail of CCHFV and ANDV had the ability to directly bind to viral RNAs through the dual zinc-finger domain or conserved basic residues flanking the zinc-finger domain, respectively (47, 57). It has been speculated that the RVFV Gn cytoplasmic tail could also interact with viral RNA although it has not been directly demonstrated (53). The exact mechanism driving RNA packaging into virions in bunyaviruses remains poorly understood.

Bunyaviruses can undergo genetic reassortment, in which two related viruses co-infect the same cell leading to progeny virions containing genomic segments from both parental viruses, thus creating a novel virus (58-65). Genetic reassortment is important for the evolution of segmented viruses by introducing antigenic variation and can affect viral fitness. Multiple reassortant RVFV strains have been characterized, revealing that each RNA segment can undergo reassortment (61). Since Gn is important for RNP incorporation and virus assembly, it is possible that Gn may be able to interact with heterologous RNPs that can lead to the emergence of reassortant viruses. This highlights the importance of studying the mechanism of RNA packaging in bunyaviruses.

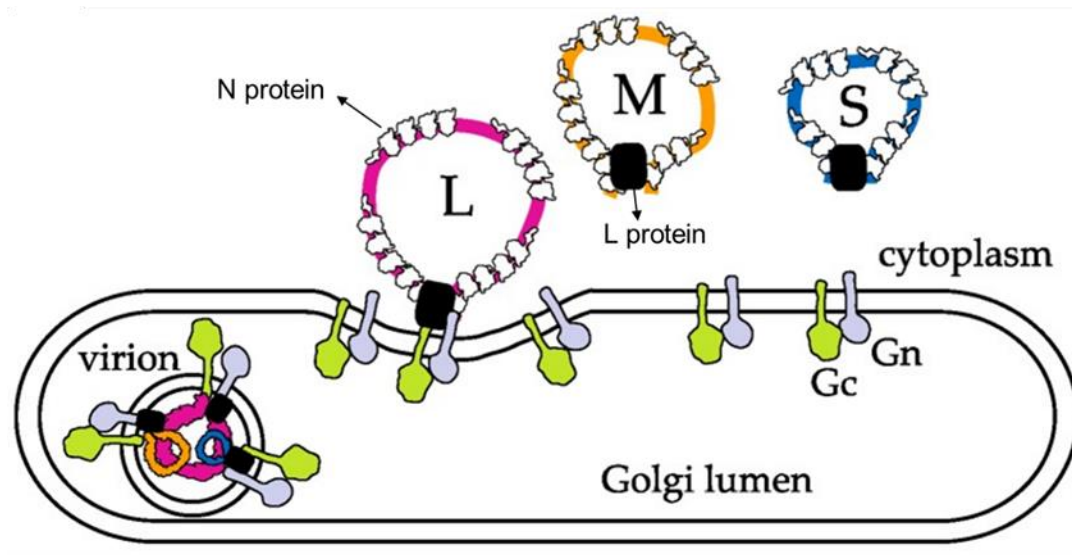


Illustration 1.2: Assembly of bunyavirus RNP complexes into mature virions

Illustration describing the assembly of bunyavirus RNP complexes in mature virions. RNPs are encapsidated by the N protein and bound by the L protein. All three genomic RNPs interact with the cytoplasmic tail of the envelope glycoprotein Gn, subsequently leading to packaging inside a mature virion. Figure adapted from Hornak et al., (36).

Rift Valley Fever phlebovirus

Rift Valley fever (RVF) is an acute mosquito-borne disease caused by RVFV. RVFV can cause severe disease in both humans and ruminants, who can become infected by bites from infected mosquitos or direct contact with infected animal tissue (4). In majority of cases, patients infected with RVFV experience an acute-febrile illness and can generally recover. However, a small percentage of patents develop a severe form of the illness characterized by ocular damage, vision loss, late-onset encephalitis, and hemorrhagic fever (4, 66-78). In ruminants, RVFV can cause high mortality rates in young animals and cause high rates of abortion in pregnant animals called “abortion storms”, resulting in an enormous negative impact on the economy of affected regions (4). RVF has already spread outside continental Africa to Saudi Arabia, Yemen, and Madagascar, highlighting its potential to spread to any area of the world, including North America (79-81). Furthermore, studies have shown that mosquito populations in the U.S. support RVFV replication (79, 82, 83). Considering the health and economic concerns, the lack of availability of licensed vaccines and anti-RVFV reagents for human or animal use is of great concern.

RNA REPLICATION

Like all bunyaviruses, RVFV is a spherical enveloped, single-stranded, segmented RNA virus. It contains three negative sense or ambisense RNA genomic segments, termed L, M, and S segments. The RNA segments are encapsidated by the N protein and bound by L protein, forming the ribonucleoprotein (RNP) complexes. Upon cell entry, RVFV releases the RNPs into the cytoplasm, where viral replication and transcription occur mediated by N and L protein (84-87). Each RNA contains non-coding regions (NCRs) flanking the open reading frames (ORF) (88). The 3' and 5' terminal ends of the NCRs are complementary that base pair to form panhandle structures. The transcriptional promoters

and termination sequences reside within the NCRs (13). In the antigenomic sense, L, M, and S RNA segments have relatively shorter 5' NCRs than their 3' NCRs, which vary in length depending on the RNA segment. The 3' NCRs of antigenomic L and M segment carry transcription termination signals for L mRNA and M mRNA, respectively (16). The S segment carries an intergenic (IGR) region, which harbors the transcription terminal signals for N and NSs mRNA, between the N and NSs ORFs (15-17).

The genomic L and M RNAs serve as templates for the synthesis of their respective antigenomic and mRNAs. The L segment encodes the L protein whereas the M segment encodes a polyprotein precursor that is cleaved to produce the two envelope glycoproteins Gn/Gc, a non-structural protein, NSm, and an accessory protein, 78-kDa. The S RNA utilizes an ambisense coding strategy for gene expression. The genomic S RNA serves as a template for the synthesis of N mRNA, encoding the N protein, while antigenomic S RNA serves as the template for the synthesis of NSs mRNA, which encodes NSs (88). mRNAs contain a host-derived cap structure at the 5' end, obtained by a cap-snatching mechanism employed by the N and L proteins, and do not contain poly (A) sequences at the 3'-end (26, 27).

The N and L proteins are presumably translated on free ribosomes in the cytoplasm. These viral proteins are indispensable for the virus. The structural properties of the N proteins vary widely among the *Bunyavirales* order (7, 36). Two crystal structures of the RVFV N protein revealed a “closed” configuration that was devoid of RNA and an “opened” configuration that showed that N proteins have N-terminal arms that can open and close over an RNA binding cleft (89, 90). The interaction important for triggering this conformational change is unclear although it is speculated to be N protein's interaction with viral RNA and/or L protein (36). The N-terminal arms were shown to mediate oligomerization with neighboring N protein monomers. Although it is known that L protein plays a central role in viral RNA synthesis, little is known about the mechanisms behind L protein's functions. Studies have reported that intermolecular and intramolecular

interactions between the N and C terminal ends of L proteins can form oligomers that play a role in viral RNA synthesis (91). The cap-snatching process requires two functions from the L protein: the ability to bind cap-structures and the activity of cleaving the structures from cellular mRNA. The first 248 residues of the L protein contain an active endonuclease domain (92). A crystal structure of the C-terminal domain of RVFV L protein revealed a functional cap-binding site (93).

NSs AND THE INNATE IMMUNE RESPONSE

Incoming RVFV RNPs are recognized by the retinoic acid-inducible gene 1 (RIG-I) mediated antiviral innate immune signaling due to the presence of the 5'-triphosphate dsRNA panhandle formed by the genome ends (94). Downstream signaling of RIG-I activates the production of type I interferon (IFN) expression, subsequently leading to the establishment of an antiviral state. RVFV is highly sensitive to IFNs and it has been reported that treatment with type I IFN inducers protected mice and hamsters from lethal RVFV infection (95-97). Additionally, during viral replication, dsRNAs are formed which can then bind to and activate the double-stranded RNA-activated protein kinase R (PKR). Activated PKR in turn phosphorylates eIF-2 α , resulting in the inhibition of the translation of both viral and cellular mRNA. PKR can also lead to the induction of apoptosis and can act as a potent restriction factor to RVFV replication (98).

As phleboviruses are extremely sensitive to IFN production and carry not just one but three RIG-I activating RNPs, they have established counterstrategies to prevent the induction of the innate immune response by expressing the NSs protein. The bunyavirus NSs protein is a multifunctional protein, displaying a variety of different mechanisms to evade the host innate immune responses. Within phleboviruses, the amino acid sequence and the subcellular localization of NSs are weakly conserved. However, their function to antagonize the type I IFN response is highly conserved, even if different strategies are employed to do so (98-100). Although the NSs protein was shown to be dispensable for

virus growth and replication in cell culture, in an IFN-competent mammalian host, the virus needs to express NSs to establish a productive infection. The RVFV-clone 13 strain, a naturally-attenuated strain with a deletion within the NSs ORF, had no inhibitory effect on IFN- β expression compared to wild-type RVFV strain ZH548, thus proving that NSs has an anti-IFN activity and is a major virulence factor (98, 101).

RVFV NSs is localized in the nucleus of infected mammalian cells, forming filamentous structures. NSs can inhibit cellular general transcription activity by interfering with the transcription factor II H (TFIIH) components. TFIIH is a transcription factor for host RNA polymerases I and II. NSs interacts with the F-box protein FBXO3 to achieve rapid proteasomal degradation of the TFIIH subunit p62 early in infection. Additionally, NSs can sequester the TFIIH subunit p44, preventing the assembly of the TFIIH complex in the nucleus (98-106). NSs can inhibit IFN induction by recruiting a transcriptional suppressor complex containing Sin3A associated protein (SAP30) to the IFN- β promoter (107). RVFV NSs also recruits the F-box proteins, FBXW11 and FBXW1, to mediate the degradation of PKR, thereby preventing eIF2- α phosphorylation and facilitating viral translation (98, 99, 108).

As stated earlier, RVFV NSs protein is translated from the mRNA transcribed from the antigenomic S RNA in infected cells. It has been shown that the NSs protein accumulates immediately after RVFV infection and that the NSs mRNA is transcribed from incoming antigenomic S RNA that was packaged in the infecting-virion (29). Additional packaging of the antigenomic S segment, along with the three genomic RNAs, facilitates a selective advantage during viral infection.

Although RVFV infection in vertebrates is well studied, information regarding RVFV infection in mosquitos is limited. As mosquitos are the vector and reservoir for RVFV, it is important that RVFV replication is tightly controlled to avoid any detrimental effects and establish a persistent infection in mosquito cells. It has been reported that the Dicer-2 and Piwi-mediated RNA interference pathways restricted RVFV growth in

mosquito cells (109). U4.4 cells, derived from *A. albopictus*, downregulated NSs expression and NSs filaments were not present in infected cells (109). Interestingly, it was reported that an abundance of virus derived siRNAs, generated by the RNAi response in *Drosophila* and mosquito cells, targeted the intergenic region of the antigenomic S RNA segment (110).

RNA PACKAGING

Packaging of the viral genome into virus particles is a critical step in the assembly of infectious viruses. For a RVFV particle to be infectious, it must contain at least one copy of each genomic RNA. Importantly, it has been shown, in both mammalian and mosquito cell lines, that along with the genomic viral RNA segments, all antigenomic RNA segments are packaged into RVFV particles (29). Additionally, the antigenomic S RNA was efficiently incorporated relative to antigenomic L and M RNA segments (29). However, the mechanism by which all viral RNPs are incorporated into nascent virions have yet to be elucidated for bunyaviruses and has remained an open question for segmented RNA viruses. Whether RVFV employs a selective or non-selective “random” packaging has been a major question asked in the bunyavirus field. To comprehend the fundamental mechanisms of RNA packaging, it is essential to understand differences in calculating RNA packaging efficiency and RNA packaging ability. RNA packaging ability can be defined as the intrinsic ability for an RNA to be efficiently packaged into virus particles as it corresponds to the ratio of viral RNA packaged in virions to its accumulation in cells. Packaging efficiency is the absolute amount of RNA per virus or VLP and monitors both the intravirion RNA amount and the level of released virus particles (111). Many studies have deployed different strategies to monitor RNA packaging in RVFV (37).

Multiple studies have focused on the NCRs of RVFV RNA segments for packaging signals. It has been reported that there was overlap between the replication and packaging signals within the terminal 15-25 nucleotides of each RNA segment in RVFV. Murakami

et al., determined the packaging efficiencies of reporter gene constructs containing intact NCRs of each viral RNA segment and found that all were efficiently incorporated into VLPs, demonstrating that the 3' and 5' NCRs of RVFV RNA segments are sufficient for the incorporation of viral RNA into virus particles (14). Minigenome studies containing the NCR of L segment, of Uukuniemi virus (UUKV) or BUNV, was maintained more efficiently than M or S RNA following serial passage. This implies that the NCRs play an important role in bunyavirus genome packaging and that L segment may potentially have stronger packaging signals (112, 113).

Studies using RVFV-clone 13 strain have reported, using P^{32} labeling, that in infected cells, viral RNA accumulates $S > M > L$ and that the L:M:S ratio of genomic segments in purified virions was 1:3.9:3.9, respectively (13). It is to be noted that this analysis of viral RNAs cannot distinguish between genomic, antigenomic, and viral mRNAs. It has been suggested that the M segment coordinates co-packaging of the S and L segments in RVFV. M RNA and an M NCR deletion mutant were packaged into VLPs efficiently but only the M segment with an intact NCR could facilitate co-packaging (114). These data would suggest a possible selective process of packaging, perhaps by the formation of a supra-molecular complex. However, multiple subsequent studies have argued for a flexible non-selective “random” packaging of RVFV. A bisegmented RVFV, that lacks an M segment, was shown to be viable when the glycoproteins ORF was in place of the NSs ORF (115). Furthermore, the flexibility in RVFV packaging was demonstrated by the generation of a 4 segmented RVFV, containing authentic L and S RNA segments and two M-type RNAs (116).

Evidence leaning towards a “random” packaging model of RVFV has been accumulating recently. A recombinant RVFV virus, in which the N and NSs ORF were swapped on the S segment, was generated (117). This study calculated the total percentage of genome to antigenome ratio in infected cells and purified virus. They reported that the accumulation of genomic and antigenomic S and M RNA packaged inside virions reflected

their relative accumulation in infected cells, wherein genomic RNA accumulated to higher levels leading to its higher abundance in virions. Notably, the proportion of antigenomic S RNA was higher when compared to antigenomic M RNA inside virions. This is consistent with studies reporting that antigenomic S RNA is efficiently incorporated into RVFV and UUKV particles (29, 118). Interestingly, in the N-NSs ORF swap virus, antigenomic S RNA accumulated to higher levels in infected cells which correlated with its higher abundance in purified virions. This virus had an attenuated phenotype in mammalian cells but resulted in cell death in mosquito cells, suggesting genome packaging variation across species and cell lines (117).

Studies using a single-molecule fluorescence *in-situ* hybridization (smFISH) method observed in cells infected with RVFV-clone 13 strain, that individual genome segments do not colocalize in the cytoplasm during replication. They also found that a significant number of cells and virions did not contain all three genome segments, further implying a non-selective “random” packaging (119). Additionally, the same group recently observed major differences in the RNA packaging efficiencies in mammalian and mosquito cells, further demonstrating that cell-type specific differences can affect RNA packaging in RVFV (120). Their study reported a higher percentage of complete virus particles, containing all three genomic RNA segments, in mosquito cells compared to mammalian cells, displaying a more efficient genomic RNA packaging in mosquito cells.

ASSEMBLY

The RVFV envelope glycoproteins, Gn/Gc, are involved in virus attachment to cell receptors, endosomal membrane fusion, and viral assembly. They are also the primary targets for the induction of neutralizing antibodies. Gn/Gc are type 1 integral membrane proteins, wherein the C-terminal tails extend towards the cytoplasmic side of the membrane, while the N-terminal ectodomains form the spikes located on the outside of the virion envelope (10, 52). The Gc protein is a class II fusion protein, which undergoes major

conformational changes depending on pH levels which is associated with membrane fusion (10). Gn/Gc are translated as a polyprotein on the endoplasmic reticulum (ER). The Gn/Gc precursor is cleaved by signal peptidase in the ER to form the individual Gn and Gc proteins (88). Gn and Gc are post-translationally modified by N-linked glycosylation (54). When expressed individually, Gc remains in the ER compartment due to a basic di-lysine motif that is conserved among phlebovirus (121). This motif is found in its relative short cytoplasmic tail and is responsible for the ER retention in the absence of Gn (56). Gn, in the absence of Gc, can translocate to the Golgi compartment due to a Golgi localization signal in the cytoplasmic tail (49, 121). Gn/Gc form heterodimers which is important for the translocation and retention of Gc at the Golgi compartment which is necessary for the assembly of the virus.

As bunyaviruses, apart from arenaviruses, lack a matrix protein, it is proposed that the Gn cytoplasmic tail interacts directly with viral RNPs which then get packaged in virus particles. The RVFV Gn cytoplasmic tail is larger than the Gc cytoplasmic tail, containing 70 amino acids compared to 5 amino acids, respectively. There is low conservation in the size and sequences of the Gn cytoplasmic tails among the bunyaviruses. Although it is to be noted that two dual zinc-finger domains located in the Gn cytoplasmic tail were conserved among the *Nairoviridae*, *Hantaviridae*, *Peribunyaviridae*, and *Tospoviridae* families but was lacking in phleboviruses (57). The zinc-finger domain of CCHFV Gn cytoplasmic tail was shown to interact with viral RNAs *in-vitro*. In contrast, the flanking regions of the zinc-finger domain in ANDV Gn cytoplasmic tail was shown to be important for the direct interaction with viral RNAs (57, 122). The packaging of viral RNA into a VLP, in the absence of N and L protein, suggested that RVFV Gn could also interact directly with viral RNA (53). Characterization of the RVFV Gn cytoplasmic tail revealed that the last 40 amino acids are responsible for the recruitment of the L protein to the site of assembly at the Golgi apparatus. This interaction can occur independently from Gn's interaction with N protein, which is proposed to occur within the first 30 amino acids of

the cytoplasmic tail (53). An in-depth analysis of the Gn cytoplasmic tail revealed that residues N43, R44, and I46 were important for Golgi localization and virus assembly. Recombinant viruses containing alanine substitutions at residues K29 and K30 displayed reduced titers but an increase in Gn to N ratio, suggesting a defect in RNP packaging (49).

Questions addressed in this dissertation

1. *Question:* Is there any preference for packaging among genomic RNA segments and antigenomic RNA segments?

Question: Is the packaging of genomic and antigenomic RNAs proportional to their accumulation levels in infected cells?

To gain an insight into viral RNA packaging mechanisms, a comprehensive quantitative analysis of the replication kinetics of genomic and antigenomic RNAs is needed. Mechanisms of bunyavirus RNA replication and packaging is limited since most assays cannot accurately distinguish between genomic, antigenomic, and cognate mRNAs in infected cells. In the second chapter, we have established a quantitative method that distinguishes between genomic and antigenomic RNAs and investigated the replication kinetics of the viral RNAs in RVFV-infected cells. We used this assay in the third chapter to determine the packaging profile of viral RNAs in RVFV particles.

2. *Question:* What factors and interactions govern the packaging of RNA segments into RVFV particles?

Question: Can RVFV envelope glycoprotein, Gn, directly interact with viral RNAs?

Many studies have suggested that the envelope glycoprotein, Gn, can interact with viral RNPs, but this interaction has not been demonstrated in bunyavirus-infected cells. The third chapter focuses on the characterization of the different interactions between Gn and viral RNPs in infected cells. We established a co-immunoprecipitation assay to characterize the interactions of Gn with viral RNPs in RVFV-infected cells. To determine if Gn can directly interact with viral RNAs, we established an ultraviolet crosslinking immunoprecipitation (CLIP) assay.

CHAPTER 2: A STRAND-SPECIFIC REAL-TIME QUANTITATIVE RT-PCR ASSAY FOR DISTINGUISHING THE GENOMIC AND ANTIGENOMIC RNAs OF RIFT VALLEY FEVER PHLEBOVIRUS

Introduction

Viruses belonging to the Order *Bunyavirales* carry segmented RNA genomes that can cause serious and important diseases in both human and domestic animals. Rift Valley fever phlebovirus (RVFV), a member of the genus *Phlebovirus*, family *Phenuiviridae*, order *Bunyavirales*, is a mosquito-borne virus that can cause severe disease in humans and ruminants. RVFV is endemic in sub-Saharan Africa but has spread to Madagascar and the Arabian Peninsula (1-4). Human infection occurs from the bite of infected mosquitoes or from direct transmission of the virus from infected animal tissues or blood. Human disease manifestations include transient incapacitating febrile illness, encephalitis, vision loss and hemorrhagic fever (2, 4-9). RVFV has the potential to spread to any area of the world, including North America, by naturally occurring mosquito populations (2, 10-12). One of the hallmarks of diseases caused by RVFV is high mortality in young ruminants and high rates of abortion in pregnant animals called “abortion storms” causing an enormous negative impact on the economy of affected regions. The lack of anti-viral treatments and licensed vaccines for use in humans or domestic animals is of great concern.

RVFV carries three genomic RNA segments, L, M, and S (Fig. 2.1). L and M segments are of negative-sense polarity, whereas S segment is of ambisense polarity. The RNA genome segments are encapsidated by the nucleocapsid protein, N, and bound to the L protein, the RNA-dependent RNA polymerase, forming the ribonucleoprotein (RNP) complexes. In virus-infected cells, three different viral RNA species are produced for each of the three viral RNA segments, which include the genomic RNA, its complementary

antigenomic RNA and cognate mRNAs. Immediately after infection, the incoming genomic L and M RNAs serve as templates for the synthesis of their respective antigenomic RNAs and mRNAs. The L mRNA encodes L protein, and the M mRNA encodes two accessory proteins, NSm and the 78-kDa protein, along with two major envelope glycoproteins, Gn and Gc. The RVFV S segment uses an ambisense strategy for gene expression. The incoming genomic S RNA serves as the template for the synthesis of N mRNA encoding the N protein, while antigenomic S RNA serves as the template for the synthesis of NSs mRNA, which encodes NSs, a nonstructural protein, which is a major viral virulence factor (8, 13-19). A host-derived cap structure is added to the 5'-end of all viral mRNAs by a cap-snatching mechanism, but viral mRNAs lack the poly(A) sequence at the 3'-end (20). The three viral RNA segments have noncoding regions (NCRs) that flank the open reading frames (ORFs). In the antigenomic sense, L, M and S segments have a relatively shorter 5' NCRs than their 3' NCRs, which vary in length, including 107 nt for L RNA, 271 nt for M RNA and 34 nt for S RNA. These NCRs carry signals necessary for viral RNA synthesis and viral RNA packaging (15, 21). The 3' NCRs of antigenomic L segment and M segment also carry transcription termination signals for L mRNA and M mRNA, respectively. The S segment carries an intergenic NCR, which harbors the transcription termination signals for N and NSs mRNAs, between the N and NSs ORFs (22-24).

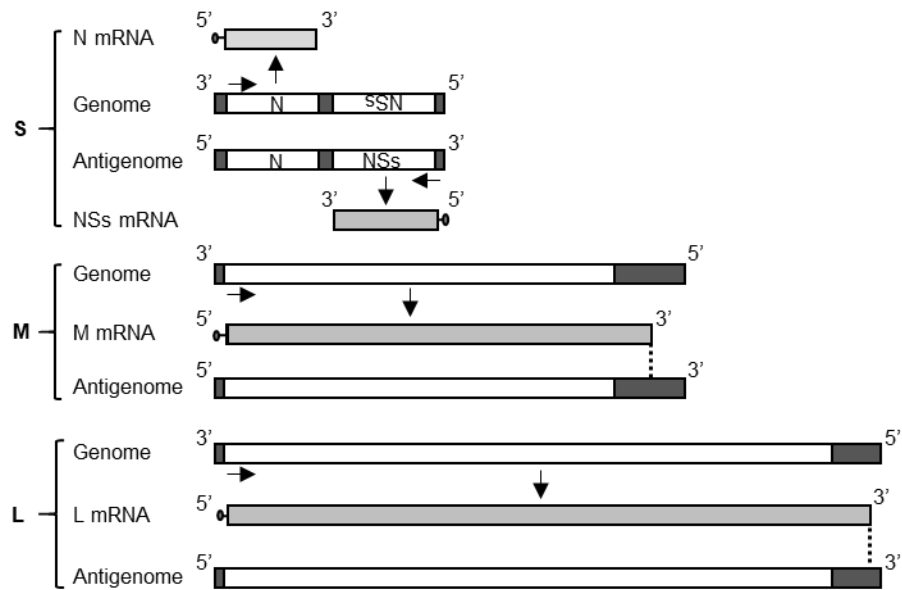


Figure 2.1: RVFV RNA species and coding strategies

Schematic showing all RNA species for each viral segment (123). Full length genomic segments are negative sense and serve as templates for the generation of complementary antigenomic RNAs. The S segment has an ambisense coding strategy wherein, the N mRNA is transcribed from the genomic RNA and NSs mRNA is transcribed from the antigenomic RNA. The genomic strands of L and M segments are used as templates to generate L and M mRNAs, respectively. The horizontal arrows indicate transcriptional start sites. The dashed lines indicate the 3'-ends of L and M mRNAs compared to the full-length antigenomic segments.

An insight into the underlying rules and mechanisms that drive viral RNA replication is valuable for understanding the regulation of virus replication and the pathogenic potential of the virus. This knowledge is also critical for the development of antiviral drugs and the design of strategies for live attenuated vaccines. Although it is well-established that L and N proteins drive viral RNA synthesis in the cytoplasm of cells infected with bunyaviruses (8, 13, 14, 16-18), our knowledge about the mechanisms of bunyavirus RNA replication is limited. In fact, due to the absence of an assay system that can accurately distinguish between genomic and antigenomic viral RNA segments, the accumulation kinetics of replicating viral RNA segments and their relative abundance during infection have not been reported for any bunyaviruses. A lack of such an assay system has also hindered the advancement of our knowledge about other aspects of the viral replication cycle, for example, clarifying the mechanism of viral RNA packaging into virus particles.

In this study, we have developed a strand-specific RT-qPCR assay that accurately distinguishes between the genomic and antigenomic RNAs of RVFV L, M and S segments. Using this assay system, we examined the accumulation kinetics of the genomic and antigenomic viral RNAs in RVFV-infected cells. Our study represents the first quantitative analysis of the kinetics of intracellular accumulation of genomic and antigenomic viral RNA segments in bunyaviruses.

Materials and methods

CELL CULTURE AND VIRUS INFECTION

Vero E6 cells (kidney epithelial cells from African green monkeys) were cultured in Dulbecco's Modified Eagle Medium (DMEM), supplemented with 5% fetal bovine serum (FBS) and 1% penicillin-streptomycin. Huh7 cells (human hepatocellular carcinoma cells) were cultured in DMEM supplemented with 10% FBS and 1% kanamycin. RVFV

MP-12 strain was generated by a reverse genetics system (25) and passaged once in Vero E6 cells. The virus titers were determined by plaque assay in Vero E6 cells. For virus infection, Vero E6 and Huh7 cells, with 90% confluency in 6-well plates, were inoculated with MP-12 at a MOI of 3. After virus absorption at 37°C for 1 h, cells were washed three times with phosphate buffered saline (PBS) and fresh medium was added to the wells.

INTRACELLULAR RNA EXTRACTION FROM VIRUS-INFECTED CELLS

Virus-infected cells were lysed at indicated time points by directly adding 1 ml of Trizol reagent (Invitrogen) to the wells. Total RNA was extracted according to the manufacturer's instructions and re-suspended in 30 µl RNase-free water. The concentration of total RNA was determined using spectrophotometry and adjusted to 100 ng/µl for cDNA synthesis.

PLASMID CONSTRUCTION

Plasmids containing the T7 promoter sequence with MP-12 genomic RNA segments pProT7-L(-), pProT7-M(-), pProT7-S(-) and antigenomic RNA segments pProT7-L(+), pProT7-M(+), pProT7-S(+) were reported previously (25). For the generation of a plasmid expressing L mRNA, we used the pProT7-L (+) plasmid as the PCR DNA template. We produced a PCR product by using a forward primer containing Spe I site (5'-TCGAAACTAGTAGCCCGCCAGGAAG-3'), and a reverse primer containing the end of the transcription termination signal of L RNA (23) with the Not I site (5'-TCGAATGCGGCCGCGTAGCACTATGCTAGTATC-3'). The purified PCR product replaced a 2.7-kb-long Spe I-Not I region, which contains a portion of the L segment ORF and the entire 3'-NCR, of pProT7-L (+), resulting in the pProT7-L-mRNA like plasmid. The pProT7-M-mRNA like plasmid was similarly generated using a 1.2-kb-long Xba I-Not I region, which contains a portion of the M segment ORF and the entire 3'-NCR, of pProT7-M (+), that was replaced by a purified PCR product. This PCR product

was obtained by using a forward primer containing Xba I (5'-CTAGTCTCTAGAGATCACAGACTTTGATGGC-3') and a reverse primer containing the end of the transcription termination signal for M segment (23) along with the Not I site (5'-TCGAATGCGGCCGCCACCCCAAATTACAAC-3') and the use of the pProT7-M(+) plasmid as a PCR DNA template. Sequence analysis confirmed that both plasmids had the expected sequences and lacked viral sequences after the transcription termination sites.

***IN-VITRO* RNA SYNTHESIS**

Plasmids were linearized by Not I digestion and subjected to *in-vitro* transcription reactions at 37°C for 4 h by using the MEGAscript T7 transcription kit (Applied Biosystems/Invitrogen). The samples were then incubated with 2 units of Turbo DNase for 15 min at 37°C, and RNA was extracted using phenol/chloroform and precipitated using ethanol. To ensure complete removal of residual DNAs, the samples were subjected to a second round of DNase treatment and RNA purification using RNeasy Mini Protocol for RNA Cleanup and On-Column DNase digestion (Qiagen). The on-column DNase treatment was extended to 30 min at room temperature. The concentrations of purified RNA transcripts were determined by using spectrophotometry and quality of RNAs were examined by agarose gel electrophoresis. The molecular copies of synthetic RNAs were calculated from the total molecular weight and length of each RNA segment. At 1 ng of RNA, the copy numbers of full-length L, M, and S segment were 2.925×10^8 copies, 4.820×10^8 copies, and 1.108×10^9 copies, respectively. The stocks of *in-vitro* synthesized viral RNAs were subsequently serially diluted to form standard curves used for our RT-qPCR studies.

REVERSE TRANSCRIPTION

cDNA synthesis of viral RNAs by using unmodified RT primers (Table 2.1) was performed by using the Superscript-III first strand synthesis system (Invitrogen). Briefly, 100 ng of *in-vitro* synthesized RNA was mixed with 2 μ M of strand-specific RT primer. The mixture was incubated at 65°C for 5 min and then cooled to 4°C. After addition of the reaction buffer and enzyme mixture, cDNA synthesis was carried out by incubating the sample at 50°C for 50 min, terminated by heating at 85°C for 5 min, cooled to 4°C, and then treated with RNase H at 37°C for 20 min. RT of viral RNA by using tagged RT primers (Table 2.3) was carried out in a similar method, except that 10 pg of *in-vitro* synthesized RNA or 100 ng of total RNA from virus-infected cells were used as the source of RNA samples. cDNA synthesis was performed by incubating the samples at 55°C, instead of 50°C, for 50 min. We used 500 ng of total RNA from virus-infected cells to detect antigenomic RNA segments at the 2 h time-point because RNA levels were lower than the detection limit early in infection with 100 ng total RNA. Accordingly, the resulting copy numbers for the antigenomic RNA segments were adjusted by dividing by a factor of 5 and plotted with the data obtained for the other time-points using 100 ng total RNA. The cDNAs were purified using an on-column PCR purification kit (Qiagen). To test for cDNA synthesis caused by RNA self-priming, RT reactions were carried out in the absence of an RT primer.

STANDARD PCR

PCRs were performed by using the SsoAdvanced™ Universal SYBR® Green Supermix (Bio Rad). For PCR of cDNAs generated by using unmodified RT primers or no RT primers, 2 μ l of cDNA was added to the PCR master mix containing the viral strand-specific PCR primers (Table 2.2). For cDNAs generated by tagged RT primers and purified by on-column purification, 1 μ l of cDNA was added to the PCR master mix containing the non-viral tagged sequence as a forward primer and a viral strand-specific PCR reverse primer (Table 2.4). For both PCRs, thermocycling conditions were as follows: 95°C for 30

sec, 35 cycles of 95°C for 15 sec and 60°C for 20 sec. PCR products were analyzed by gel electrophoresis. Gel Images are scanned, cropped, and assembled by AlphaEase FC Software.

QUANTITATIVE PCR

The real time qPCR assays were prepared using the SsoAdvanced™ Universal SYBR® Green Supermix (BioRad). Total RNAs from virus-infected cells were subjected to RT using tagged strand-specific RT primers as stated before. After cDNA purification, 1 µl of cDNA was added to the PCR master mix containing the non-viral tagged sequence as a forward primer and a viral strand-specific PCR reverse primer (Table 2.4). Thermocycling conditions were the same as standard PCR, followed by melting curve analysis. The assays were performed by the CFX96 Touch Real-time PCR detection system and analyzed using the provided software (BioRad CFX Manager 3.1).

Results

STRAND-SPECIFIC RT-PCR ASSAY DESIGN USING UNMODIFIED PRIMERS FAILS TO SELECTIVELY AMPLIFY TARGET VIRAL RNA SEGMENTS

Our initial approach for quantifying RVFV genomic and antigenomic segments was to synthesize cDNAs by using RT primers, each of which specifically bind to the 3' NCR of each viral RNA segment (Fig. 2.1), and subsequent amplification of the cDNA products by PCR. Antigenomic L segment and M segment have the same orientation as L mRNA and M mRNA, respectively (Fig. 2.1). As transcription of both mRNAs is terminated at the transcription termination site (16, 17) located within the 3' NCR of these antigenomic segments, both mRNAs lack sequences present downstream of the transcription termination sites. To determine the abundances of antigenomic L and M segments, we designed RT primers that bind downstream of their transcription termination sites such that the RT primers would not bind to L and M mRNAs and only amplify full-length

antigenomic segments. Genomic S segment and antigenomic S segment serve as templates for N mRNA and NSs mRNA, respectively (Fig. 2.1). The RT primers used for the cDNA synthesis of genomic S segment and antigenomic S segment have the same sequence as N mRNA and NSs mRNA, respectively. Therefore, these primers would not bind to these mRNAs. Table 2.1 lists the RT primers used for each viral segment. Our initial experimental design used the PCR primer sets reported by others (124-126) (Table 2.2).

RVFV RNA	Target strand	Sequence (5'- 3')	Genome position (Genomic sense)
L segment	Genome	acacaaaggcgcccaatc	1-18 ^a
	Antigenome	cacaaagaccgccaat	6403-6387 ^a
M segment	Genome	acacaaagacggtgcattaa	1-20 ^b
	Antigenome	cagctaactctggcaaaagac	3844-3825 ^b
S segment	Genome	acacaaagctccctagag	1-18 ^c
	Antigenome	cccctagtgccttatcaag	1680-1663 ^c
a From Rift Valley Fever virus strain MP-12 L segment, DQ375404.1 b From Rift Valley Fever virus strain MP-12 M segment, DQ380208.1 c From Rift Valley Fever virus strain MP-12 S segment, DQ380154.1			

Table 2.1: Unmodified RT primers

RVFV RNA	Target strand	Sequence (5'- 3')	Genome position (Genomic sense)
L segment	*Genome	cctcactattacacaccattc	3296-3316 ^a
		atcatcagctgggaagct	3453-3436 ^a
	Antigenome	gctaggctaagaccagtaagc	6288-6308 ^a
		cacaaagaccgccaat	6403-6387 ^a
M segment	**Genome	ctagccgtttcacaactggg	2656-2676 ^b
		caattgcatacccttgcctgggc	2766-2743 ^b
	Antigenome	atccaagcttagaaacttatgcaat	3707-3731 ^b
		cagctaactctggcaaaagac	3844-3825 ^b
S segment	***Genome	aaggcaaagcaactgtggag	271-290 ^c
		cagtgcaggaagccactca	407-426 ^c
	Antigenome	ccatagaataaggtatcctgg	1551-1571 ^c
		cccctagtgccttatcaag	1680-1663 ^c
* Primers used are from Wilson et al., 2013			
** Primers used are from Maquart et al., 2013			
*** Primers used are from Naslund et al., 2008			
^a From Rift Valley Fever virus strain MP-12 L segment, DQ375404.1			
^b From Rift Valley Fever virus strain MP-12 M segment, DQ380208.1			
^c From Rift Valley Fever virus strain MP-12 S segment, DQ380154.1			

Table 2.2: Unmodified PCR primers

To test whether this experimental design worked, we generated full-length genomic and antigenomic viral RNAs for each segment by using *in-vitro* transcription. After DNase treatment of the samples, these RNAs were subjected to cDNA synthesis by using RT primers, each of which binds to genomic L, M and S segment, and subsequent PCR amplification by using the PCR primer sets reported by others (124-126). Surprisingly, we detected PCR products of the expected sizes from target genomic segments, whereas we also detected PCR products of the same sizes from corresponding antigenomic segments (Fig. 2.2A) (123). We performed similar experiments, in which *in-vitro* synthesized genomic L, M and S segment, antigenomic L, M and S segment, and L and M mRNAs, were subjected to cDNA synthesis by using RT primers, each of which designed to bind to each full-length antigenomic segment. Amplification of the cDNAs by using the reported PCR primers resulted in generation of the PCR products of the expected sizes from both antigenomic and genomic segment RNAs and an unexpected PCR product of ~500 bp from L mRNA (Fig. 2.2B) (123). These data showed that this experimental design was unable to selectively amplify target RNAs. To exclude the possibility of incomplete DNA digestion after *in-vitro* transcription leading to the generation of the PCR products from low levels of residual DNAs, the RNA samples were directly subjected to the PCR reaction. No PCR products were generated (Fig. 2.3), demonstrating absence of DNA contamination in the RNA samples (123).

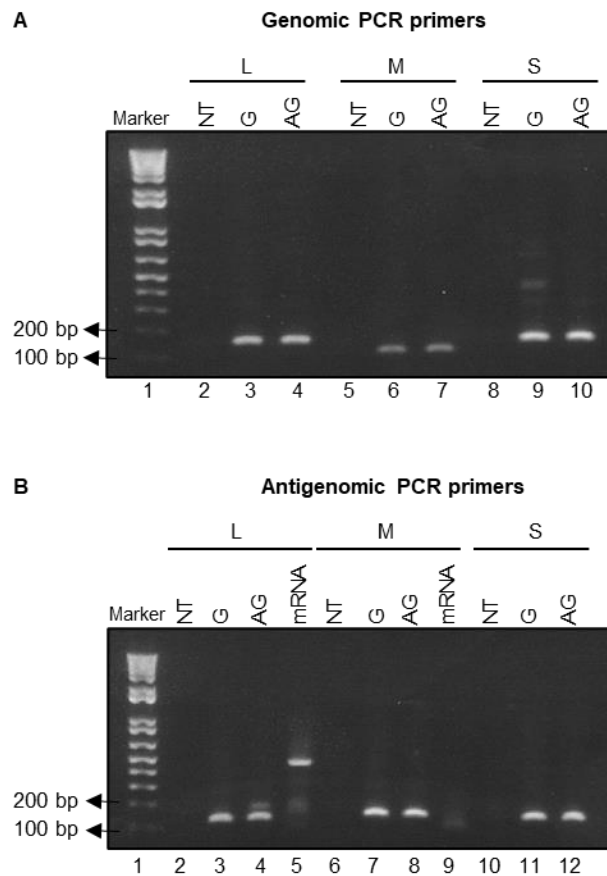


Figure 2.2: Standard RT-PCR using modified primers does not display strand-specificity

(A) 100 ng of *in-vitro* synthesized RNAs corresponding to the genomic (G) and antigenomic (AG) segments of L, M, and S RNAs were used for cDNA synthesis using unmodified RT primers specific for genomic L, M, and S segments respectively. The corresponding cDNAs were subjected to PCR by using unmodified PCR primer sets, specific for genomic L (lanes 2-4), M (lanes 5-7) and S (lanes 8-10) segments. NT represents the "no template" control for RT-PCR analysis (lanes 2, 5 and 8). (B) 100 ng of *in-vitro* synthesized RNAs corresponding to the genomic (G), antigenomic (AG) segments of L, M, and S RNAs, and cognate mRNAs (mRNA) of L and M segments were used for cDNA synthesis using unmodified RT primers specific for antigenomic L, M, and S segments respectively. The corresponding cDNAs were subjected to PCR by using an unmodified PCR primer set, specific for antigenomic L (lanes 2-5), M (lanes 6-9) and S (lanes 10-

12) segments. Lane 1 in (A) and (B) represents the DNA size marker, and the location of the markers having 100 and 200 base pairs (bp) bands are indicated by arrows. The PCR products were analyzed by agarose gel electrophoresis. NT represents the no template control for RT-PCR analysis (lanes 2, 6 and 10) (123).

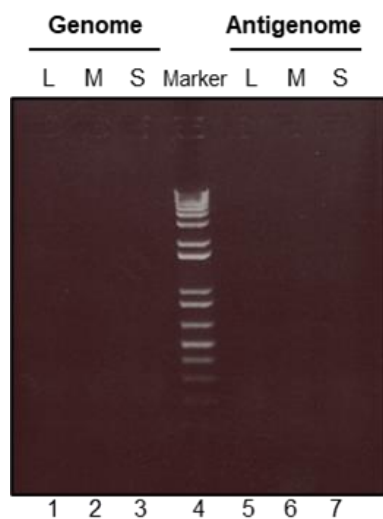


Figure 2.3: Absence of residual plasmid DNA after DNase treatment in RNA preparations

In-vitro synthesized RNAs corresponding to genomic and antigenomic segments of L, M, and S RNAs were treated with DNase and directly subjected to PCR using unmodified PCR primer sets that specifically target genomic L (lane 1), M (lane 2), and S (lane 3) segments and PCR primer sets that specifically target antigenomic L (lane 5), M (lane 6) and S (lane 7) segments. The PCR products were analyzed by agarose gel electrophoresis. Lane 4 represents the DNA size marker (123).

PRIMER-INDEPENDENT cDNA SYNTHESIS PREVENTS SELECTIVE AMPLIFICATION OF TARGET VIRAL RNAs

Multiple studies have reported a phenomenon known as self-primed reverse transcription, where cDNA can be generated in the absence of an RT primer (127-136). The self-priming in the absence of the RT primer is most probably due to the intrinsic ability of the RNA itself or the presence of small RNA fragments in RNA preparations that can serve as primers. To test whether self-primed reverse transcription occurred in this assay system, we performed cDNA synthesis from synthetic genomic and antigenomic viral segments along with RNAs isolated from RVFV-infected cells in the absence of RT primers. The samples were then subjected to PCR. In all samples, we detected PCR products of the same sizes as those generated by amplification of the correct cDNAs by using PCR primer sets (Fig. 2.4) (123), suggesting that cDNA was synthesized in the absence of the RT primer from these viral RNAs. Therefore, we concluded that cDNAs produced by false-priming, possibly due to RNA self-priming, underwent PCR-mediated amplification, preventing strand-specificity of the assay system.

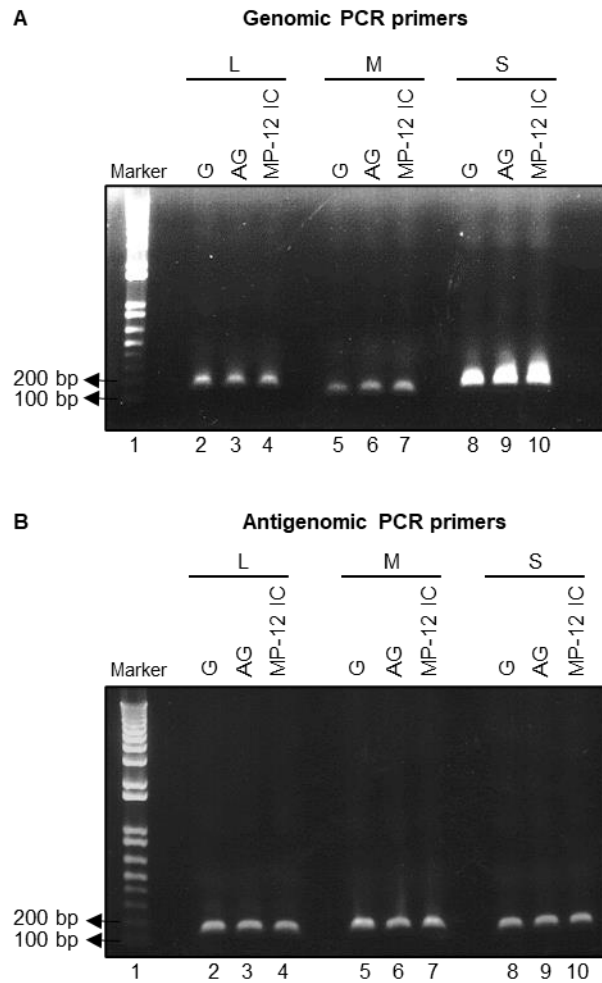


Figure 2.4: Primer-independent cDNA synthesis of viral RNA impairs standard RT-PCR strand-specificity

100 ng of *in-vitro* synthesized RNAs corresponding to the genomic (G) and antigenomic (AG) segments of L, M, and S RNAs and intracellular RNAs from RVFV-infected cells (MP-12 IC) were used for cDNA synthesis without the use of specific RT primers. (A) After cDNA synthesis, the samples underwent PCR using unmodified PCR primer sets, specific for genomic L (lanes 2-4), M (lanes 5-7), and S (lanes 8-10) segments. (B) Experiments were done like (A), except that the samples underwent PCR using unmodified PCR primer sets, specific for antigenomic L (lanes 2-4), M (lanes 5-7), and S (lanes 8-10) segments. Lane 1 in (A) and (B) represents the DNA size

marker, and the location of the markers having 100 and 200 base pairs (bp) bands are indicated by arrows. The PCR products were analyzed by agarose gel electrophoresis (123).

STRAND-SPECIFIC RT-PCR USING ‘TAGGED’ RT PRIMERS SELECTIVELY AMPLIFIES THE TARGET VIRAL RNA SEGMENT

To establish a strand-specific RT-qPCR assay, we modified our assay by increasing the annealing temperature during reverse transcription from 50°C to 55°C and by using ‘tagged’ RT primers (Table 2.3). Increasing the annealing temperature in the reverse transcription step has been shown to reduce non-specific primer binding (129, 131, 132). The tagged primer method has been used in numerous studies to overcome false-priming issues (117, 132-140). In this modified assay, cDNA synthesis was performed by using a tagged RT primer complementary to each of the target RNA segments (Fig. 2.5) (123). Each tagged RT primer had a non-viral tag sequence, modified from Brennan et al (117), at the 5’-end. Hence, cDNAs that are synthesized by using the tagged RT primer, but not those synthesized by false-priming, carry the ‘tag’ sequence at the 5’-end. The tagged RT primer for the antigenomic M segment and that for the antigenomic L segment were designed not to bind to M mRNA and L mRNA, respectively. The tag sequence of the RT primer was used as the forward primer (5’-GGCCGTCATGGTGGCGAATA-3’) and a strand-specific primer was used as the reverse primer in PCR. Use of the tag sequence as the forward primer ensures that only primer-driven tagged cDNA, but not those generated by false-priming, gets amplified during PCR.

RVFV RNA	Target strand	Sequence (5' - 3')	Genome position (Genomic sense)
L segment	Genome	<u>GGCCGTCATGGTGGCGAATA</u> gccaatcatggattctat	11-29 ^a
	Antigenome	<u>GGCCGTCATGGTGGCGAATA</u> caaagaccgccaatattg	6401-6383 ^a
M segment	Genome	<u>GGCCGTCATGGTGGCGAATA</u> actaaccagagatgattg	124-141 ^b
	Antigenome	<u>GGCCGTCATGGTGGCGAATA</u> ctggcaaaagacgattacg	3836-3818 ^b
S segment	Genome	<u>GGCCGTCATGGTGGCGAATA</u> cactattacaataatggac	26-41 ^c
	Antigenome	<u>GGCCGTCATGGTGGCGAATA</u> gtatatcatggattactt	1663-1646 ^c

^a From Rift Valley Fever virus strain MP-12 L segment, DQ375404.1

^b From Rift Valley Fever virus strain MP-12 M segment, DQ380208.1

^c From Rift Valley Fever virus strain MP-12 S segment, DQ380154.1

Tagged RT primers were used for strand-specific reverse transcription. The Tag sequence is in capital letters and underlined.

Table 2.3: Tagged primers used for reverse transcription

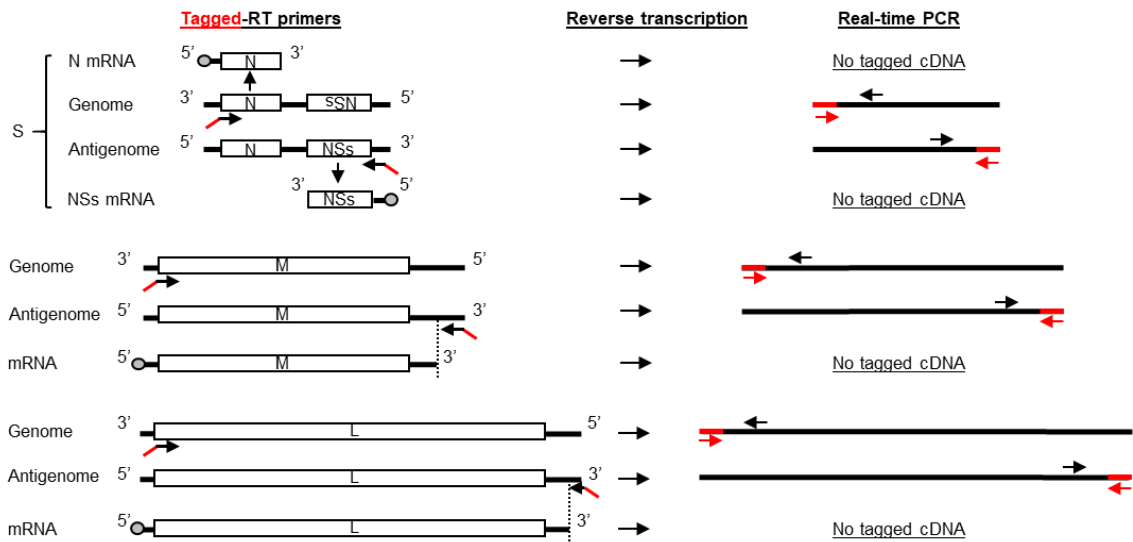


Figure 2.5: Schematic diagram of modified RT-qPCR with tagged RT primers and modified PCR primer sets

Left panel shows schematic diagram of RVFV RNAs and binding sites of tagged RT primers to viral RNA segments. cDNA synthesis is performed using a tagged RT primer complementary to either genomic or antigenomic viral RNA segments. The tagged non-viral sequence, shown in red, is attached to the 5'-end of each strand-specific RT primer. For genomic segments, the tagged genomic RT primers bind to the 3'-end of these RNAs. Note that the tagged genomic RT primer binds to the 3'-end of genomic S segment, but not N mRNA, as the RT primer is in the same orientation as N mRNA. The same principle is applied for the tagged RT primer for antigenomic S segment, which does not bind to NSS mRNA. The tagged RT primers for antigenomic M and L segments bind downstream of the transcription termination sites of these segments. The dashed lines indicate the 3'-ends of L and M mRNAs compared to the full-length antigenomic segments. The right panel outlines the PCR of the cDNA products by using the forward PCR primer (red arrows), which is the tag portion of the RT primer, and a strand-specific reverse PCR primer (black arrows). Use of the tagged portion as a forward PCR primer ensures that only primer-driven tagged cDNAs undergo amplification (123).

To determine whether a combination of forward tag PCR primer and strand-specific reverse PCR primer amplifies cDNAs synthesized by false-priming, we performed cDNA synthesis from *in-vitro* synthesized genomic and antigenomic viral segments and RNAs from RVFV-infected cells in the absence of the RT primers. The samples were then subjected to PCR amplification by using a forward tag PCR primer and strand-specific reverse PCR primer for each of the genomic and antigenomic viral segments (Table 2.4). No PCR products were generated (Fig. 2.6), demonstrating that a combination of the forward tag PCR primer and the strand-specific reverse PCR primer did not amplify cDNAs produced by false-priming (123).

We next tested whether use of the tagged RT primer for cDNA synthesis and subsequent PCR using forward tag PCR primer and strand-specific reverse PCR primer sets lead to selective amplification of the target RNA. We used *in-vitro* synthesized genomic and antigenomic L, M and S segments and L and M mRNAs as source RNAs. As residual RT primer present during PCR amplification can also cause false-priming (128, 129, 132, 133, 136), we purified the cDNAs after reverse transcription to remove residual tagged RT primers and reverse transcriptase, and then subjected them to PCR amplification using the forward tag PCR primer and strand-specific reverse PCR primer for each target RNA (Table 2.4). We detected PCR products of the expected sizes only from the target RNA templates (Fig. 2.7), demonstrating selective amplification of the target RNAs (123).

RVFV RNA	Target strand	Sequence (5'-3')	Genome position (Genomic sense)
L segment	Genome	ccagattgaagtctatgg	169-152 ^a
	Antigenome	gctaggctaagaccagtaagc	6288-6308 ^a
M segment	Genome	caagccatcagcagcaatg	278-260 ^b
	Antigenome	atccaagcttagaaacttatgcaat	3836-3818 ^b
S segment	*Genome	aactctacgggcatcaaacc	152-133 ^c
	Antigenome	ccatagaataaggtatcctgg	1551-1571 ^c
Tag		**GGCCGTCATGGTGGCGAATA	
* Primer used is from Brennan et al., 2014			
** Tag sequence is adapted from Brennan et al., 2014			
^a From Rift Valley Fever virus strain MP-12 L segment, DQ375404.1			
^b From Rift Valley Fever virus strain MP-12 M segment, DQ380208.1			
^c From Rift Valley Fever virus strain MP-12 S segment, DQ380154.1			

Table 2.4: Primers used for strand-specific PCR

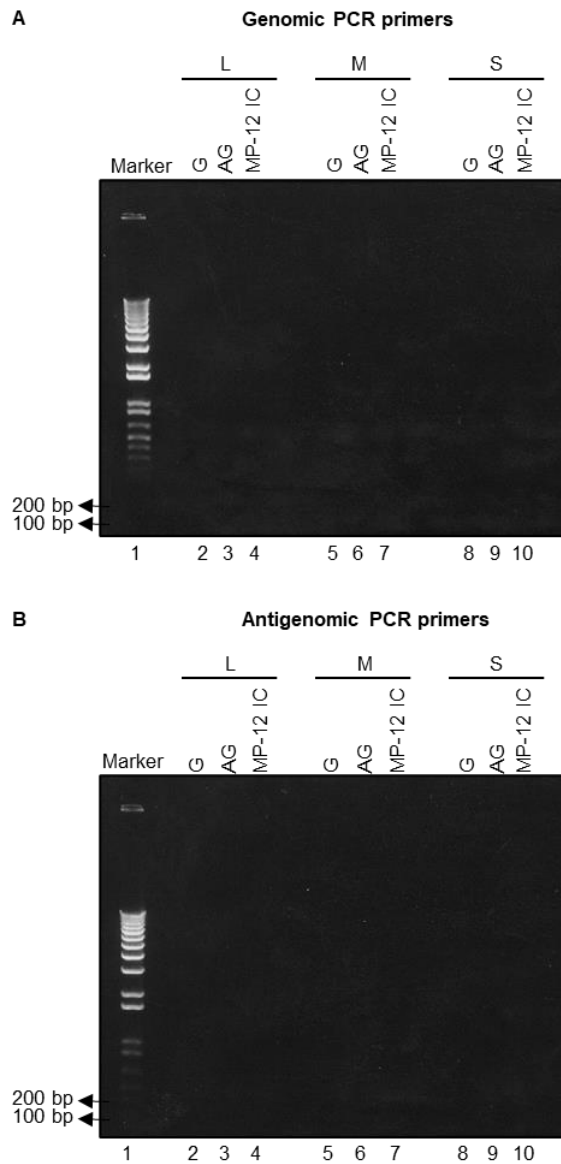


Figure 2.6: Modified tagged PCR primer sets do not amplify cDNAs generated by primer-independent reverse transcription

100 ng of *in-vitro* synthesized RNAs corresponding to the genomic (G) and antigenomic (AG) segments of L, M, and S RNAs and intracellular RNAs from RVFV-infected cells (MP-12 IC) were used for cDNA synthesis without the use of specific RT primers. (a) After reverse transcription, cDNAs underwent PCR using primer sets with the forward PCR primer having a tagged sequence and a segment-specific reverse PCR primer designed to selectively amplify

genomic L (lanes 2-4), M (lanes 5-7), and S (lanes 8-10) segments. (b) Experiments were done similar to (a) except that the samples underwent PCR using a set of forward PCR primers having a tagged sequence and a segment-specific reverse PCR primer specific for antigenomic L (lanes 2-4), M (lanes 5-7), and S (lanes 8-10) segments. Lane 1 in (a) and (b) represents the DNA size marker, and the location of the 100 and 200 base pair (bp) bands of the marker are indicated by arrows. The PCR products were analyzed by agarose gel electrophoresis (123).

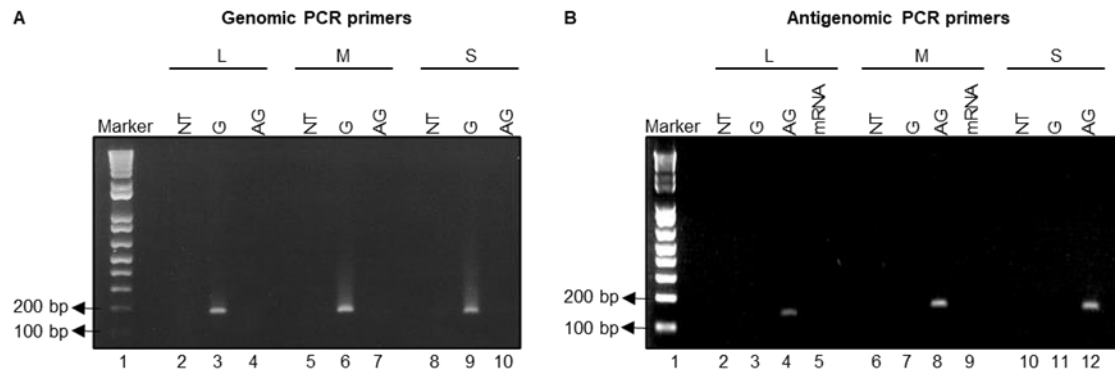


Figure 2.7: Validation of a strand-specific RT-qPCR using modified tagged RT primers and PCR primer sets

(A) 10 pg of *in-vitro* synthesized RNAs corresponding to the genomic (G) and antigenomic (AG) segments of L, M, and S RNAs were used for cDNA synthesis using tagged RT primers specific for genomic L, M, and S segments. The corresponding cDNAs were subjected to PCR by using PCR primer sets with the 'tag' sequence as the forward primer and a segment-specific reverse primer that selectively amplifies genomic L (lanes 2-4), M (lanes 5-7) and S (lanes 8-10) segments. NT represents the "no template" control for RT-PCR analysis (lanes 2, 5 and 8). (B) 10 pg of *in-vitro* synthesized RNAs corresponding to the genomic (G), antigenomic (AG) segments of L, M, and S RNAs, and cognate mRNAs (mRNA) of L and M segments were used for cDNA synthesis by using tagged RT primers specific for antigenomic L, M, and S segments. The corresponding cDNAs were subjected to PCR using PCR primer sets with the 'tag' sequence as the forward primer and a segment-specific reverse primer that selectively amplifies antigenomic L (lanes 2-5), M (lanes 6-9) and S (lanes 10-12) segments. NT represents the "no template" control for RT-PCR analysis (lanes 2, 6 and 10). Lane 1 in (A) and (B) represents the DNA size marker, and the location of the markers having 100 and 200 base pairs (bp) bands are indicated by arrows. The PCR products were analyzed by agarose gel electrophoresis (123).

ESTABLISHMENT OF STRAND-SPECIFIC RT-QPCR ASSAYS FOR GENOMIC AND ANTIGENOMIC RVFV RNAs

As the experimental approach described above successfully amplified the target viral RNAs, we proceeded to further validate and establish the RT-qPCR assay and examined its specificity and limit of detection. To determine absolute copy number for target viral RNAs that are detectable in this assay, we performed an RT-qPCR assay by using known copy numbers of *in-vitro* transcribed RNA and established standard curves for each viral segment, where 10^3 to 10^{10} copies of genomic and antigenomic L and M segments and 10^4 to 10^{11} copies of genomic and antigenomic S segments showed strong linearity with 0.992 or better correlation coefficient (R^2) values (Fig. 2.8 and Table 2.5) (123).

We next tested whether this assay was capable of quantifying target viral RNAs in the presence of RNAs in the opposite sense. We prepared RNA samples, where 10^4 - 10^8 copies of target genomic or antigenomic L or M segments were mixed with 10^6 copies of their opposite-strand RNA and 10^5 - 10^9 copies of target genomic or antigenomic S segment were mixed with 10^7 copies of their opposite-strand RNA, and used them as RNA sources for cDNA synthesis. After cDNA synthesis using specific tagged RT primers for the target RNA, we purified cDNAs and performed qPCR. The amounts of all target RNAs were accurately determined under this experimental condition, demonstrating that this strand-specific RT-qPCR assay was able to measure the amounts of the target RNAs in the presence of up to ~100-fold excess amounts of their opposite-strand RNAs (Table 2.6) (123). Taken together, these data demonstrate that the modified strand-specific RT-qPCR assay was effective for overcoming false priming and allowed us to distinguish between all the genomic and antigenomic RVFV RNAs.

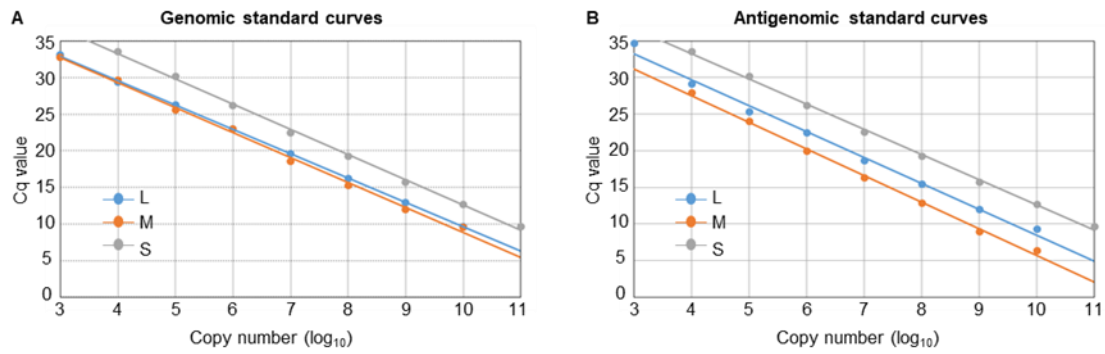


Figure 2.8: Standard curves for genomic and antigenomic segments

Standard curves for (A) genomic and (B) antigenomic viral segments were generated by plotting the quantification cycle (Cq) value against the input of *in-vitro* transcribed RNA of known copy numbers. *In-vitro* synthesized genomic RNA segments (A) and antigenomic RNA segments (B) were serially diluted ten-fold, (10^{10} to 10^3 copies) for L (blue) and M (orange) segments and (10^{11} to 10^4 copies) for S segment (grey) and were used to generate standard curves.

Limit of Detection (Copies)		Linear Regression			
Genome		<i>Slope</i>	<i>Intercept</i>	<i>Amplification efficiency (%)</i>	<i>R² value</i>
L segment	10 ³	-3.329	44.471	99.7	0.998
M segment	10 ³	-3.408	45.288	96.5	0.996
S segment	10 ⁴	-3.446	47.207	95.1	0.998
Antigenome					
L segment	10 ³	-3.535	45.480	91.8	0.992
M segment	10 ⁴	-3.645	44.609	88.1	0.997
S segment	10 ⁴	-3.222	44.611	104.3	0.995

Table 2.5: Validation parameters for qPCR

Linear regression of standard curves	Genome (in the presence of antigenome)			Antigenome (in the presence of genome)		
	L segment	M segment	S segment	L segment	M segment	S segment
R ² value	0.998	0.997	0.999	0.983	0.995	0.997

Table 2.6: Demonstration of strand-specific RT-qPCR in the presence of opposite-sense RNA transcripts

KINETICS OF VIRAL RNA ACCUMULATION IN RVFV-INFECTED CELLS

We used this newly established strand-specific RT-qPCR assay to investigate the intracellular accumulation kinetics of RVFV RNAs following infection in Vero E6 cells and Huh7 cells, a hepato-cellular carcinoma cell line (141), at a multiplicity of infection (MOI) of 3. We determined the amounts of intracellular genomic and antigenomic L, M and S segments at 2, 4, 6, 8, 12, 16, and 20 h post-infection (p.i.) (Fig. 2.9).

In both cell lines, accumulation of all three genomic RNA segments were substantially higher than their antigenomic counterparts throughout the course of infection, with the exception of M segment at 6-8 h p.i., in Vero E6 cells and 4-12 h p.i. in Huh7 cells, showing similar levels of accumulation for genomic and antigenomic RNAs. Accumulation of antigenomic M segment in both cell lines were higher relative to antigenomic L and S segment after 4 h p.i., being more prominent in Huh7 cells (Fig. 2.10). We also noted that early in infection (4-6 h p.i.), genomic S segment copy numbers were higher compared to genomic L and M segments (Fig. 2.9 and 2.10).

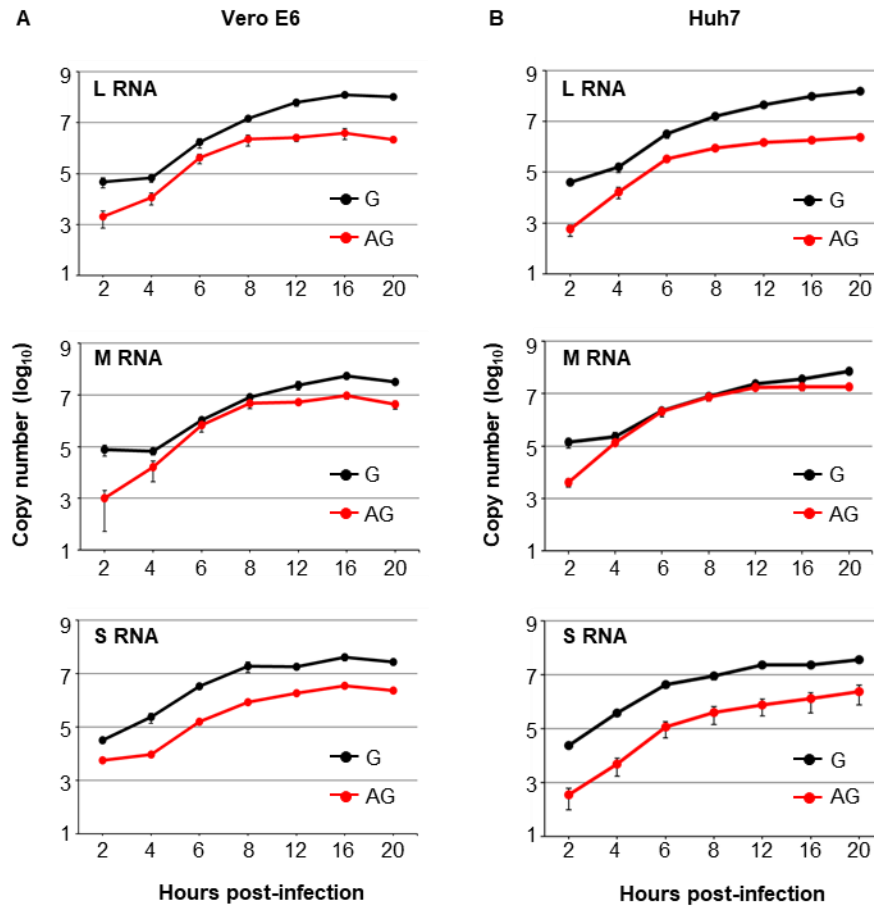


Figure 2.9: Accumulation kinetics of genomic and antigenomic viral RNA segments in RVFV-infected cells

(A) Vero E6 and (B) Huh7 cells were infected with RVFV at an MOI of 3. Total intracellular RNAs were extracted in triplicate at the indicated times p.i. Total RNAs were subjected to strand-specific RT-qPCR and the copy numbers for each viral segment, which were determined with synthetic viral RNA as a reference standard, are plotted. Error bars represent the mean (+/- the standard deviation) of biological triplicate experiments (123).

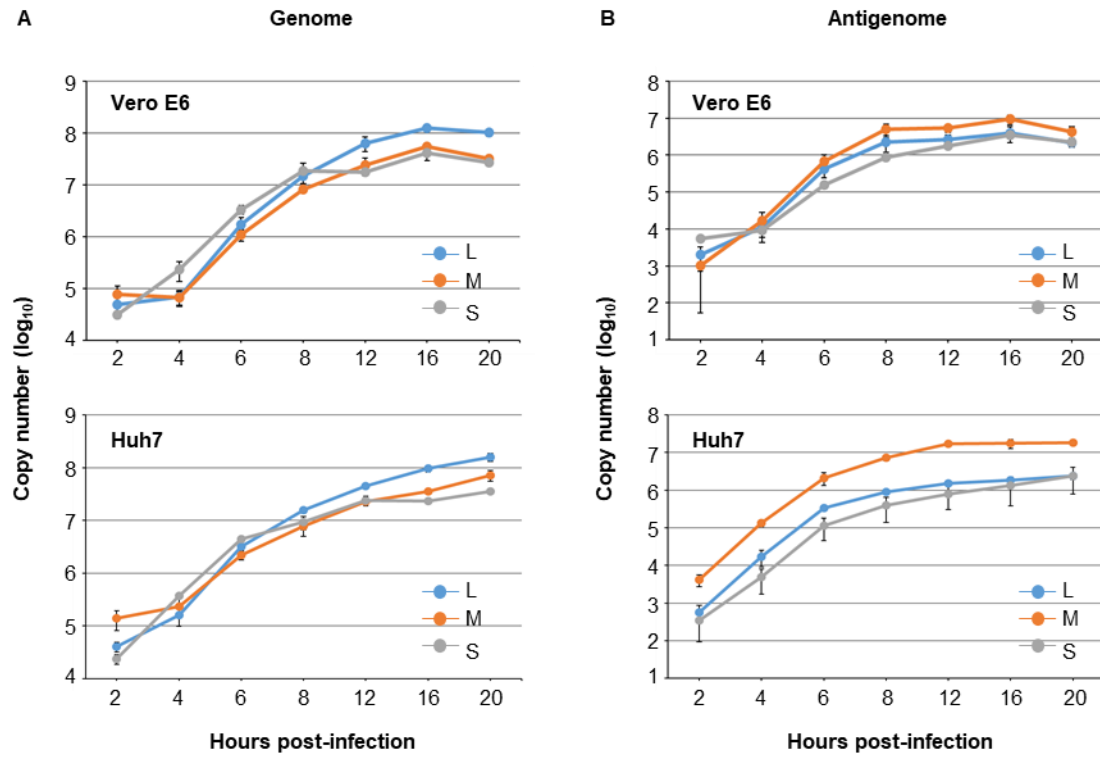


Figure 2.10: Comparison of accumulation kinetics of L, M and S segments in RVFV-infected cells

Alternate representation of the data shown in Fig.2.9 for the accumulation kinetics of a) all three genomic segments and b) all three antigenomic segments. Blue, red, and grey lines represent L segment, M segment and S segment, respectively (123).

Discussion

The present study reported the development of a RT-qPCR assay that determines the amounts of genomic and antigenomic L, M and S segments of RVFV; this assay represents the first system that can distinguish and measure the accumulation of all genomic and antigenomic viral RNA segments in any bunyaviruses. Several methods have been used to detect and quantify the different viral RNA species generated during RVFV infection, including radiolabeling, Northern blot, *in-situ* hybridization, and RT-qPCR assays (13, 29, 117, 119, 124-126, 142). Limitations of these studies include limited sensitivity, different probe efficiencies, and the inability to distinguish antigenomic RNA from mRNA and genomic RNA from antigenomic RNA. Multiple groups have reported the use of RT-qPCR approaches to quantitate RVFV RNA load, however these assays were not designed to specifically target individual replicative RNA species (124-126, 142). Additionally, these assays do not consider cDNA synthesized due to false priming.

The assay developed in this study incorporated the combined use of the tagged RT primer and the forward tag and the strand-specific reverse PCR primers, which eliminated amplification of cDNAs generated by false-priming (Fig. 2.7). This modified assay excluded amplification of viral mRNAs (Fig. 2.7B) and accurately measured between 10^3 to 10^{10} copies of the genomic and antigenomic L and M segments and between 10^4 to 10^{11} copies of the genomic and antigenomic S segments in samples (Figure 2.8). The assay was also able to accurately determine the amounts of target viral RNAs present in up to ~100-fold excess amounts of their opposite-strand RNAs (Table 2.6). Brennan et al., reported a similar RT-qPCR assay, where tagged RT primer and sets of forward tag and strand-specific reverse PCR primers were used to determine the amounts of the genomic and antigenomic RVFV M and S segments, however their assay did not include the measuring method for the genomic and antigenomic L segments (117). Our RT-qPCR assay design benefited from their study; we used the same tag sequence used in their tagged RT primers,

except that our tag sequence had an extra 'A' at the 3'-end, and used the same strand-specific reverse PCR primer for the genomic-sense S RNA. As the transcription termination signal for L mRNA is located very close to the 3'-end of the antigenomic L RNA (16, 17), it was necessary to determine an appropriate binding site of the tagged RT primer for cDNA synthesis of antigenomic L segment, but not for cDNA synthesis of L mRNA, within ~20 nt from the 3'-end of antigenomic L segment. After testing several tagged RT primer candidates, we were able to identify an appropriate tagged RT primer for antigenomic L segment.

Like other past studies that have reported self-primed reverse transcription in various viruses (127-136), our data suggested synthesis of cDNAs in the absence of an RT primer from *in-vitro* synthesized RVFV RNAs as well as intracellular RNAs obtained from RVFV-infected cells (Fig. 2.3). A possible mechanism for primer-independent cDNA synthesis in RVFV RNAs is self-primed RNA due to the existence of a thermostable secondary structure that serves as a primer during reverse transcription (Fig. 2.11A). Another possibility is random priming due to small cellular nucleic acids, such as tRNAs and microRNAs, in RVFV-infected cells. As the 5'- and 3'-ends of both genomic and antigenomic RVFV RNA segments have a stretch of short complementary sequences (7, 36, 61, 143), fragmented or degraded RNAs could possibly serve as primers during reverse transcription (Fig. 2.11B).

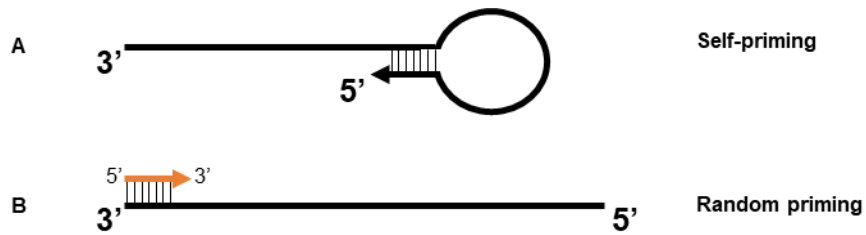


Figure 2.11: Possible mechanisms for primer-independent cDNA synthesis

(A) Self-priming RNA due to the existence of a thermostable secondary structure at the terminal end of the genomic or antigenomic RNA template that serves as a primer (indicated by black arrow) for the reverse transcriptase. (B) Random priming (indicated by orange arrow) by short cellular RNAs, such as tRNAs and microRNAs, or fragmented viral RNAs generated during RNA preparation.

By using our newly developed RT-qPCR assay, we examined the accumulation kinetics of replicating RVFV RNAs in Vero E6 and Huh7 cells (Fig. 2.9); the former is widely used for studies of RVFV replication and preparation of virus stocks (144) and the latter, a hepato-cellular carcinoma cell line (141), was selected because one of the major target organs of RVFV in mammals is the liver (145, 146). To our knowledge, this is the first study demonstrating the accumulation kinetics of replicating viral RNA species in bunyavirus-infected cells. We noted similar accumulation kinetics of viral RNAs in both cell lines. The amounts of the genomic RNA segments were always higher than corresponding antigenomic RNA segments throughout the infection, except that the amounts of genomic and antigenomic M segments were similar at 6-8 h p.i. in Vero cells and at 4-12 h p.i. in Huh7 cells. Our finding of similar levels of the genomic and antigenomic M segments in RVFV-infected cells are a marked contrast to accumulation of viral RNAs in cells infected with positive-stranded RNAs, where abundances of genomic RNAs always exceed antigenomic RNAs. Currently, it is unclear why only M segment showed similar accumulations of genomic and antigenomic RNAs at certain times p.i. Notably, the antigenomic segment ratios differed between Vero and Huh 7 cells, whereas in Huh 7 cells the replication kinetics of antigenomic M RNA was substantially higher than antigenomic L and S RNA throughout the entire course of infection.

In both cell lines, genomic S RNA, but not genomic L and M RNAs, rapidly accumulated from 2 to 4 h p.i. (Fig. 2.9 and Fig. 2.10). Antigenomic S RNA is packaged efficiently into RVFV particles, and we previously reported that the incoming antigenomic S RNA serves as template for the synthesis of NSs mRNA immediately following RVFV infection, leading to NSs expression early in infection (29). Expression of NSs immediately after infection would be critical for efficient virus replication in mammalian hosts, as the incoming RVFV RNPs trigger RIG-I-mediated antiviral innate immune signaling (100, 146, 147). Rapid accumulation of genomic S segment from 2 to 4 h p.i. suggest that the incoming antigenomic S segment also serves as the template for genomic S RNA

replication. This results in efficient genomic S RNA accumulation, which was higher than the accumulation of genomic L and M segments from 4-6 h p.i. (Fig. 2.10). Efficient accumulation of genomic S RNA, which serves as the template for N mRNA, during the early phase of infection may lead to efficient accumulation of N protein early in infection resulting in optimal virus replication.

In conclusion, our strand-specific RT-qPCR assay determined the amounts of genomic and antigenomic RVFV RNAs with accuracy and specificity, allowing us to determine the accumulation kinetics of these viral RNAs in infected cells. Overall, our assay system will be a valuable tool to examine the replication mechanisms of RVFV.

**CHAPTER 3: CHARACTERIZATION OF THE MOLECULAR INTERACTIONS
THAT GOVERN THE PACKAGING OF RIFT VALLEY FEVER PHLEBOVIRUS
RNA SEGMENTS INTO VIRUS PARTICLES**

Introduction

Bunyaviruses are enveloped RNA viruses that consist of segmented, negative/ambisense polarity, single-stranded RNA genome. Rift Valley Fever phlebovirus (RVFV), within the family *Phenuiviridae*, is one of the most widely studied bunyaviruses. RVFV carries a tripartite genome composed of L, M, and S RNA segments that are negative and ambisense polarity. The virion consists of two envelope glycoproteins, Gn and Gc, and the three viral RNA segments packaged in the form of ribonucleoprotein complexes (RNPs). These RNPs consist of the viral RNAs encapsidated by the nucleocapsid, N, protein and the RNA-dependent RNA polymerase, L, protein. The L segment encodes the L protein while the M RNA encodes a polyprotein precursor that is cleaved in the endoplasmic reticulum to generate the Gn/Gc proteins. Two non-structural accessory proteins, NSm and 78kDa, are also encoded in the M segment. The S segment utilizes an ambisense coding strategy, in which the N protein is encoded from N mRNA transcribed from the genomic S RNA and the non-structural protein, NSs, is encoded from the NSs mRNA transcribed from the antigenomic S RNA (7). The 3' and 5' terminal ends of each viral RNA segment contain non-coding regions (NCRs) that include important replication and transcription terminal signals (13, 16). They also contain incorporation signals that are required for the packaging of viral RNA segments into virus particles (14). RVFV replication and transcription, driven by N and L proteins, occur in the cytoplasm of infected cells while virus assembly and budding takes place at the Golgi apparatus (7, 36, 84-87, 148).

An infectious RVFV particle must contain at least one copy of each viral RNA segment. (12, 36, 47, 49, 52, 149). A cryo-electron microscopy study of RVFV particles has revealed that intra-virion space can incorporate additional RNA segments (12, 37). Furthermore, the flexibility of RVFV packaging with the production of a four segmented virus has been demonstrated (116). Past studies have observed that along with the three genomic RNA segments, RVFV also packages all three complementary antigenomic RNAs (29). The 5' and 3' terminal ends of the viral RNA segments are complementary to each other forming a panhandle structure (7). RVFV RNPs are strong activators of the RIG-I-mediated antiviral innate immune response due to the presence of these 5'-triphosphorylated dsRNA panhandle formations (94). To overcome the RIG-I mediated antiviral innate immune signaling, the virus needs to express the virulence factor NSs immediately after infection. NSs is a type I interferon (IFN) antagonist that inhibits host transcription and suppresses interferon- β gene expression. It has also been shown to induce protein kinase R (PKR) degradation, which facilitates viral mRNA translation (95, 98, 100, 101, 103-108). We have previously shown that NSs mRNA is transcribed from incoming antigenomic S segment, leading to the synthesis of NSs protein early in infection (29).

The mechanisms that govern the packaging of RVFV RNA segments are poorly understood. The main determinants of RVFV assembly are the glycoproteins, Gn/Gc, which have been shown to produce virus-like particles (VLPs) in the absence of other viral proteins (36, 53). A characteristic of bunyaviruses is the lack of a matrix protein, and it has been suggested that the cytoplasmic tail of Gn functions as a matrix protein surrogate through its interaction with the viral RNPs (10, 12, 47, 49, 52, 53). It has been hypothesized that this interaction drives the packaging of viral RNAs into bunyaviruses. However, demonstration of Gn interaction with viral RNPs has not been biochemically demonstrated in bunyavirus-infected cells. An insight into the mechanisms driving RNA packaging is valuable for understanding virus replication, evolution, and genetic reassortment in bunyaviruses.

In this study, we investigated the mechanism of viral RNA packaging into RVFV particles. We determined the packaging abilities of RVFV RNAs into virus particles and found that the packaging ability of antigenomic S RNA, compared to antigenomic L and M RNAs, was significantly higher, suggesting a preferential incorporation of antigenomic S RNA into virus particles among the antigenomic segments. We also characterized the interactions of Gn with viral RNPs in RVFV-infected cells for the first time. Our study revealed that Gn can directly interact with all viral RNAs and that this interaction correlates with the packaging abilities of viral RNAs to be packaged inside RVFV particles.

Materials and methods

CELL CULTURE

Vero E6 cells were cultured in Dulbecco's modified eagle medium (DMEM), supplemented with 5% fetal bovine serum (FBS) and 1% penicillin-streptomycin. Huh7 cells (141) were cultured in DMEM supplemented with 10% FBS and 1% kanamycin. BSRT7-5 cells, stably expressing T7 RNA polymerase (150), were cultured in Glasgow minimum essential medium supplemented with 10% FBS, 10% TPB, 1X MEM amino acid solution, and 1X geneticin.

VIRUS INFECTION

The recombinant RVFV MP-12, MP-12-V5-L, and MP-12-rLuc viruses were generated by a previously established reverse genetics system (144). MP-12-rLuc was generated with the *Renilla* luciferase (rLuc) ORF in place of the NSs ORF in the S segment (144). The MP-12-V5-L virus has a V5 tag inserted between amino acid position 1852 and 1853 of the L polymerase (151). Rescued viruses were amplified once in VeroE6 cells, titrated by plaque assay, and used for virus infections. For virus infection, cells (10-cm dish) were inoculated at a MOI of 3. After virus absorption at 37°C for 1 h, cells were

washed three times with phosphate buffered saline (PBS) and fresh medium was added. Cell lysates and virus supernatant were harvested either 8- or 16-hours post-infection.

VIRUS AND VLP PURIFICATION

Supernatant harvested from plasmid-transfected cells or virus-infected cells were clarified by centrifugation at 3,000 rpm for 15 minutes. The clarified supernatant was then layered on top of a discontinuous sucrose gradient consisting of 20, 30, 50, and 60% sucrose (wt/vol) and centrifuged for 3 hours at 26,000 rpm at 4°C using a Beckman SW28 rotor. The interface between 30 and 50% sucrose was collected with a fractionator, diluted with 4 volumes of NTE buffer (0.1M NaCl, 10mM, Tris-HCl pH 7.5, 1mM EDTA) and subjected to a second discontinuous sucrose gradient centrifugation consisting of 20, 30, 50, and 60% sucrose for 18 hours at 26,000 rpm at 4°C. The particles at the interface of 30 and 50% sucrose were collected and pelleted down through a 20% cushion at 38,000 rpm for 2 hours at 4°C using a Beckman SW41 rotor (114). The pellets were suspended in 1ml Trizol reagent for RNA analysis.

CO-IMMUNOPRECIPITATION ASSAY

Cytoplasmic cell lysates were prepared at 16 h post-infection with a mild lysis buffer (50mM Tris-HCl pH 7.5, 5mM MgCl₂, 100mM KCl, 1% Triton-X-100) containing 1X protease-phosphatase inhibitor cocktail (Cell-Signaling) and RNase inhibitor (New England Biolabs). MP-12-infected and MP-12-V5-L-infected lysates were pre-cleared using protein G dynabeads (Invitrogen) conjugated with non-RVFPV mouse antibody H2K^{KD} (H2K) for 15 minutes at 4°C with rotation. Protein G dynabeads were conjugated by incubating with specific antibodies in PBS-0.02% Tween-20 for 30 minutes at 4°C with rotation. Intracellular MP-12-specific proteins and RNA were immunoprecipitated using protein G dynabeads conjugated with either mouse monoclonal anti-Gn antibody (R1-4D4), rabbit GST-N peptide antibody (R1-GST-N), and a non-RVFPV mouse antibody H2K

for 3 hours at 4°C with rotation. For protein analysis, immunoprecipitated lysates were washed 3X with mild lysis buffer and incubated with 2X Laemmli SDS sample buffer for 5 minutes at 100°C. For RNA analysis, immunoprecipitated lysates were washed 3X with mild lysis buffer and incubated with proteinase K (0.5mg/ml) in proteinase K buffer (0.2M Tris-HCl, pH 7.5, 25mM EDTA, 0.3M NaCl, 2% w/v SDS) for 30 minutes at 37°C. After proteinase K digestion, viral RNA was extracted using phenol-chloroform/ethanol precipitation and resuspended in 16 µl of sterile DNase/RNase free H₂O. MP-12-V5-L-infected lysates were subjected to immunoprecipitation using magnetic beads conjugated with mouse anti-V5 monoclonal IgG antibody (MBL). For protein analysis, immunoprecipitated lysates were washed 3X with mild lysis buffer as well as two additional washes with TBS-0.1% Tween-20 and incubated with 2X Laemmli SDS sample buffer for 5 minutes at 100°C.

WESTERN BLOT

Intracellular and immunoprecipitated MP-12-specific proteins were run on a 4-20% SDS-polyacrylamide gel and transferred to a PVDF membrane (BioRad). For Gn and N protein detection, the following antibodies were used: mouse monoclonal anti-Gn (R1-4D4) at a dilution of 1:1000, mouse monoclonal anti-N (R1-P2E7) antibody at a dilution of 1:500, conformation specific rat monoclonal anti-mouse IgG HRP-linked antibody (Abcam) at a dilution of 1:5000, and a goat anti-mouse IgG HRP-linked antibody (Cell-signaling) at a dilution of 1:5000. For V5 tagged-L protein detection, IC and IPed MP-12-V5-L specific proteins were run on a 7.5% SDS-polyacrylamide gel and transferred to a PVDF membrane. A rabbit monoclonal anti-V5 antibody (Cell-signaling) was used at a dilution of 1:1000 followed by an incubation with goat anti-rabbit IgG HRP-linked antibody (Cell-signaling) at a dilution of 1:5000. ECL 2 western blotting HRP substrate (Thermo-Scientific Pierce) was used for film-based imaging. Membrane images are scanned, cropped, and assembled by AlphaEase FC Software.

NORTHERN BLOT

For RNA analysis, intracellular lysates were harvested in Trizol reagent (Invitrogen), followed by RNA extraction following manufacturer's specifications. Immunoprecipitated RNA was extracted as stated earlier. 0.5µg of intracellular RNA and 3µl of immunoprecipitated RNAs were denatured and separated on a 1% agarose gel containing formaldehyde. After electrophoresis, Northern blot analysis was performed as previously described with digoxigenin-labeled probes specific to genomic L, M, and S viral RNAs (29). The viral RNAs were visualized with the DIG luminescent detection kit (Roche Applied Science) and imaged using AlphaEase FC Software.

REVERSE TRANSCRIPTION

Reverse transcription of viral RNAs using a strand-specific assay was previously described (123). Briefly, cDNA synthesis of viral RNAs was performed by using the Superscript-III first strand synthesis system (Invitrogen). Viral RNA was mixed with 2 µM of strand-specific RT primer. The mixture was incubated at 65°C for 5 min and then cooled to 4°C. After addition of the reaction buffer and enzyme mixture, cDNA synthesis was carried out by incubating the sample at 50°C for 55 min, terminated by heating at 85°C for 5 min, cooled to 4°C, and then treated with RNase H at 37°C for 20 min. The cDNAs were purified using an on-column PCR purification kit (Qiagen).

STANDARD PCR

Standard PCRs were performed by using AccuPrime *Pfx* DNA polymerase (Invitrogen). 3 µl of cDNA was added to the PCR master mix containing the non-viral tagged sequence as a forward primer and a viral strand-specific PCR reverse primer. Thermocycling conditions were as follows: 95°C for 2 mins, 35 cycles of 95°C for 15 sec, 55°C for 30 sec and an extension at 68°C for 30 secs. PCR products were analyzed by gel

electrophoresis. Gel Images are scanned, cropped, and assembled by AlphaEase FC Software.

QUANTITATIVE PCR

The strand-specific real time qPCR assays were conducted using SsoAdvanced™ Universal SYBR® Green Supermix (BioRad) and followed the established protocol previously described (123). Total RNAs from virus-infected cells were subjected to RT using tagged strand-specific RT primers as stated before. After cDNA purification, 3 µl of cDNA was added to the PCR master mix containing the non-viral tagged sequence as a forward primer and a viral strand-specific PCR reverse primer. Thermocycling conditions were as follows: 95°C for 30 sec, 35 cycles of 95°C for 15 sec and 60°C for 20 sec followed by melting curve analysis. The assays were performed by the CFX96 Touch Real-time PCR detection system and analyzed using the provided software (BioRad CFX Manager 3.1).

VLP RNA PACKAGING ASSAY

Plasmids used for this assay were previously described (144). To collect the 1st set of VLPs, BSRT7/5 cells were transfected with protein expression plasmids, pCAGGS-G, pT7-IRES-vL, and pT7-IRES-vN, as well as an RNA expression plasmid expressing either S or M antigenomic RNA using *Transit* LT1 reagent (Mirus). After 2 days post-transfection, the supernatant was harvested from the plasmid-transfected cells and clarified by centrifugation at 3,000rpm for 15 mins at 4°C. BSRT7/5 cells, co-expressing L, N, and Gn/Gc proteins, were then inoculated with the 1st set of VLPs containing either S or M RNA. After 2 days post-inoculation, supernatant containing the 2nd set of VLPs was collected and purified by sucrose gradient ultracentrifugation. The total intracellular RNAs were collected by adding 1ml of Trizol directly to the plate. After VLP purification, 1ml of Trizol was added to the virus pellet for extraction of VLP-associated RNAs using the

manufacturer's instructions. Total RNA and VLP-associated RNA were then subjected to DNase treatment and RNA purification using RNeasy mini protocol for RNA cleanup and On-column DNase digestion (Qiagen). The on-column DNase treatment was extended to 30 mins at room temperature. The concentrations of intracellular RNAs were determined using spectrophotometry and adjusted to 100ng/μl for cDNA synthesis.

UV LIGHT CROSS-LINKING IMMUNOPRECIPITATION (CLIP)

The reagents and protocol of Conrad et al., (152) was followed with some modifications. Briefly, MP-12-infected or MP-12-V5-L-infected cells were irradiated with UV light at 254nm wavelength with 250 mJ/cm². The cells were then lysed with 140μl of SDS lysis buffer (0.5% SDS, 50mM Tris-HCl pH 6.8, 1mM EDTA, 1mM DTT, 2.5mg/ml Torula yeast tRNA, 10mM VRC), containing 1X protease-phosphatase inhibitor cocktail and RNase inhibitor, and heated to 65°C for 5 minutes. RIPA correction buffer (1.25% NP40, 0.625% sodium deoxycholate, 62.5mM Tris-HCl pH 8.0, 2.25mM EDTA, 187.5mM NaCl, 2.5mg/ml Torula yeast tRNA, 10mM VRC) was added to the lysates for a total volume of 700μl. To reduce viscosity, samples were passed through a QIAshredder spin column (Qiagen) twice. Intracellular MP-12 and MP-12-V5-L specific proteins were immunoprecipitated using protein G dynabeads conjugated with either mouse monoclonal anti-Gn antibody (R1-4D4) or rabbit GST-N peptide antibody (R1-GST-N). Lysates were incubated with conjugated magnetic beads overnight at 4°C and subsequently washed 5X with high salt RIPA buffer (1% NP40, 0.5% sodium deoxycholate, 0.1% SDS, 500mM NaCl, 50mM Tris-HCl pH 8.0, 2mM EDTA). After washing, beads were resuspended in 200μl high salt RIPA buffer where 20μl of the sample was removed and put aside for protein analysis. Samples used for protein analysis were suspended in 2X Laemmli SDS lysis buffer and incubated at 100°C for 5 minutes. The remaining sample was used for RNA analysis and was resuspended in proteinase K solution (0.5mg/ml Proteinase K, 0.5% SDS, 20mM Tris-HCl pH 7.5, 5mM EDTA, 0.1mg/ml Torula yeast tRNA) and incubated

at 37° for 2 hours. After proteinase K digestion, 3M NaOAc (pH 5.2) was added to the samples followed by phenol chloroform/ethanol precipitation RNA extraction. RNA pellets were resuspended in 13µl of sterile DNase/RNase free H₂O.

PROTEIN DOT BLOT

Intracellular and UV-crosslinked immunoprecipitated protein lysates were added directly to a nitrocellulose membrane. The membrane was dried for 30 minutes at room temperature. After drying, non-specific sites were blocked by using 5% dry milk in TBS-0.1% Tween-20 for 1 hour at room temperature. The same primary and secondary antibodies for Gn, N, and V5-L protein western blot detection were used for the protein dot blot analysis. After antibody incubations, the membrane was washed 4X with TBS-0.1% Tween-20. ECL 2 western blotting HRP substrate (Thermo-Scientific Pierce) was used for film-based imaging. Membrane images are scanned, cropped, and assembled by AlphaEase FC Software.

Results

ANTIGENOMIC S RNA IS EFFICIENTLY INCORPORATED INTO PURIFIED RVFV-VIRIONS

We previously reported that antigenomic S RNA was efficiently packaged into RVFV purified virions relative to antigenomic L and M RNA segments (29). Using our previously established strand-specific RT-qPCR assay (123), we conducted a quantitative analysis that determined a packaging profile of the viral RNAs by using RVFV live-attenuated vaccine strain, MP-12. We first examined the packaging abilities of viral RNAs during early and late infection. We infected Vero E6 with MP-12 at an MOI of 3 and collected the intracellular lysate as well as the culture supernatant at 8-hour and 16-hour post infection. Using our strand-specific RT-qPCR assay, we determined the levels of genomic and antigenomic RNAs in infected cells and purified virus particles. We

calculated the packaging abilities of the viral RNA segments as the ratio of RNA copy number in purified virus to that in infected cells. At both time points, the packaging abilities among the genomic RNA segments were similar, indicating no preferential packaging among genomic RNAs. In contrast, the packaging ability of antigenomic S RNA was significantly higher than that of antigenomic L and M RNAs at both 8 h and 16 h post infection, suggesting a preferential packaging of antigenomic S RNA into virions (Fig. 3.1A and B). We also calculated the packaging abilities of viral RNAs at 8 h post infection in Huh 7 cells, a type I IFN competent cell line. The packaging profile remained the same, in which antigenomic S RNA was incorporated more efficiently among the antigenomic viral RNAs (Fig. 3.1C).

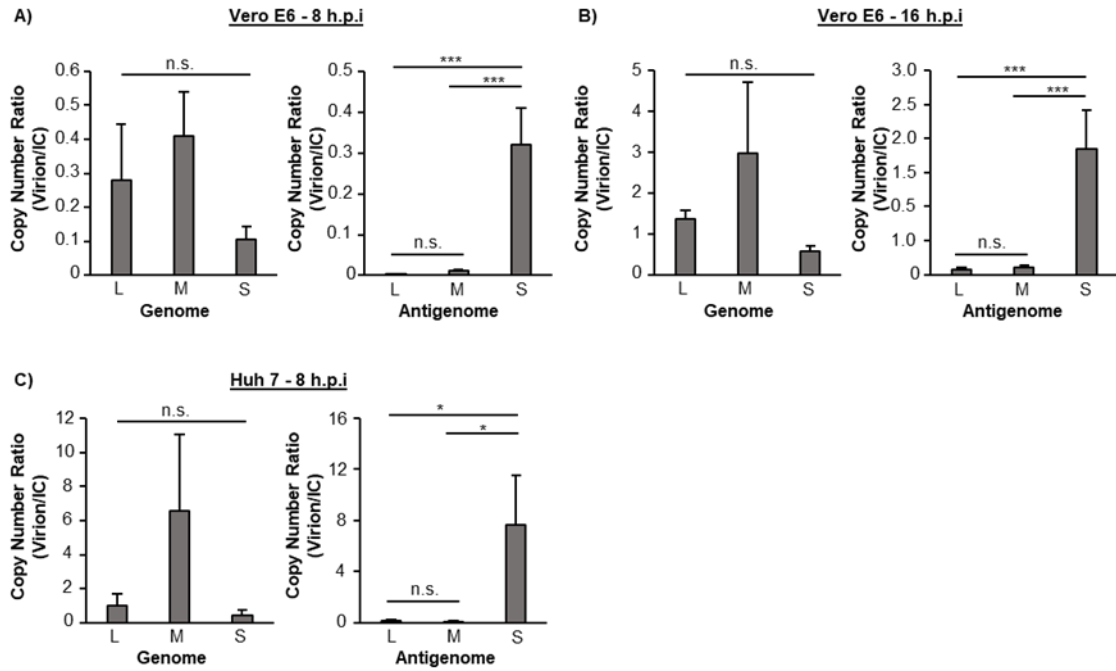


Figure 3.1: Quantitative analysis of RVFV RNA segments packaged inside purified virus.

Packaging abilities of viral RNAs from MP-12-infected cells. (A and B) Vero E6 cells and (C) Huh 7 cells were infected with MP-12 at an MOI of 3. Intracellular (IC) lysates and culture supernatant were collected at 8 hours post-infection (h.p.i). (b) IC lysates and culture supernatant were also collected from VeroE6 cells at 16 h.p.i Culture supernatant was purified by sucrose gradient ultracentrifugation. RNA from infected cell lysate and purified virus were extracted. Copy numbers of genomic and antigenomic L, M, and S RNAs were determined by RT-qPCR assay. RNA packaging ability was calculated as the ratio of the copy number of viral RNA inside purified virions to the copy number of intracellular viral RNA in infected cells (Virion/IC). Data represent the mean of biological triplicate experiments and error bars indicate the standard deviation. Statistical analysis was done using a one-way ANOVA with Tukey's multiple comparison post-test. N.S., not significant. * $P < 0.05$, ** $P < 0.01$, *** $P < 0.001$

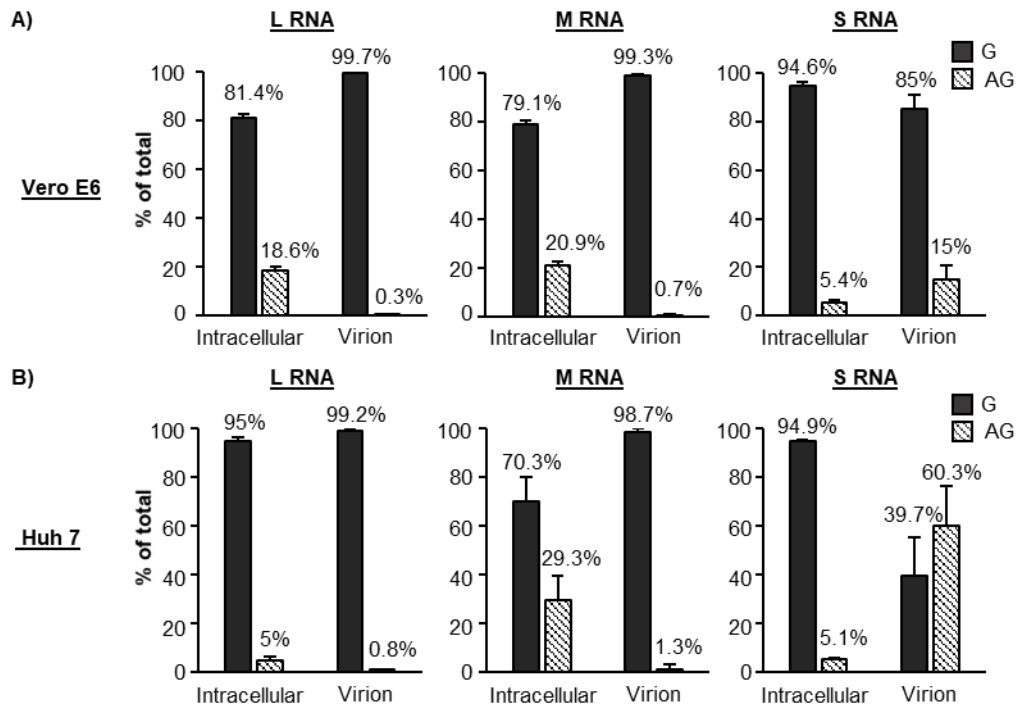


Figure 3.2: Alternative representation of RVFV RNA packaged inside virions.

(A) Vero E6 cells and (B) Huh 7 cells were infected with MP-12 at an MOI of 3. Intracellular (IC) lysates and culture supernatant were collected at 8 hours post-infection (h.p.i). Culture supernatant was purified by sucrose gradient ultracentrifugation. RNA from infected cell lysate (Intracellular) and purified virus (Virion) were extracted. Copy numbers of genomic (G) and antigenomic (AG) L, M, and S RNAs were determined by RT-qPCR assay. The proportion of genomic and antigenomic RNAs in virus-infected cells and in purified virions is represented as a percentage of the total viral RNA. Data represent the mean of biological triplicate experiments and error bars indicate the standard deviation.

Fig. 3.2 shows an alternative representation of the mean ratio of genomic to antigenomic RNAs in infected cells and purified virus for both Vero and Huh 7 cells. The total percentage of genomic RNA for all three viral segments was substantially higher than antigenomic RNA in infected cells and purified virus in Vero cells (Fig. 3.2A). There was a trend that the antigenomic L and M RNAs, relative to antigenomic S RNA, were inefficiently packaged into virus particles in both cells, whereas the proportional packaging of antigenomic S RNA in virions was higher compared to that of antigenomic L and M RNAs in both cells. Strikingly, we observed a more prominent packaging of antigenomic S RNA inside virions produced from infected Huh 7 cells than in Vero cells (Fig 3.2B). This data showed that antigenomic S RNA underwent efficient packaging in both cell lines.

As the antigenomic S RNA serves as the template for the transcription of NSs mRNA, we tested if the presence of the NSs ORF was important for the efficient packaging of antigenomic S RNA into RVFV-particles. To this end, we determined the packaging ability of viral RNAs in MP-12-rLuc virus, whose S segment contains the *Renilla* (rLuc) ORF in place of the NSs ORF, in VeroE6 cells. Although MP-12 and MP-12-rLuc produced similar levels of infectious viruses in Vero cells (144), western blot analysis showed that MP-12-rLuc produced higher levels of virus particles than MP-12 (Fig 3.3A). Among the three genomic RNA segments, the packaging ability of genomic M RNA was significantly higher than L and S genomic RNAs. However, the packaging abilities among the antigenomic RNA segments remained consistent to MP-12, wherein relative to antigenomic L and M RNA, the packaging ability of antigenomic S was significantly higher (Fig 3.3B). These data suggest that the efficient packaging of antigenomic S RNA does not require the presence of the NSs ORF or protein. Taken together, these data demonstrated an efficient incorporation of antigenomic S RNA into virions and suggest a differential packaging ability among the antigenomic RNA segments.

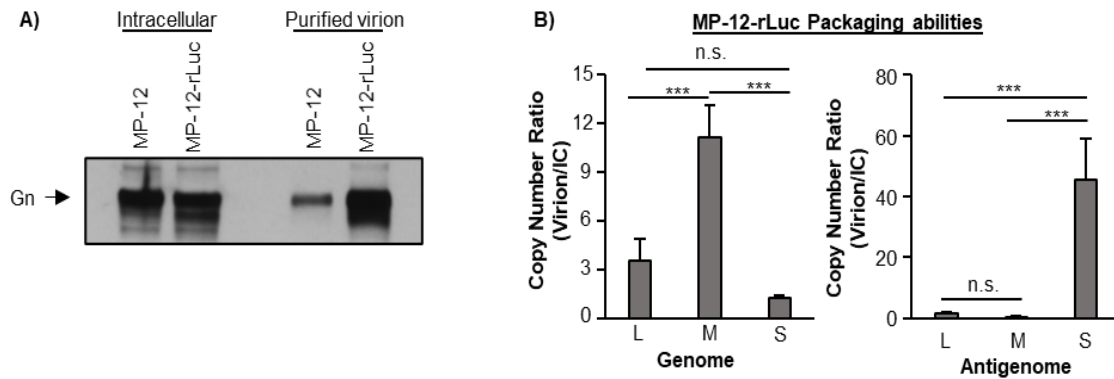


Figure 3.3: Packaging abilities of viral RNAs in MP-12-rLuc virus.

Vero E6 cells were infected with MP-12 and MP-12-rLuc at an MOI of 3. Intracellular (IC) lysates and culture supernatant were collected at 16 hours post-infection (h.p.i). Culture supernatant was purified by sucrose gradient ultracentrifugation. (A) Particle production from MP-12 vs MP-12-rLuc-infected cells. Protein from infected cells and purified virus were subjected to western blot analysis using anti-Gn antibody. The levels of Gn protein (indicated by black arrow) are shown in each lane in the intracellular and purified virus samples. (B) Quantitative analysis of packaged viral RNA from MP-12-rLuc-infected cells. RNA from infected cell lysate (IC) and purified virus were extracted. Copy numbers of genomic and antigenomic L, M, and S RNAs were determined by RT-qPCR assay. RNA packaging ability was calculated as the ratio of the copy number of viral RNA inside purified virions to the copy number of intracellular viral RNA in infected cells (Virion/IC). Data represent the mean of biological triplicate experiments and error bars indicate the standard deviation. Statistical analysis was done using a one-way ANOVA with Tukey's multiple comparison post-test. N.S., not significant. * $P < 0.05$, ** $P < 0.01$, *** $P < 0.001$

PACKAGING PROFILES OF S AND M RNAs IN VLPs

We addressed the possibility that the relatively smaller size of antigenomic S RNA, compared to antigenomic L and M RNAs, allows it to be passively packaged more efficiently into infectious RVFV particles, carrying the three genomic RNA segments. To this end, we established a single-segment RNA packaging assay to analyze the packaging abilities of S and M RNAs, when expressed individually in the absence of any other viral RNA segment, into VLPs (Fig. 3.4A). Previously, we have reported that S genomic RNA and M genomic RNA are efficiently packaged into VLPs, which are produced from cells expressing Gn/Gc, N and L proteins along with replicating S RNA and M RNA, respectively (14). Accordingly, we prepared two types of VLPs, one carrying S RNA and another carrying M RNA, and inoculated each of these VLPs into BSRT7/5 cells, co-expressing L, N, and Gn/Gc proteins (Fig. 3.4A). The replication and transcription of incoming S or M RNA, driven by L and N proteins, and the expression of Gn/Gc proteins in the VLP-inoculated cells resulted in the production of the 2nd set of VLPs, carrying S or M RNAs, respectively (Fig. 3.4A).

We determined the copy numbers of genomic and antigenomic S and M RNAs in the VLP-inoculated cells and in purified VLPs (2nd set), produced from these cells, by using strand-specific RT-qPCR assay. We calculated the proportion of genomic and antigenomic S and M RNAs in VLP-inoculated cells and in purified VLPs to evaluate the packaging profiles of S and M RNAs in VLPs. The profiles of intracellular accumulation and packaging of genomic and antigenomic S and M RNAs into VLPs were similar to that observed in RVFV-infected cells, wherein, a higher level of antigenomic S RNA was packaged into VLPs that did not correlate with its relative abundance in VLP-inoculated cells (Fig. 3.4B). The packaging profile of genomic and antigenomic M RNA in VLPs reflected its relative abundance in VLP-inoculated cells (Fig. 3.4B). These data showed that antigenomic S RNA is preferentially packaged into VLPs, which recapitulated the

observed phenomenon of efficient antigenomic S RNA packaging in MP-12-infected cells, suggesting the presence of an active mechanism for the selection and recognition of antigenomic S RNA that facilitates its efficient incorporation into virus particles.

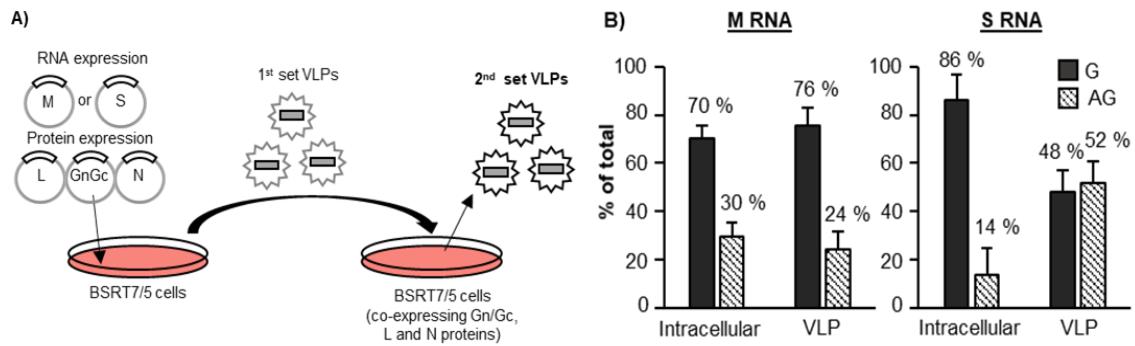


Figure 3.4: Single-segment RNA packaging assay.

A) Schematic of the RNA packaging assay. BSRT7/5 cells, stably expressing T7 polymerase, were transfected with plasmids expressing L, N, and Gn/Gc proteins, along with a plasmid expressing M or S RNA. At 2 days post-transfection, VLPs produced from transfected cells were collected and inoculated into BSRT7/5 cells, co-expressing Gn/Gc, L, and N proteins. The replication and transcription of incoming S or M RNA, along with the expression of Gn/Gc proteins in the VLP-inoculated cells resulted in the production of the 2nd set of VLPs carrying S or M RNA, respectively. At 2 days post-inoculation, the 2nd set of VLPs were collected and purified by sucrose gradient ultracentrifugation. B) Quantitative analysis of S and M RNA accumulation in VLP-inoculated cells and in purified VLPs. RNA from VLP-inoculated cells (intracellular) and purified VLPs (VLP) were extracted and the copy numbers of genomic (G) and antigenomic (AG) S and M RNAs were determined by RT-qPCR assay. The proportion of genomic and antigenomic S and M RNAs in VLP-inoculated cells and in purified VLPs is represented as a percentage of the total. Data represent the mean of biological triplicate experiments and error bars indicate the standard deviation.

DEMONSTRATION OF THE INTERACTION OF GN WITH VIRAL RNPs IN RVFV-INFECTED CELLS

We next delineated the factor(s) governing the differential packaging abilities among the antigenomic RNAs. It has been suggested that the interaction of the cytoplasmic tail of Gn with viral RNPs is important for viral RNA packaging in bunyaviruses (10, 12, 36, 37, 47, 49, 52, 53, 122, 149). However, this interaction has not been biochemically demonstrated in infected cells. Therefore, we first characterized the molecular interactions between Gn and viral RNPs in infected cells by a co-immunoprecipitation (Co-IP) assay. To examine the interaction of Gn with N protein, Vero E6 cells were infected with MP-12 at an MOI of 3 and intracellular lysates were collected at 16 hours post infection using a mild, containing a non-ionic detergent, lysis buffer. The lysates underwent immunoprecipitation using antibodies against Gn and N proteins. The anti-Gn antibody, but not the non-specific antibody H2K^KD^K, efficiently co-immunoprecipitated N protein (Fig. 3.5A) and the three genomic RNAs (Fig. 3.5C). The anti-N antibody co-immunoprecipitated Gn protein, confirming this interaction in infected cells (Fig. 3.5A). Consistent with a notion that N and viral genomic RNAs form viral RNPs, the anti-N antibody also co-immunoprecipitated the three viral genomic RNAs (Fig. 3.5C). We also tested whether L protein interacts with Gn in infected cells. Due to the lack of a suitable antibody for co-IP analysis of L protein, we used a recombinant MP-12 mutant containing a V5-epitope tag within the L protein, MP-12-V5-L (153). We performed the co-IP analysis of intracellular lysates, from MP-12-V5-L infected Vero E6 cells at 16 h p.i. using anti-Gn and anti-V5 antibodies. The Gn antibody efficiently pull down V5-tagged L protein. A reciprocal co-IP analysis showed the co-immunoprecipitation of Gn protein by anti-V5 (Fig 3.5B). Taken together, these data demonstrate the interaction of Gn with each component of the viral RNPs, including viral RNAs, N protein and L protein, for the first time in bunyavirus-infected cells.

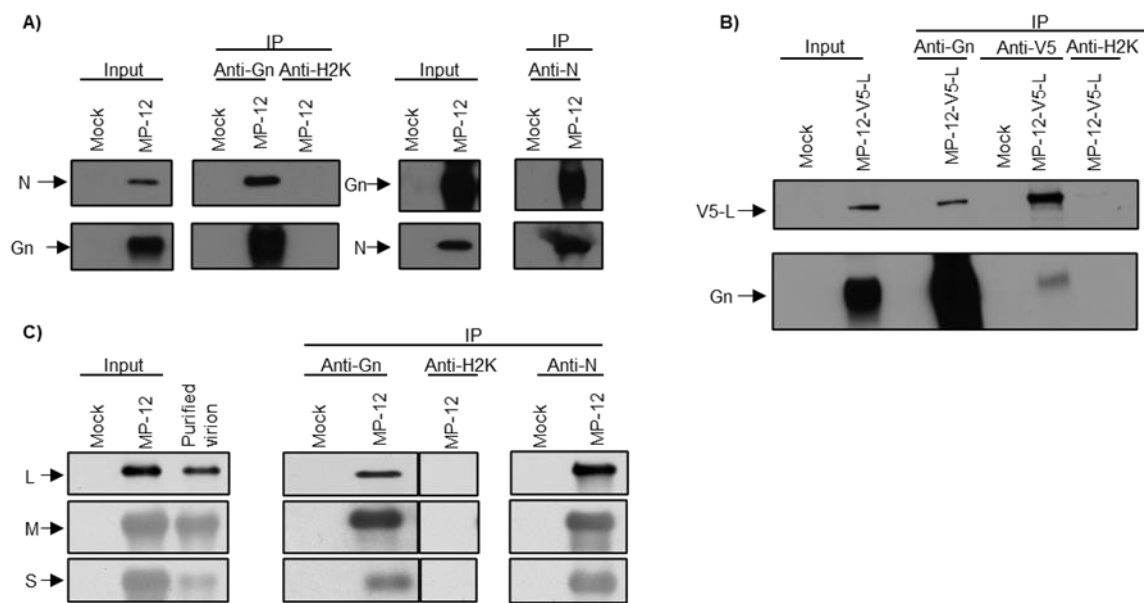


Figure 3.5: Gn-RNP interaction in RVFV-infected cells.

Protein analysis of Gn-RNP interactions. Vero E6 cells were infected at an MOI-3 with (A) MP-12 and (B) MP-12-V5-L viruses or mock infection. Cell extracts were collected 16 h post-infection. (A) Cell extracts were subjected to co-immunoprecipitation (IP) using anti-Gn antibody (Left panel), anti-N antibody (Right panel), and a non-specific antibody H2K^KD^K (H2K). Intracellular (Input) and IP protein samples were subjected to western blot analysis using anti-Gn and anti-N antibodies. The levels of Gn and N proteins (indicated by black arrows) are shown in each lane in the input and IP samples. B) Cell extracts, infected with MP-12-V5-L virus, were subjected to IP using anti-Gn, anti-V5, and H2K antibodies. Input and IP protein samples were subjected to western blot analysis using anti-Gn and anti-V5 antibodies. The levels of Gn and V5-tagged L protein (indicated by black arrows) are shown in each lane in the input and IP samples. (C) RNA analysis of Gn-RNP interaction. Vero E6 cells were infected at an MOI-3 with MP-12 or mock infection and intracellular and supernatant were collected 16 h post-infection. Culture supernatant was purified by sucrose gradient ultracentrifugation. Cell extracts were subjected to IP using anti-Gn, anti-N and H2K antibodies. RNA was extracted from intracellular lysates, purified virus, and IP samples and subjected to northern blot analysis. The RNAs were detected using digoxigenin-

labeled RNA probes that specifically hybridized with genomic viral RNAs. The levels of L, M, and S segment (indicated by black arrows) are shown in each lane in the input, purified virion, and IP samples.

GN DIRECTLY INTERACTS WITH VIRAL RNAs IN INFECTED CELLS

In CCHFV and hantavirus, a direct interaction between the Gn cytoplasmic tail and viral RNAs was shown in an *in-vitro* assay (57, 122). For RVFV, it was suggested that Gn could possibly interact with viral RNAs as well (53), however a direct Gn and viral RNA interaction has not been shown in bunyavirus-infected cells. In order to determine whether Gn interacts directly with viral RNAs, we utilized a UV-crosslinking and immunoprecipitation (CLIP) method (152). VeroE6 cells infected with MP-12 or MP-12-V5-L were irradiated with UV light to covalently crosslink RNA to protein at zero-length. Cell extracts were then prepared in a high stringency lysis buffer, containing an ionic detergent, and subjected to co-IP analysis using anti-Gn and anti-N antibodies. The stringent buffer conditions did not affect the IP efficiency of Gn but disrupted any interactions of Gn with either N or L protein, thereby eliminating any indirect pull down of viral RNA through N and L protein (Fig 3.6A and B). Notably, RT-PCR analysis revealed that the anti-Gn antibody co-immunoprecipitated all viral RNAs in UV-irradiated samples but not in the non-irradiated samples. We noted that the interaction between viral RNAs to N protein was retained in both UV-irradiated and non-irradiated samples, demonstrating that N-viral RNA interaction was resistant to the stringent buffer conditions (Fig. 3.6C). This UV-induced crosslinking of Gn with the viral RNAs is the first experimental evidence of a direct interaction between Gn and viral RNA in bunyavirus-infected cells.

To evaluate the relationship between the direct Gn-viral RNA interaction and RNA packaging ability, we conducted the UV-CLIP assay in Huh 7 cells and performed a quantitative analysis on the binding ability of Gn to viral RNAs. We calculated the binding ability of Gn as the ratio of RNA copy number, pulled down by Gn, to that of intracellular RNA in UV-irradiated cells (Fig. 3.7). Gn exhibited a similar ability to directly interact with genomic RNAs, suggesting no preference for direct Gn-viral RNA binding among the

genomic RNA segments. Strikingly, relative to antigenomic L and M RNA, Gn exhibited a significantly higher ability to directly interact with antigenomic S RNA, suggesting a preference for Gn to bind to the antigenomic S segment. Altogether, our data demonstrated a positive correlation between the ability of Gn to directly interact with viral RNA and the packaging ability of RNA into RVFV-particles.

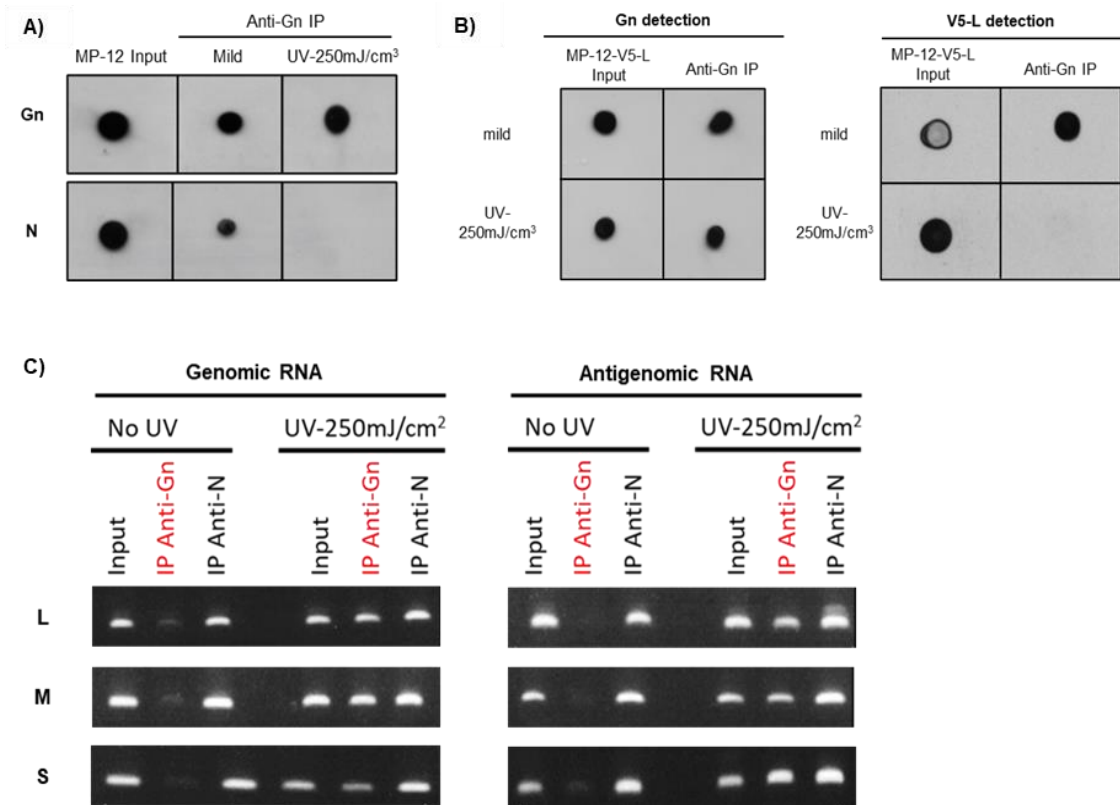


Figure 3.6: Direct interaction of Gn with viral RNAs in RVFV-infected cells.

(A and B) Disruption of protein-protein interactions in Ultraviolet (UV)-irradiated samples. Vero E6 cells were infected with (A) MP-12 or (B) MP-12-V5-L viruses at an MOI-3. Cell extracts were collected 16 hours post-infection (h.p.i) using a mild lysis buffer, as previously used in Fig. 3.5, or cells were irradiated with 250mJ/cm² UV light and extracts were collected using a high stringent lysis buffer. Cell extracts were subjected to co-immunoprecipitation (IP) using anti-Gn antibody. Intracellular (input) and IP protein samples were subjected to protein dot-blot analysis using anti-Gn, anti-N, and anti-V5 antibodies. (A) The levels of Gn and N proteins are shown in each box in the input and IP samples. (B) The levels of Gn (left square) and V5-tagged L protein (right square) are shown in each box in the input and IP samples. (c) RNA analysis in UV-irradiated samples. Vero E6 cells were infected with MP-12 at an MOI-3. Cells were irradiated with 250mJ/cm² UV light and extracts were collected using a high stringent lysis buffer. Non-irradiated cells were used as a negative control. Cells extracts were subjected to IP using anti-Gn and anti-N antibody. Anti-

N was used as a positive control. RNA was extracted from intracellular lysates (input) and IP samples from both non-irradiated and UV-irradiated cells and subjected to RT-PCR. Genomic RNA (left panel) and antigenomic RNA (right panel) PCR products were analyzed by agarose gel electrophoresis.

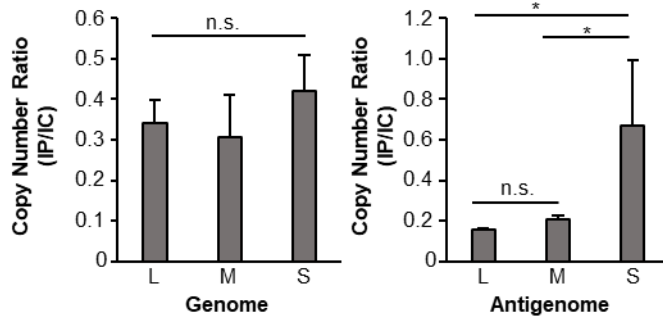


Figure 3.7: Quantitative analysis of RNA directly bound to Gn in RVFV-infected cells.

Binding ability of Gn to viral RNAs in ultraviolet (UV)-irradiated cells. Huh 7 cells were infected with MP-12 at an MOI-3. Cells were irradiated 8 hours post-infection with 250mJ/cm² UV light. Cell extracts were collected with a high stringent lysis buffer. Cell extracts were subjected to co-immunoprecipitation (IP) using anti-Gn antibody. RNA was extracted from intracellular lysates (IC) and IP samples from UV-irradiated cells. Copy numbers of genomic and antigenomic L, M, and S RNAs were determined by RT-qPCR assay. Gn binding ability was calculated as the ratio of the copy number of viral RNA directly bound to Gn (IP) to the copy number of intracellular viral RNA in UV-irradiated infected cells (IP/IC). Data represent the mean of biological triplicate experiments and error bars indicate the standard deviation. Statistical analysis was done using a one-way ANOVA with Tukey's multiple comparison post-test. N.S., not significant. * P < 0.05

Discussion

As RVFV RNPs trigger the RIG-I mediated antiviral innate immune signaling, it is vital for the virus to establish a strategy to overcome this response throughout virus replication, including early in infection (94). Efficient packaging of antigenomic S RNA, which serves as the template for the transcription of NSs mRNA, would ensure that the NSs protein, an IFN antagonist, would be expressed early during infection, enabling the virus to establish a productive infection in an IFN-competent host. Therefore, a positive selection mechanism for the efficient packaging of antigenomic S RNA would facilitate the NSs-mediated evasion of the early innate immune response.

The present study aimed to clarify the fundamental mechanisms that drive viral RNA packaging in RVFV particles. We previously reported that along with the three genomic viral RNAs, all three antigenomic RNAs are packaged into RVFV particles (29). In this study, we determined the amounts of genomic and antigenomic viral RNAs in infected cells and in the purified virus and established a packaging profile of all viral RNAs. Using our established RT-qPCR assay (123), we observed that the packaging abilities of the genomic RNAs were similar, indicating no preferential incorporation among the genomic RNA segments. However, we saw that the intrinsic packaging ability of antigenomic S RNA was significantly higher than antigenomic L and M RNA packaging abilities, suggesting an efficient incorporation of antigenomic S RNA into virus particles (Fig 3.1).

Interestingly, although viral RNA kinetics are similar between Vero and Huh7 cells (123), we noticed that the packaging of antigenomic S RNA was more pronounced in Huh7 cells (Fig 3.2). Brennan et al., previously reported that the packaging of genomic and antigenomic M and S RNAs were dependent on their relative abundance in infected cells (117). Consistent with this notion, the ratio of genome to antigenome for all viral RNAs were similar in infected Vero cells and purified virus (Fig 3.2A). In Huh 7 cells, we saw

similar results for L and M RNA, wherein the RNAs packaged inside virions correlated with the intracellular abundance in infected cells. In contrast, we observed that the packaging of antigenomic S RNA into virions did not reflect its relative amount accumulated in infected cells (Fig 3.2B). These data suggest the presence of an active mechanism for the selection and recognition of antigenomic S RNA that facilitates its efficient incorporation into virus particles. Our data are also consistent with reports that genome segment ratios can differ among cell types (37, 120, 123, 154), suggesting the possibility that cell-type specific differences can alter packaging efficiencies.

We also determined the packaging profile of a recombinant MP-12 virus containing the rLuc ORF in place of the NSs ORF located on the S RNA, thereby lacking the NSs nucleotide sequence and NSs protein expression. We found that among the genomic RNA segments, there was a higher packaging ability of M RNA compared to S and L RNAs (Fig 3.3B). Despite comparable titers of MP-12 and MP-12-rLuc in Vero cells (144), we observed that MP-12-rLuc had increased particle production suggesting the production of non-infectious particles (Fig 3.3A). These non-infectious particles could potentially carry genomic M segment and lack L and/ S RNA. Our data are consistent with previous reports that RVFV-clone 13 virus, which contains a truncated NSs ORF, showed enhanced recruitment of the genomic M segment at the Golgi assembly site and can generate non-infectious virus particles carrying less than the three genomic RNA segments (119). Despite this, the packaging ability of antigenomic S RNA of MP-12-rLuc was significantly higher relative to antigenomic L and M RNAs (Fig 3.3B). These data demonstrate that the presence of the NSs ORF is not required for the efficient incorporation of antigenomic S RNA.

We noted that the packaging profiles of S and M RNA in our single-segment RNA packaging analysis, were similar to those in MP-12-infected cells (Fig 3.4). Genomic and antigenomic M RNA packaged into purified VLPs mirrored their accumulation in VLP-inoculated cells, whereas antigenomic S RNA was efficiently packaged into VLPs that did

not correlate with its abundance in VLP-inoculated cells. These data suggest the presence of an active RNA element(s), within antigenomic S RNA, that facilitates the efficient incorporation of antigenomic S RNA into particles. As our VLP packaging assay recapitulated the observed RNA packaging profiles in infected cells, this assay could be used in future studies to identify a putative RNA signal(s) that drive efficient packaging of the antigenomic S RNA.

It has been proposed that the cytoplasmic tail of Gn serves as a surrogate matrix protein through its interaction with viral RNPs which drives the packaging of bunyaviral RNAs into particles (10, 12, 36, 37, 47, 49, 52, 53, 57, 122, 149). As viral RNPs consist of viral RNA, N protein and L protein, we tested interactions of Gn with each component of viral RNPs. Co-IP analysis, using anti-Gn antibody, revealed interactions of Gn with N and L protein as well as genomic RNAs. Reciprocal experiments using anti-N protein or anti-V5 antibody further confirmed the presence of Gn-N interaction and Gn-L interaction (Fig 3.5). We employed a UV-CLIP analysis to test whether viral RNAs directly bind to Gn in infected cells. We demonstrated that a highly stringent lysis buffer was able to break any interactions that Gn had with N and L protein (Fig 3.6A and B). Importantly, our results strongly indicate that Gn can directly interact with all genomic RNAs as well as their antigenomic counterparts (Fig 3.6C). This data is the first demonstration of a direct interaction of an envelope glycoprotein to viral RNA in bunyavirus-infected cells. Quantitative analysis revealed that the binding ability of Gn to antigenomic S was significantly higher than antigenomic L and M RNAs (Fig. 3.6). Our data showed that the binding ability of Gn to the viral RNAs correlated with their packaging ability into virus particles. These data strongly suggest that direct viral RNA-Gn interaction plays a central role in determining the incorporation efficiencies of each viral RNA.

In summary, our study showed that among RVFV antigenomic segments, there was a preferential incorporation of antigenomic S RNA relative to antigenomic L and M RNAs into virus particles. We discovered the presence of a direct interaction between Gn and

viral RNAs for the first time in bunyavirus-infected cells. We observed a positive correlation between the ability of Gn to directly interact with viral RNAs and their packaging abilities into RVFV particles, which suggests that the direct interaction between Gn and specific RNA element(s) in the viral RNAs governs their efficiency of incorporation into RVFV particles.

CHAPTER 4: SUMMARY AND FUTURE PERSPECTIVES

Rift valley fever phlebovirus (RVFV) is an enveloped virus that has a trisegmented, single-stranded, negative-sense RNA genome, consisting of L, M and S segments. The virion carries two envelope glycoproteins, Gn and Gc, along with ribonucleoprotein complexes (RNPs), composed of encapsidated genomes carrying the nucleocapsid protein, N, and the RNA-dependent RNA polymerase, L protein. The S RNA segment uses an ambisense coding strategy to encode the N protein and a nonstructural protein, NSs, an IFN antagonist, which is a major viral virulence factor. Previous studies have shown that in addition to the three genomic RNA segments, the antigenomic S RNA segment is also packaged into RVFV particles, facilitating the synthesis of NSs immediately after infection to counter the early innate immune response.

A comprehensive analysis of the replication kinetics and packaging abilities of the different replicative RNA species of RVFV has not been reported due to the lack of a quantitative assay system that can selectively distinguish between the genomic and antigenomic RNAs of each of the three RVFV RNA segments. To study the accumulation kinetics and packaging profile of RVFV RNAs into virions, we established a novel tagged strand-specific real time RT-PCR assay that selectively quantifies the genomic and antigenomic RNAs of each of the three RVFV RNA segments. A previous study documented the intracellular ratio of RVFV-clone 13 virus RNA replication at a single point in time as $S > M > L$ by radiolabeling and gel electrophoresis (13). As stated earlier, quantification by radiolabeling does not differentiate between genomic and antigenomic segments for L, M, and S and between antigenomic and mRNA for L and M segments due to similar migration sizes. Using a different quantification approach by in-situ hybridization, another group observed intracellular ratios of genomic RVFV-clone 13 virus replication as $L = M = S$ early in infection and varying slightly later in infection (119). In our study, the intracellular ratios of genomic RNA vary depending on the time during

infection but overall was similar to $L = M = S$. Intracellular ratios of antigenomic segments are slightly similar throughout infection in VeroE6 cells, however in Huh-7 cells, antigenomic M segment is noticeably higher throughout the course of infection relative to L and S segment. As antigenomic M RNA contains a longer 3'-NCR, a possible explanation for its higher replication could be that the long 3'-NCR increases the stability of the RNA (155). We observed that the genomic RNA levels, for all three viral RNA segments, were in at least 10-fold excess over their corresponding antigenomic RNAs throughout the course of infection, with the exception of antigenomic M RNA at 8 h.p.i in both mammalian cell lines. This differs from the observed replication kinetics in positive-sense viruses where the positive strands outnumber the negative strands by about 30- to 70-fold throughout the course of infection (156).

The mechanisms of viral RNA packaging in RVFV and other bunyaviruses are largely unknown. In both mammalian and mosquito cell lines, all three antigenomic RNAs were packaged inside purified virions with a higher amount of antigenomic S RNA relative to antigenomic L and M RNAs (29). This packaging profile has only been observed for the phleboviruses, RVFV and UUKV. The NSs mRNA is transcribed from the incoming antigenomic S RNA which leads to the synthesis of NSs protein early in infection (29). Incoming RVFV RNPs trigger the RIG-I mediated antiviral immune signaling pathway which leads to the induction of the type I IFN response (94). The NSs protein is a major virulence factor for RVFV and a known IFN antagonist (98, 101, 147). The efficient packaging of antigenomic S RNA would ensure that NSs protein is made early during infection to evade the early innate immune response triggered by the incoming RNPs. This suggests a positive selection mechanism for the efficient incorporation of antigenomic S RNA.

Using our strand-specific RT-qPCR assay, we quantified the packaging abilities of genomic and antigenomic RNA in purified RVFV particles. The packaging abilities of genomic RNA segments were similar with no appreciable difference between the

segments, suggesting the lack of any preferential packaging among genomic RNA segments. In contrast, the packaging ability of antigenomic S RNA was substantially higher than that of antigenomic L and M RNAs, indicating that among the antigenomic RNA segments, the antigenomic S RNA is preferentially packaged into virions. We also determined that this observed packaging profile does not require the presence of the NSs ORF. Interestingly, infection of Vero E6 cells with the MP-12-rLuc virus, which lacks the NSs ORF, resulted in a higher production of virus particles compared to MP-12. Although both viruses grow to similar titers in Vero E6 cells (144), we speculate that MP-12-rLuc virus generates empty or incomplete virus particles. An earlier study observing the composition of RVFV-clone 13 virions, also lacking a full NSs ORF, displayed a high percentage of empty or incomplete virions (119). The question is does the NSs protein directly or indirectly affect the production of infectious RVFV particles?

Using our single-segment VLP RNA packaging assay, we report that the relatively smaller size of antigenomic S RNA cannot be the sole reason for its efficient packaging inside particles, suggesting the presence of an additional RNA element(s) within antigenomic S RNA. Brennan et al., observed that the ORFs located on the S RNA may play a role in the ratio of genome to antigenome packaging inside virions (117). As our data suggests that the NSs ORF is not required for the efficient packaging of antigenomic S RNA, it is possible that an additional RNA element(s) may reside within the N ORF. Our single-segment packaging assay recapitulated the observed packaging profile in infected cells, indicating that this assay could be used to identify the putative RNA packaging element(s) within antigenomic S RNA. Future studies will involve generating mutant S RNAs, carrying mutations within the NCRs or carrying a nonviral gene in place of the N ORF, and testing the packaging efficiency of antigenomic S RNA into VLPs.

To delineate the factor(s) governing the differential packaging abilities of RVFV RNA segments, we characterized the molecular interactions between Gn and viral RNPs in RVFV-infected cells, which is predicted to be required for the incorporation of

bunyavirus RNAs into virions. Co-immunoprecipitation analysis, using anti-Gn antibody, demonstrated the proposed interaction of Gn with viral RNPs in infected cells. Furthermore, UV-crosslinking and immunoprecipitation analysis showed that Gn also directly binds to genomic and antigenomic viral RNAs, revealing the presence of a direct interaction between Gn and viral RNAs in infected cells for the first time in bunyaviruses. Strikingly, among the antigenomic RNAs, Gn exhibited a significantly higher binding ability to antigenomic S RNA, which correlated with its higher packaging ability, suggesting the presence of a mechanism for the preferential packaging of antigenomic S RNA. These findings are surprising because Gn is a transmembrane viral envelope glycoprotein with no known RNA binding motifs including zinc-finger domains that were found in other bunyaviruses but not phleboviruses. Overall, our data indicated a positive correlation between the ability of Gn to directly interact with RVFV RNA segments and their packaging abilities, strongly suggesting that a direct interaction between Gn and specific RNA elements in viral RNAs could be the primary factor that governs the packaging efficiency of RVFV RNA segments into virus particles. As it has been shown that RVFV N protein can non-specifically bind to viral RNAs (157) and L protein can bind to cellular mRNAs for cap-snatching (26, 27), it is possible that the direct interaction of Gn with viral RNAs is required for the recognition and selection of viral RNAs to be packaged. Whereas N and L proteins take part in the replication of viral RNAs, Gn binding to viral RNAs could be an important step in the switch from replication to packaging by marking the RNA templates for packaging. The direct interaction of Gn with viral RNAs could also be important for the stability of the RNP complex with Gn that ensures the packaging of RNPs into virions.

Another implication of Gn directly interacting with viral RNAs could be a regulatory role in viral RNA synthesis (47). The IAV M1 matrix protein has been shown to repress viral transcription through its RNA-binding domains (158, 159). It was also reported that the matrix proteins of filoviruses and rhabdoviruses contribute to the

regulation of viral RNA synthesis (46, 160). The arenavirus Z matrix protein acts as a viral transcriptional repressor by binding directly to the catalytic domain, the highly conserved SDD motif, of the L protein (23). Along with a direct interaction of RVFV Gn with viral RNAs, we also demonstrated that Gn could bind to L protein in infected cells. It is possible that the interaction of Gn with L protein could not only ensure the incorporation of L protein into virions but also may have a regulatory role in viral RNA transcription. These interactions may be important for the late stages of infection, where the decrease of viral mRNA production triggers the packaging of the viral genome.

In conclusion, this study provided valuable insight into the mechanism driving RNA packaging into RVFV particles. Interestingly, our study suggests a possible additional RNA element located on the antigenomic S RNA segment that may be responsible for the efficient incorporation of antigenomic S RNA into virus particles. As we demonstrated that Gn can directly interact with viral RNAs using a UV-CLIP method, this assay could be modified to identify the binding sites for Gn in each of the viral RNA segments using high-throughput sequencing of RNA isolated by crosslinking immunoprecipitation (HITS-CLIP). Identification of this putative RNA element(s) could lead to the generation of an RVFV mutant, lacking the RNA element(s), that cannot efficiently package antigenomic S RNA into virions. Infections with this RVFV mutant could result in a delayed NSs response due to low transcription of the NSs mRNA and expression of the NSs protein needed early in infection to circumvent the early innate immune response (Illustration 4.1). These studies can examine the biological significance of antigenomic S RNA packaging for RVFV replication in type I IFN-competent cells.

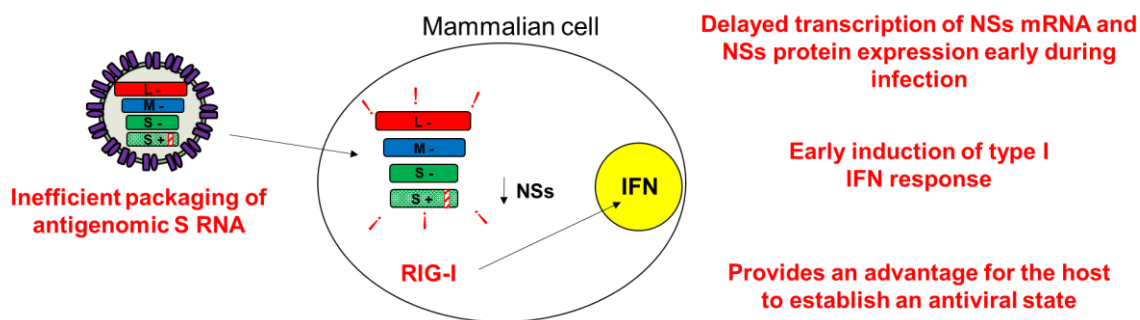


Illustration 4.1: Future studies examining the biological significance of efficient antigenomic S RNA packaging

Generation of a recombinant RVFV carrying a mutation within the putative RNA element(s) that is responsible for the efficient incorporation of antigenomic S RNA into virions. As the direct interaction of Gn with viral RNAs is most probably the major factor governing RNA packaging efficiency, the disruption of the direct interaction of Gn with this putative RNA element(s) could lead to inefficient packaging of antigenomic S RNA, resulting in a delay in the transcription of NSs mRNA and NSs protein expression. The delayed NSs response could potentially provide an advantage for the host to induce the type I IFN response and establish an anti-viral state.

References

1. Abudurexiti A, Adkins S, Alioto D, Alkhovsky SV, Avsic-Zupanc T, Ballinger MJ, Bente DA, Beer M, Bergeron E, Blair CD, Briesse T, Buchmeier MJ, Burt FJ, Calisher CH, Chang C, Charrel RN, Choi IR, Clegg JCS, de la Torre JC, de Lamballerie X, Deng F, Di Serio F, Digiaro M, Drebot MA, Duan X, Ebihara H, Elbeaino T, Ergunay K, Fulhorst CF, Garrison AR, Gao GF, Gonzalez JJ, Groschup MH, Gunther S, Haenni AL, Hall RA, Hepojoki J, Hewson R, Hu Z, Hughes HR, Jonson MG, Junglen S, Klempa B, Klingstrom J, Kou C, Laenen L, Lambert AJ, Langevin SA, Liu D, Lukashevich IS, et al. 2019. Taxonomy of the order Bunyavirales: update 2019. *Arch Virol* 164:1949-1965.
2. Brisse ME, Ly H. 2019. Hemorrhagic Fever-Causing Arenaviruses: Lethal Pathogens and Potent Immune Suppressors. *Front Immunol* 10:372.
3. Dowall SD, Carroll MW, Hewson R. 2017. Development of vaccines against Crimean-Congo haemorrhagic fever virus. *Vaccine* 35:6015-6023.
4. Fawzy M, Helmy YA. 2019. The One Health Approach is Necessary for the Control of Rift Valley Fever Infections in Egypt: A Comprehensive Review. *Viruses* 11.
5. Liu R, Ma H, Shu J, Zhang Q, Han M, Liu Z, Jin X, Zhang F, Wu X. 2019. Vaccines and Therapeutics Against Hantaviruses. *Front Microbiol* 10:2989.
6. Sakkas H, Bozidis P, Franks A, Papadopoulou C. 2018. Oropouche Fever: A Review. *Viruses* 10.
7. Sun Y, Li J, Gao GF, Tien P, Liu W. 2018. Bunyavirales ribonucleoproteins: the viral replication and transcription machinery. *Crit Rev Microbiol* 44:522-540.
8. Endalew AD, Faburay B, Wilson WC, Richt JA. 2019. Schmallenberg Disease-A Newly Emerged Culicoides-borne Viral Disease of Ruminants. *Viruses* 11.
9. Sevik MA, Arli-Sokmen, M. 2012. Estimation of the effect of *Tomato spotted wilt virus* (TSWV) infection on some yield components of tomato. *Phytoparasitica* doi:<https://doi.org/10.1007/s12600-011-0192-2>:87-93.
10. Guardado-Calvo P, Rey FA. 2017. The Envelope Proteins of the Bunyavirales. *Adv Virus Res* 98:83-118.
11. Baird NL, York J, Nunberg JH. 2012. Arenavirus infection induces discrete cytosolic structures for RNA replication. *J Virol* 86:11301-10.
12. Sherman MB, Freiberg AN, Holbrook MR, Watowich SJ. 2009. Single-particle cryo-electron microscopy of Rift Valley fever virus. *Virology* 387:11-5.
13. Gauthier N, Billecocq A, Flick R, Bouloy M. 2006. Rift Valley fever virus noncoding regions of L, M and S segments regulate RNA synthesis. *Virology* 351:170-9.
14. Murakami S, Terasaki K, Narayanan K, Makino S. 2012. Roles of the coding and noncoding regions of rift valley Fever virus RNA genome segments in viral RNA packaging. *J Virol* 86:4034-9.

15. Albarino CG, Bird BH, Nichol ST. 2007. A shared transcription termination signal on negative and ambisense RNA genome segments of Rift Valley fever, sandfly fever Sicilian, and Toscana viruses. *J Virol* 81:5246-56.
16. Ikegami T, Won S, Peters CJ, Makino S. 2007. Characterization of Rift Valley fever virus transcriptional terminations. *J Virol* 81:8421-38.
17. Lara E, Billecocq A, Leger P, Bouloy M. 2011. Characterization of wild-type and alternate transcription termination signals in the Rift Valley fever virus genome. *J Virol* 85:12134-45.
18. Bergeron E, Zivcec M, Chakrabarti AK, Nichol ST, Albarino CG, Spiropoulou CF. 2015. Recovery of Recombinant Crimean Congo Hemorrhagic Fever Virus Reveals a Function for Non-structural Glycoproteins Cleavage by Furin. *PLoS Pathog* 11:e1004879.
19. Mittler E, Dieterle ME, Kleinfelter LM, Slough MM, Chandran K, Jangra RK. 2019. Hantavirus entry: Perspectives and recent advances. *Adv Virus Res* 104:185-224.
20. Hewson R, Chamberlain J, Mioulet V, Lloyd G, Jamil B, Hasan R, Gmyl A, Gmyl L, Smirnova SE, Lukashev A, Karganova G, Clegg C. 2004. Crimean-Congo haemorrhagic fever virus: sequence analysis of the small RNA segments from a collection of viruses world wide. *Virus Res* 102:185-9.
21. Barnwal B, Karlberg H, Mirazimi A, Tan YJ. 2016. The Non-structural Protein of Crimean-Congo Hemorrhagic Fever Virus Disrupts the Mitochondrial Membrane Potential and Induces Apoptosis. *J Biol Chem* 291:582-92.
22. Shi M, Lin XD, Chen X, Tian JH, Chen LJ, Li K, Wang W, Eden JS, Shen JJ, Liu L, Holmes EC, Zhang YZ. 2018. Author Correction: The evolutionary history of vertebrate RNA viruses. *Nature* 561:E6.
23. Hallam SJ, Koma T, Maruyama J, Paessler S. 2018. Review of Mammarenavirus Biology and Replication. *Front Microbiol* 9:1751.
24. Tercero B, Makino S. 2020. Reverse genetics approaches for the development of bunyavirus vaccines. *Curr Opin Virol* 44:16-25.
25. Borucki MK, Kempf BJ, Blitvich BJ, Blair CD, Beaty BJ. 2002. La Crosse virus: replication in vertebrate and invertebrate hosts. *Microbes Infect* 4:341-50.
26. Hopkins K, Cherry S. 2013. Bunyaviral cap-snatching vs. decapping: recycling cell cycle mRNAs. *Cell Cycle* 12:3711-2.
27. Olschewski S, Cusack S, Rosenthal M. 2020. The Cap-Snatching Mechanism of Bunyaviruses. *Trends Microbiol* 28:293-303.
28. Patterson JL, Kolakofsky D. 1984. Characterization of La Crosse virus small-genome transcripts. *J Virol* 49:680-5.
29. Ikegami T, Won S, Peters CJ, Makino S. 2005. Rift Valley fever virus NSs mRNA is transcribed from an incoming anti-viral-sense S RNA segment. *Journal of Virology* 79:12106-12111.

30. Fontana J, Lopez-Montero N, Elliott RM, Fernandez JJ, Risco C. 2008. The unique architecture of Bunyamwera virus factories around the Golgi complex. *Cell Microbiol* 10:2012-28.
31. Shafiuddin M, Boon ACM. 2019. RNA Sequence Features Are at the Core of Influenza A Virus Genome Packaging. *J Mol Biol* 431:4217-4228.
32. Masters PS. 2019. Coronavirus genomic RNA packaging. *Virology* 537:198-207.
33. Rumenapf T, Strauss EG, Strauss JH. 1994. Subgenomic mRNA of Aura alphavirus is packaged into virions. *J Virol* 68:56-62.
34. Rein A. 2020. The heart of the HIV RNA packaging signal? *Proc Natl Acad Sci U S A* 117:19621-19623.
35. Rein A. 2019. RNA Packaging in HIV. *Trends Microbiol* 27:715-723.
36. Hornak KE, Lanchy JM, Lodmell JS. 2016. RNA Encapsidation and Packaging in the Phleboviruses. *Viruses* 8.
37. Wichgers Schreur PJ, Kormelink R, Kortekaas J. 2018. Genome packaging of the Bunyavirales. *Curr Opin Virol* 33:151-155.
38. Comas-Garcia M. 2019. Packaging of Genomic RNA in Positive-Sense Single-Stranded RNA Viruses: A Complex Story. *Viruses* 11.
39. Narayanan K, Makino S. 2001. Cooperation of an RNA packaging signal and a viral envelope protein in coronavirus RNA packaging. *J Virol* 75:9059-67.
40. Narayanan K, Chen CJ, Maeda J, Makino S. 2003. Nucleocapsid-independent specific viral RNA packaging via viral envelope protein and viral RNA signal. *J Virol* 77:2922-7.
41. Bolte H, Rosu ME, Hagelauer E, Garcia-Sastre A, Schwemmler M. 2019. Packaging of the Influenza Virus Genome Is Governed by a Plastic Network of RNA- and Nucleoprotein-Mediated Interactions. *J Virol* 93.
42. Noda T, Kawaoka Y. 2012. Packaging of influenza virus genome: robustness of selection. *Proc Natl Acad Sci U S A* 109:8797-8.
43. Chou YY, Vafabakhsh R, Doganay S, Gao Q, Ha T, Palese P. 2012. One influenza virus particle packages eight unique viral RNAs as shown by FISH analysis. *Proc Natl Acad Sci U S A* 109:9101-6.
44. Noton SL, Medcalf E, Fisher D, Mullin AE, Elton D, Digard P. 2007. Identification of the domains of the influenza A virus M1 matrix protein required for NP binding, oligomerization and incorporation into virions. *J Gen Virol* 88:2280-2290.
45. Gomis-Ruth FX, Dessen A, Timmins J, Bracher A, Kolesnikowa L, Becker S, Klenk HD, Weissenhorn W. 2003. The matrix protein VP40 from Ebola virus octamerizes into pore-like structures with specific RNA binding properties. *Structure* 11:423-33.
46. Finke S, Conzelmann KK. 2003. Dissociation of rabies virus matrix protein functions in regulation of viral RNA synthesis and virus assembly. *J Virol* 77:12074-82.

47. Strandin T, Hepojoki J, Vaheri A. 2013. Cytoplasmic tails of bunyavirus Gn glycoproteins-Could they act as matrix protein surrogates? *Virology* 437:73-80.
48. Urata S, Yasuda J. 2012. Molecular mechanism of arenavirus assembly and budding. *Viruses* 4:2049-79.
49. Carnec X, Ermonval M, Kreher F, Flamand M, Bouloy M. 2014. Role of the cytosolic tails of Rift Valley fever virus envelope glycoproteins in viral morphogenesis. *Virology* 448:1-14.
50. Huiskonen JT, Overby AK, Weber F, Grunewald K. 2009. Electron cryo-microscopy and single-particle averaging of Rift Valley fever virus: evidence for GN-GC glycoprotein heterodimers. *J Virol* 83:3762-9.
51. Shi X, Kohl A, Li P, Elliott RM. 2007. Role of the cytoplasmic tail domains of Bunyamwera orthobunyavirus glycoproteins Gn and Gc in virus assembly and morphogenesis. *J Virol* 81:10151-60.
52. Spiegel M, Plegge T, Pohlmann S. 2016. The Role of Phlebovirus Glycoproteins in Viral Entry, Assembly and Release. *Viruses* 8.
53. Piper ME, Sorenson DR, Gerrard SR. 2011. Efficient cellular release of Rift Valley fever virus requires genomic RNA. *PLoS One* 6:e18070.
54. Phoenix I, Nishiyama S, Lokugamage N, Hill TE, Huante MB, Slack OA, Carpio VH, Freiberg AN, Ikegami T. 2016. N-Glycans on the Rift Valley Fever Virus Envelope Glycoproteins Gn and Gc Redundantly Support Viral Infection via DC-SIGN. *Viruses* 8.
55. Acuna R, Cifuentes-Munoz N, Marquez CL, Bulling M, Klingstrom J, Mancini R, Lozach PY, Tischler ND. 2014. Hantavirus Gn and Gc glycoproteins self-assemble into virus-like particles. *J Virol* 88:2344-8.
56. Overby AK, Popov VL, Pettersson RF, Neve EP. 2007. The cytoplasmic tails of Uukuniemi Virus (Bunyaviridae) G(N) and G(C) glycoproteins are important for intracellular targeting and the budding of virus-like particles. *J Virol* 81:11381-91.
57. Estrada DF, De Guzman RN. 2011. Structural characterization of the Crimean-Congo hemorrhagic fever virus Gn tail provides insight into virus assembly. *J Biol Chem* 286:21678-86.
58. Borucki MK, Chandler LJ, Parker BM, Blair CD, Beaty BJ. 1999. Bunyavirus superinfection and segment reassortment in transovarially infected mosquitoes. *J Gen Virol* 80 (Pt 12):3173-3179.
59. Bowen MD, Trappier SG, Sanchez AJ, Meyer RF, Goldsmith CS, Zaki SR, Dunster LM, Peters CJ, Ksiazek TG, Nichol ST, Force RVFT. 2001. A reassortant bunyavirus isolated from acute hemorrhagic fever cases in Kenya and Somalia. *Virology* 291:185-90.
60. Briese T, Bird B, Kapoor V, Nichol ST, Lipkin WI. 2006. Batai and Ngari viruses: M segment reassortment and association with severe febrile disease outbreaks in East Africa. *J Virol* 80:5627-30.

61. Gaudreault NN, Indran SV, Balaraman V, Wilson WC, Richt JA. 2019. Molecular aspects of Rift Valley fever virus and the emergence of reassortants. *Virus Genes* 55:1-11.
62. Liu J, Sun Y, Shi W, Tan S, Pan Y, Cui S, Zhang Q, Dou X, Lv Y, Li X, Li X, Chen L, Quan C, Wang Q, Zhao Y, Lv Q, Hua W, Zeng H, Chen Z, Xiong H, Jiang C, Pang X, Zhang F, Liang M, Wu G, Gao GF, Liu WJ, Li A, Wang Q. 2017. The first imported case of Rift Valley fever in China reveals a genetic reassortment of different viral lineages. *Emerg Microbes Infect* 6:e4.
63. Sall AA, Zannotto PM, Sene OK, Zeller HG, Digoutte JP, Thiongane Y, Bouloy M. 1999. Genetic reassortment of Rift Valley fever virus in nature. *J Virol* 73:8196-200.
64. Klempa B. 2018. Reassortment events in the evolution of hantaviruses. *Virus Genes* 54:638-646.
65. Briese T, Calisher CH, Higgs S. 2013. Viruses of the family Bunyaviridae: are all available isolates reassortants? *Virology* 446:207-16.
66. Abdel-Wahab KS, El Baz LM, El-Tayeb EM, Omar H, Ossman MA, Yasin W. 1978. Rift Valley Fever virus infections in Egypt: Pathological and virological findings in man. *Trans R Soc Trop Med Hyg* 72:392-6.
67. Adam AA, Karsany MS, Adam I. 2010. Manifestations of severe Rift Valley fever in Sudan. *Int J Infect Dis* 14:e179-80.
68. Al-Hazmi A, Al-Rajhi AA, Abboud EB, Ayoola EA, Al-Hazmi M, Saadi R, Ahmed N. 2005. Ocular complications of Rift Valley fever outbreak in Saudi Arabia. *Ophthalmology* 112:313-8.
69. Alrajhi AA, Al-Semari A, Al-Watban J. 2004. Rift Valley fever encephalitis. *Emerg Infect Dis* 10:554-5.
70. Deutman AF, Klomp HJ. 1981. Rift Valley fever retinitis. *Am J Ophthalmol* 92:38-42.
71. Laughlin LW, Girgis NI, Meegan JM, Strausbaugh LJ, Yassin MW, Watten RH. 1978. Clinical studies on Rift Valley fever. Part 2: Ophthalmologic and central nervous system complications. *J Egypt Public Health Assoc* 53:183-4.
72. Maar SA, Swanepoel R, Gelfand M. 1979. Rift Valley fever encephalitis. A description of a case. *Cent Afr J Med* 25:8-11.
73. Schrire L. 1951. Macular changes in rift valley fever. *S Afr Med J* 25:926-30.
74. Siam AL, Meegan JM. 1980. Ocular disease resulting from infection with Rift Valley fever virus. *Trans R Soc Trop Med Hyg* 74:539-41.
75. Siam AL, Meegan JM, Gharbawi KF. 1980. Rift Valley fever ocular manifestations: observations during the 1977 epidemic in Egypt. *Br J Ophthalmol* 64:366-74.

76. Strausbaugh LJ, Laughlin LW, Meegan JM, Watten RH. 1978. Clinical studies on Rift Valley fever, Part I: Acute febrile and hemorrhagic-like diseases. *J Egypt Public Health Assoc* 53:181-2.
77. Swanepoel R, Manning B, Watt JA. 1979. Fatal Rift Valley fever of man in Rhodesia. *Cent Afr J Med* 25:1-8.
78. Yassin W. 1978. Clinico-pathological picture in five human cases died with Rift Valley fever. *J Egypt Public Health Assoc* 53:191-3.
79. Balkhy HH, Memish ZA. 2003. Rift Valley fever: an uninvited zoonosis in the Arabian peninsula. *Int J Antimicrob Agents* 21:153-7.
80. Andriamandimby SF, Randrianarivo-Solofoniaina AE, Jeanmaire EM, Ravololomanana L, Razafimanantsoa LT, Rakotojoelinandrasana T, Razainirina J, Hoffmann J, Ravalohery JP, Rafisandratantsoa JT, Rollin PE, Reynes JM. 2010. Rift Valley fever during rainy seasons, Madagascar, 2008 and 2009. *Emerg Infect Dis* 16:963-70.
81. Madani TA, Al-Mazrou YY, Al-Jeffri MH, Mishkhas AA, Al-Rabeah AM, Turkistani AM, Al-Sayed MO, Abodahish AA, Khan AS, Ksiazek TG, Shobokshi O. 2003. Rift Valley fever epidemic in Saudi Arabia: epidemiological, clinical, and laboratory characteristics. *Clin Infect Dis* 37:1084-92.
82. Gargan TP, 2nd, Clark GG, Dohm DJ, Turell MJ, Bailey CL. 1988. Vector potential of selected North American mosquito species for Rift Valley fever virus. *Am J Trop Med Hyg* 38:440-6.
83. Rolin AI, Berrang-Ford L, Kulkarni MA. 2013. The risk of Rift Valley fever virus introduction and establishment in the United States and European Union. *Emerg Microbes Infect* 2:e81.
84. Accardi L, Prehaud C, Di Bonito P, Mochi S, Bouloy M, Giorgi C. 2001. Activity of Toscana and Rift Valley fever virus transcription complexes on heterologous templates. *J Gen Virol* 82:781-785.
85. Blakqori G, Kochs G, Haller O, Weber F. 2003. Functional L polymerase of La Crosse virus allows in vivo reconstitution of recombinant nucleocapsids. *J Gen Virol* 84:1207-1214.
86. Dunn EF, Pritlove DC, Jin H, Elliott RM. 1995. Transcription of a recombinant bunyavirus RNA template by transiently expressed bunyavirus proteins. *Virology* 211:133-43.
87. Flick K, Hooper JW, Schmaljohn CS, Pettersson RF, Feldmann H, Flick R. 2003. Rescue of Hantaan virus minigenomes. *Virology* 306:219-24.
88. Bouloy M, Weber F. 2010. Molecular biology of rift valley Fever virus. *Open Virol J* 4:8-14.
89. Raymond DD, Piper ME, Gerrard SR, Smith JL. 2010. Structure of the Rift Valley fever virus nucleocapsid protein reveals another architecture for RNA encapsidation. *Proc Natl Acad Sci U S A* 107:11769-74.

90. Ferron F, Li Z, Danek EI, Luo D, Wong Y, Coutard B, Lantéz V, Charrel R, Canard B, Walz T, Lescar J. 2011. The hexamer structure of Rift Valley fever virus nucleoprotein suggests a mechanism for its assembly into ribonucleoprotein complexes. *PLoS Pathog* 7:e1002030.
91. Zamoto-Niikura A, Terasaki K, Ikegami T, Peters CJ, Makino S. 2009. Rift valley fever virus L protein forms a biologically active oligomer. *J Virol* 83:12779-89.
92. Holm T, Kopicki JD, Busch C, Olschewski S, Rosenthal M, Uetrecht C, Gunther S, Reindl S. 2018. Biochemical and structural studies reveal differences and commonalities among cap-snatching endonucleases from segmented negative-strand RNA viruses. *J Biol Chem* 293:19686-19698.
93. Gogrefe N, Reindl S, Gunther S, Rosenthal M. 2019. Structure of a functional cap-binding domain in Rift Valley fever virus L protein. *PLoS Pathog* 15:e1007829.
94. Weber M, Gawanbacht A, Habjan M, Rang A, Borner C, Schmidt AM, Veitinger S, Jacob R, Devignot S, Kochs G, Garcia-Sastre A, Weber F. 2013. Incoming RNA virus nucleocapsids containing a 5'-triphosphorylated genome activate RIG-I and antiviral signaling. *Cell Host Microbe* 13:336-46.
95. Habjan M, Pichlmair A, Elliott RM, Overby AK, Glatter T, Gstaiger M, Superti-Furga G, Unger H, Weber F. 2009. NSs protein of rift valley fever virus induces the specific degradation of the double-stranded RNA-dependent protein kinase. *J Virol* 83:4365-75.
96. Kende M. 1985. Prophylactic and therapeutic efficacy of poly(I,C)-LC against Rift Valley fever virus infection in mice. *J Biol Response Mod* 4:503-11.
97. Peters CJ, Reynolds JA, Slone TW, Jones DE, Stephen EL. 1986. Prophylaxis of Rift Valley fever with antiviral drugs, immune serum, an interferon inducer, and a macrophage activator. *Antiviral Res* 6:285-97.
98. Wuerth JD, Weber F. 2016. Phleboviruses and the Type I Interferon Response. *Viruses* 8.
99. Eifan S, Schnettler E, Dietrich I, Kohl A, Blomstrom AL. 2013. Non-structural proteins of arthropod-borne bunyaviruses: roles and functions. *Viruses* 5:2447-68.
100. Ly HJ, Ikegami T. 2016. Rift Valley fever virus NSs protein functions and the similarity to other bunyavirus NSs proteins. *Virol J* 13:118.
101. Billecocq A, Spiegel M, Vialat P, Kohl A, Weber F, Bouloy M, Haller O. 2004. NSs protein of Rift Valley fever virus blocks interferon production by inhibiting host gene transcription. *J Virol* 78:9798-806.
102. Ikegami T, Peters CJ, Makino S. 2005. Rift valley fever virus nonstructural protein NSs promotes viral RNA replication and transcription in a minigenome system. *J Virol* 79:5606-15.
103. Kainulainen M, Habjan M, Hubel P, Busch L, Lau S, Colinge J, Superti-Furga G, Pichlmair A, Weber F. 2014. Virulence factor NSs of rift valley fever virus recruits the F-box protein FBXO3 to degrade subunit p62 of general transcription factor TFIIH. *J Virol* 88:3464-73.

104. Kalveram B, Lihoradova O, Ikegami T. 2011. NSs protein of rift valley fever virus promotes posttranslational downregulation of the TFIIEH subunit p62. *J Virol* 85:6234-43.
105. Le May N, Dubaele S, Proietti De Santis L, Billecocq A, Bouloy M, Egly JM. 2004. TFIIEH transcription factor, a target for the Rift Valley hemorrhagic fever virus. *Cell* 116:541-50.
106. Terasaki K, Ramirez SI, Makino S. 2016. Mechanistic Insight into the Host Transcription Inhibition Function of Rift Valley Fever Virus NSs and Its Importance in Virulence. *PLoS Negl Trop Dis* 10:e0005047.
107. Le May N, Mansuroglu Z, Leger P, Josse T, Blot G, Billecocq A, Flick R, Jacob Y, Bonnefoy E, Bouloy M. 2008. A SAP30 complex inhibits IFN-beta expression in Rift Valley fever virus infected cells. *PLoS Pathog* 4:e13.
108. Ikegami T, Narayanan K, Won S, Kamitani W, Peters CJ, Makino S. 2009. Rift Valley fever virus NSs protein promotes post-transcriptional downregulation of protein kinase PKR and inhibits eIF2alpha phosphorylation. *PLoS Pathog* 5:e1000287.
109. Leger P, Lara E, Jagla B, Sismeiro O, Mansuroglu Z, Coppee JY, Bonnefoy E, Bouloy M. 2013. Dicer-2- and Piwi-mediated RNA interference in Rift Valley fever virus-infected mosquito cells. *J Virol* 87:1631-48.
110. Sabin LR, Zheng Q, Thekkat P, Yang J, Hannon GJ, Gregory BD, Tudor M, Cherry S. 2013. Dicer-2 processes diverse viral RNA species. *PLoS One* 8:e55458.
111. Ferrer M, Henriot S, Chamontin C, Laine S, Mougél M. 2016. From Cells to Virus Particles: Quantitative Methods to Monitor RNA Packaging. *Viruses* 8.
112. Kohl A, Lowen AC, Leonard VH, Elliott RM. 2006. Genetic elements regulating packaging of the Bunyamwera orthobunyavirus genome. *J Gen Virol* 87:177-87.
113. Flick K, Katz A, Overby A, Feldmann H, Pettersson RF, Flick R. 2004. Functional analysis of the noncoding regions of the Uukuniemi virus (Bunyaviridae) RNA segments. *J Virol* 78:11726-38.
114. Terasaki K, Murakami S, Lokugamage KG, Makino S. 2011. Mechanism of tripartite RNA genome packaging in Rift Valley fever virus. *Proc Natl Acad Sci U S A* 108:804-9.
115. Brennan B, Welch SR, McLees A, Elliott RM. 2011. Creation of a recombinant Rift Valley fever virus with a two-segmented genome. *J Virol* 85:10310-8.
116. Wichgers Schreur PJ, Oreshkova N, Moormann RJ, Kortekaas J. 2014. Creation of Rift Valley fever viruses with four-segmented genomes reveals flexibility in bunyavirus genome packaging. *J Virol* 88:10883-93.
117. Brennan B, Welch SR, Elliott RM. 2014. The consequences of reconfiguring the ambisense S genome segment of Rift Valley fever virus on viral replication in mammalian and mosquito cells and for genome packaging. *PLoS Pathog* 10:e1003922.

118. Simons JF, Hellman U, Pettersson RF. 1990. Uukuniemi virus S RNA segment: ambisense coding strategy, packaging of complementary strands into virions, and homology to members of the genus Phlebovirus. *J Virol* 64:247-55.
119. Wichgers Schreur PJ, Kortekaas J. 2016. Single-Molecule FISH Reveals Non-selective Packaging of Rift Valley Fever Virus Genome Segments. *PLoS Pathog* 12:e1005800.
120. Erick Bermudez-Mendez EK, Cindy Spruit, Jeroen Kortekaas, Paul Wichgers Schreur. 2020. Visualizing the RNP content of single bunyavirus virions reveals more efficient genome packaging in the arthropod host. PREPRINT doi:<https://doi.org/10.21203/rs.3.rs-49677/v1>.
121. Gerrard SR, Nichol ST. 2002. Characterization of the Golgi retention motif of Rift Valley fever virus G(N) glycoprotein. *J Virol* 76:12200-10.
122. Strandin T, Hepojoki J, Wang H, Vaheri A, Lankinen H. 2011. The cytoplasmic tail of hantavirus Gn glycoprotein interacts with RNA. *Virology* 418:12-20.
123. Tercero B, Terasaki K, Nakagawa K, Narayanan K, Makino S. 2019. A strand-specific real-time quantitative RT-PCR assay for distinguishing the genomic and antigenomic RNAs of Rift Valley fever phlebovirus. *J Virol Methods* 272:113701.
124. Maquart M, Temmam S, Heraud JM, Leparac-Goffart I, Cetre-Sossah C, Dellagi K, Cardinale E, Pascalis H. 2014. Development of real-time RT-PCR for the detection of low concentrations of Rift Valley fever virus. *J Virol Methods* 195:92-9.
125. Naslund J, Lagerqvist N, Lundkvist A, Evander M, Ahlm C, Bucht G. 2008. Kinetics of Rift Valley Fever Virus in experimentally infected mice using quantitative real-time RT-PCR. *Journal of Virological Methods* 151:277-282.
126. Wilson WC, Romito M, Jaspersen DC, Weingartl H, Binopal YS, Maluleke MR, Wallace DB, van Vuren PJ, Paweska JT. 2013. Development of a Rift Valley fever real-time RT-PCR assay that can detect all three genome segments. *J Virol Methods* 193:426-31.
127. Beiter T, Reich E, Weigert C, Niess AM, Simon P. 2007. Sense or antisense? False priming reverse transcription controls are required for determining sequence orientation by reverse transcription-PCR. *Anal Biochem* 369:258-61.
128. Craggs JK, Ball JK, Thomson BJ, Irving WL, Grabowska AM. 2001. Development of a strand-specific RT-PCR based assay to detect the replicative form of hepatitis C virus RNA. *J Virol Methods* 94:111-20.
129. Feng L, Lintula S, Ho TH, Anastasina M, Paju A, Haglund C, Stenman UH, Hotakainen K, Orpana A, Kainov D, Stenman J. 2012. Technique for strand-specific gene-expression analysis and monitoring of primer-independent cDNA synthesis in reverse transcription. *Biotechniques* 52:263-70.
130. Haist K, Ziegler C, Botten J. 2015. Strand-Specific Quantitative Reverse Transcription-Polymerase Chain Reaction Assay for Measurement of Arenavirus Genomic and Antigenomic RNAs. *PLoS One* 10:e0120043.

131. Lanford RE, Chavez D. 1999. Strand-Specific rTth RT-PCR for the Analysis of HCV Replication. *Methods Mol Med* 19:471-81.
132. Lim SM, Koraka P, Osterhaus AD, Martina BE. 2013. Development of a strand-specific real-time qRT-PCR for the accurate detection and quantitation of West Nile virus RNA. *J Virol Methods* 194:146-53.
133. Peyrefitte CN, Pastorino B, Bessaud M, Tolou HJ, Couissinier-Paris P. 2003. Evidence for in vitro falsely-primed cDNAs that prevent specific detection of virus negative strand RNAs in dengue-infected cells: improvement by tagged RT-PCR. *J Virol Methods* 113:19-28.
134. Plaskon NE, Adelman ZN, Myles KM. 2009. Accurate strand-specific quantification of viral RNA. *PLoS One* 4:e7468.
135. Tuiskunen A, Leparac-Goffart I, Boubis L, Monteil V, Klingstrom J, Tolou HJ, Lundkvist A, Plumet S. 2010. Self-priming of reverse transcriptase impairs strand-specific detection of dengue virus RNA. *J Gen Virol* 91:1019-27.
136. Vashist S, Urena L, Goodfellow I. 2012. Development of a strand specific real-time RT-qPCR assay for the detection and quantitation of murine norovirus RNA. *J Virol Methods* 184:69-76.
137. Bannister R, Rodrigues D, Murray EJ, Laxton C, Westby M, Bright H. 2010. Use of a highly sensitive strand-specific quantitative PCR to identify abortive replication in the mouse model of respiratory syncytial virus disease. *Virology Journal* 7.
138. Chatterjee SN, Devhare PB, Lole KS. 2012. Detection of negative-sense RNA in packaged hepatitis E virions by use of an improved strand-specific reverse transcription-PCR method. *J Clin Microbiol* 50:1467-70.
139. Kawakami E, Watanabe T, Fujii K, Goto H, Watanabe S, Noda T, Kawaoka Y. 2011. Strand-specific real-time RT-PCR for distinguishing influenza vRNA, cRNA, and mRNA. *J Virol Methods* 173:1-6.
140. Strydom E, Pietersen G. 2018. Development of a strand-specific RT-PCR to detect the positive sense replicative strand of Soybean blotchy mosaic virus. *J Virol Methods* 259:39-44.
141. Nakabayashi H, Taketa K, Miyano K, Yamane T, Sato J. 1982. Growth of Human Hepatoma-Cell Lines with Differentiated Functions in Chemically Defined Medium. *Cancer Research* 42:3858-3863.
142. Garcia S, Crance JM, Billecocq A, Peinnequin A, Jouan A, Bouloy M, Garin D. 2001. Quantitative real-time PCR detection of Rift Valley fever virus and its application to evaluation of antiviral compounds. *J Clin Microbiol* 39:4456-61.
143. Ikegami T. 2012. Molecular biology and genetic diversity of Rift Valley fever virus. *Antiviral Res* 95:293-310.
144. Ikegami T, Won S, Peters CJ, Makino S. 2006. Rescue of infectious Rift Valley fever virus entirely from cDNA, analysis of virus lacking the NSs gene, and expression of a foreign gene. *Journal of Virology* 80:2933-2940.

145. Gommet C, Billecocq A, Jouvion G, Hasan M, Zaverucha do Valle T, Guillemot L, Blanchet C, van Rooijen N, Montagutelli X, Bouloy M, Panthier JJ. 2011. Tissue tropism and target cells of NSs-deleted rift valley fever virus in live immunodeficient mice. *PLoS Negl Trop Dis* 5:e1421.
146. Terasaki K, Makino S. 2015. Interplay between the Virus and Host in Rift Valley Fever Pathogenesis. *Journal of Innate Immunity* 7:450-458.
147. Bouloy M, Janzen C, Vialat P, Khun H, Pavlovic J, Huerre M, Haller O. 2001. Genetic evidence for an interferon-antagonistic function of Rift Valley fever virus nonstructural protein NSs. *J Virol* 75:1371-7.
148. Lopez N, Muller R, Prehaud C, Bouloy M. 1995. The L protein of Rift Valley fever virus can rescue viral ribonucleoproteins and transcribe synthetic genome-like RNA molecules. *J Virol* 69:3972-9.
149. Overby AK, Pettersson RF, Neve EP. 2007. The glycoprotein cytoplasmic tail of Uukuniemi virus (Bunyaviridae) interacts with ribonucleoproteins and is critical for genome packaging. *J Virol* 81:3198-205.
150. Buchholz UJ, Finke S, Conzelmann KK. 1999. Generation of bovine respiratory syncytial virus (BRSV) from cDNA: BRSV NS2 is not essential for virus replication in tissue culture, and the human RSV leader region acts as a functional BRSV genome promoter. *J Virol* 73:251-9.
151. Baer A, Shafagati N, Benedict A, Ammosova T, Ivanov A, Hakami RM, Terasaki K, Makino S, Nekhai S, Kehn-Hall K. 2016. Protein Phosphatase-1 regulates Rift Valley fever virus replication. *Antiviral Res* 127:79-89.
152. Conrad NK. 2008. Chapter 15. Co-immunoprecipitation techniques for assessing RNA-protein interactions in vivo. *Methods Enzymol* 449:317-42.
153. Brennan B, Li P, Elliott RM. 2011. Generation and characterization of a recombinant Rift Valley fever virus expressing a V5 epitope-tagged RNA-dependent RNA polymerase. *J Gen Virol* 92:2906-2913.
154. Rossier C, Raju R, Kolakofsky D. 1988. LaCrosse virus gene expression in mammalian and mosquito cells. *Virology* 165:539-48.
155. Tushev G, Glock C, Heumuller M, Biever A, Jovanovic M, Schuman EM. 2018. Alternative 3' UTRs Modify the Localization, Regulatory Potential, Stability, and Plasticity of mRNAs in Neuronal Compartments. *Neuron* 98:495-511 e6.
156. Novak JE, Kirkegaard K. 1991. Improved method for detecting poliovirus negative strands used to demonstrate specificity of positive-strand encapsidation and the ratio of positive to negative strands in infected cells. *J Virol* 65:3384-7.
157. Raymond DD, Piper ME, Gerrard SR, Skinotis G, Smith JL. 2012. Phleboviruses encapsidate their genomes by sequestering RNA bases. *Proc Natl Acad Sci U S A* 109:19208-13.
158. Liu T, Ye Z. 2002. Restriction of viral replication by mutation of the influenza virus matrix protein. *J Virol* 76:13055-61.

159. Perez DR, Donis RO. 1998. The matrix 1 protein of influenza A virus inhibits the transcriptase activity of a model influenza reporter genome in vivo. *Virology* 249:52-61.
160. Hoenen T, Jung S, Herwig A, Groseth A, Becker S. 2010. Both matrix proteins of Ebola virus contribute to the regulation of viral genome replication and transcription. *Virology* 403:56-66.

Vita

Breanna Renee Tercero was born in El Paso, TX on July 23, 1992 to Luci Rios and was raised in San Antonio, TX by Luci, and Rene Rios. Breanna received her Bachelors in Science degree from The University of the Incarnate Word and while attending, studied the effects of Herpes B virus encoded microRNAs on the cellular differentiation factor, ID2 at Texas Biomedical Research Institute in San Antonio, TX. While in high school, Breanna became interested in infectious diseases, particularly those caused by viruses. Her internship at Texas Biomed solidified her career choice to pursue a Ph.D. in microbiology. Breanna continued her scientific training at The University of Texas Medical Branch in Galveston, TX as a post-baccalaureate student within the post-baccalaureate research education program (PREP) under the guidance of Shinji Makino. Breanna got in-depth virology training and was involved in the studies investigating the RNA packaging mechanism of Rift Valley Fever phlebovirus as well as the generation of single-cycle replicable mutant viruses. After her PREP year, Breanna got a direct admission into Shinji Makino's laboratory for her dissertation studies that addresses the RNA packaging mechanism of genomic and antigenomic viral RNAs in RVFV particles.

While attending UTMB, Breanna has been the recipient of several competitive awards. She received the National Institute of Allergy and Infectious Diseases Diversity Supplement in 2016. She held a pre-doctoral T32 Emerging and Tropical Infectious diseases training grant from 2019-2020. She received the McLaughlin Colloquium Travel Award in 2018 and 2019. Breanna received travel awards from both the Mikiten Graduate Research Symposium in 2019 and the American Society for Virology in 2019 and 2020. In 2019, Breanna received the Mardelle Susman Scientific Writing Award. In 2019, Breanna participated in the BENCH Mentor High School program where her and her mentee received the Team Science Award. Breanna also held a position on the review committee in the Biomedical Research Training Program for High school students in

support of science education. Breanna was also invited as a guest speaker for high school AP chemistry students at McCollum High School. Additionally, Breanna was a student course instructor in 2018 for the critical reading of scientific literature course at UTMB. Breanna held the position as co-chair of the Virology/Immunology Journal Club at UTMB in 2019.

Education

B.S., December 2013, The University of the Incarnate Word, San Antonio, TX

Publications

- 1) Tercero, B., Makino S. 2020. Reverse genetics approaches for the development of bunyavirus vaccines. *Curr Opin Virol* 44:16-25.
- 2) Tercero B., Terasaki K., Nakagawa K., Narayanan K., Makino S. 2019. A strand-specific real-time quantitative RT-PCR assay for distinguishing the genomic and antigenomic RNAs of Rift Valley fever phlebovirus. *J Virol Methods* 272:113701
- 3) Terasaki K., Tercero B., Makino S. 2016. Single-cycle replicable Rift Valley fever virus mutants as safe vaccine candidates. *Virus Res* 216:55-65

Permanent address: 3102 Cove View Blvd, Apt. D303
Galveston, TX 77554

This dissertation was typed by Breanna R. Tercero.